2-24-2014 12:00 AM

Static and Seismic Performance of Geosynthetics-Strengthened Pile Foundations

Ahmed M. Taha
The University of Western Ontario

Supervisor
Dr. M. Hesham El Naggar
The University of Western Ontario

Graduate Program in Civil and Environmental Engineering
A thesis submitted in partial fulfillment of the requirements for the degree in Doctor of Philosophy

STATIC AND SEISMIC PERFORMANCE OF GEOSYNTHETICS-STRENGTHENED PILE FOUNDATIONS

by

Ahmed Taha

Graduate Program in Civil and Environmental Engineering

A thesis submitted in partial fulfillment
of the requirements for the degree of
Doctor of Philosophy

The School of Graduate and Postdoctoral Studies
The University of Western Ontario
London, Ontario, Canada

Abstract

Geosynthetic reinforcement in earth structures has been used extensively over the last two decades. Extensive research has been carried out to investigate solutions to enhance the lateral stability of pile foundations. This research is motivated by the need to install piles in sites characterized by soft subsurface soil conditions, and often times, in seismic active areas. This research work explores an innovative use of geosynthetics to enhance the lateral performance of pile foundations. The static and seismic soil-structure-interaction behaviors of geosynthetics-reinforced pile foundation systems were evaluated using a series of reduced scale physical model tests performed on a shaking table in a 1G environment. A laminar shear box containing a pile foundation model supporting a single degree of freedom structure installed in different soil bed models was used in the experiments. The soil models included: a layer of synthetic clay (Modified Glyben) underlain by a sand layer (simulating a base case of soft soil); a layer of synthetic clay sandwiched between a sand layer and an aggregate layer (simulating the case of conventional ground replacement for the top soft soil); and a layer of synthetic clay sandwiched between a sand layer and a geosynthetic-reinforced aggregate layer (simulating the case of ground replacement of the top soft soil combined with geosynthetic reinforcement using a microgrid mesh). A series of sine-sweep, harmonic and scaled earthquake tests have been performed to identify the amplification and resonance conditions of the foundation system and to identify various aspects of seismic-soil-pile-geosynthetic reinforcement interaction effects. Lateral static load tests of this system were performed using a one directional load system that was fixed on the laminar shear box. The dynamic and static tests were simulated employing numerical models developed using the finite element program Plaxis 3D. The results of both static and dynamic tests showed that the microgrid reinforcement improved the lateral performance of the pile foundation and reduced the vibration amplitudes of the supported structure. The numerical analysis results were in close agreement with the dynamic and static experimental results. The results of a parametric study for the investigated foundation configuration and seismic loading demands showed that the requirements for engineered

backfill can be reduced by more than 50% and the lateral seismic response can be reduced by 50% by using geosynthetic reinforcement.

Key words: Seismic, static, piles, polymer strips reinforcement, microgrid mesh, geogrid, soft clay, Shaking table tests, Scaled model tests, Layered soil, Plaxis 3D.

Co-Authorship Statement

This thesis is prepared in accordance with the regulation for Integrated-Article format thesis stipulated by the school of graduate and post graduate studies at Western University, London, Ontario, Canada. All the field testing, numerical modeling, interpretation of results and writing of the draft and the final thesis were carried out by the candidate himself, under the supervision of Dr. M. Hesham El Naggar. The supervisor's contribution consisted of providing advice throughout the research program, and reviewing the draft and the final thesis and publications results from this research. The results of the field tests, and numerical modeling presented will be used in journals and conferences publications, which will be co-authored with Dr. El Naggar.

Chapters 2, 3 and 4 of this thesis are the current versions of manuscripts that will be submitted for publication as papers. Chapters 2 to 4 inclusive are coauthored by A. M. Taha, M.H. El Naggar and A. Turan as described below:

Chapter 2: Experimental and Numerical Study on Lateral Behavior of Model Geosynthetic-Reinforced Pile-Foundation Systems Subjected to Static Horizontal Loading.

A version of chapter 2 will be submitted to the Geotextiles and Geomembranes Journal

Chapter 3: Experimental Study on the Dynamic Lateral Behavior of Geogrid Reinforced Pile Foundation System

A version of chapter 3 will be submitted to the Geotextiles and Geomembranes Journal

Chapter 4: Numerical Study on the Dynamic Lateral Behavior of Geosynthetics-Reinforced Pile Foundation System

A version of chapter 4 will be submitted to the Journal of Soil Dynamics and Earthquake Engineering.

Acknowledgments

In the name of God, who is most compassionate and most merciful. All my praise is to Allah, the Lord of the worlds. He is the Master of the Day of Judgment and keeps us on the right path. We all depend on Him.

I would like to express my heartfelt appreciation and thanks to my supervisors Dr. M. H. El Naggar and Dr. Alper Turan. The outcomes of this research could not have been achieved without their partnership and support. I would like to acknowledge their continuous support during my research. They were always friendly available with their wise guidance and expertise.

I would like to thank Dr. Ashraf El-Damaty and Dr. Tim Newson and other members of UWO Civil Engineering faculty, from which a gained lots of knowledge related to my research work. I would also like to express my thanks for the kind assistance given by the staff of the Boundary Layer Wind Tunnel (BLWTL) and University Machine Services (UMS). I would like to specially thank Mr. Anthony Burggraaf and Gerry Dafoe for training me on the shaking table and measuring instruments. I would like to thank M. Richardson, W. Logan and Lama El-Naggar for their support in geotechnical laboratory tests. I would like to thank Cody Ruthman and other UMS staff, who helped with the assembling and mounting of the laminar soil container, this work could not have been established without them.

I would like to express my gratitude to my father Mohammed Taha and my mother Khadiga Saleh for their support and worm feelings during my study period. I would like to express special thanks to my wife Hana and my brother Abdullah and all of my family members for their extraordinary support and sacrifices.

I would like to express my deep thanks to Taibah University and the Saudi Cultural Bureau of the Saudi Arabian Embassy for funding my scholarship and a great part of this research at the University of Western Ontario.

Table of Contents

Abstract ii

Co-Authorship Statement iv

Acknowledgments v

List of Tables xi

List of Figures xiii

NOMENCLATURE xviii

Chapter 1 1

1.1 Introduction and problem overview 1

1.2 Problem Definition and Methodology 2

1.3 Research Objectives and plan 3

1.4 Literature Review on Related Studies 3

1.4.1 Dynamic performance of geogrid reinforced retaining walls 4

1.4.2 Numerical modeling of seismic behavior of geogrid reinforced earth retaining structures 5

1.4.3 Nonlinear seismic performance of piles 6

1.4.4 Geogrid reinforced soils and piled supported systems. 7

1.4.5 Background on polymer strips 9

1.5 Contributions 10

1.6 Scope of work 10

1.7 Thesis Layout 12

2. EXPERIMENTAL AND NUMERICAL STUDY ON LATERAL BEHAVIOR OF MODEL GEOSYNTHETIC-REINFORCED PILE-FOUNDATION SYSTEMS SUBJECTED TO STATIC HORIZONTAL LOADING 17

2.1 Introduction 18

2.2 Background 20

2.3 Methodology 21
2.3.1 Model soil 21
2.3.2 Soil parameters 22
2.3.3 The model foundation system 25
2.3.4 The Model geogrid 27
2.3.5 Model Stratigraphy 28
2.3.6 Placement of geogrid-reinforced engineered granular fill 29
2.3.7 Loading System and Instrumentation 30
2.3.8 Numerical model 33
2.3.9 Experimental and numerical test cases 36
2.4 Results and discussion 37
2.4.1 Pile cap translation 37
2.4.2 Extension of microgrid (in Deep backfill case) 42
2.4.3 Results of Numerical Analysis 45
2.5 Summary and Conclusions 49
3. EXPIRMENTAL STUDY ON THE DYNAMIC LATERAL BEHAVIOR OF GEOGRID REINFORCED PILE FOUNDATION SYSTEM 54
3.1 Introduction 55
3.2 Background 56
3.3 Methodology 57
3.3.1 Reduced scale physical model 57
3.3.2 The shaking table and soil container 59
3.3.3 The model soil column 60
3.3.4 Model Foundation System 62
3.3.5 Model Geosynthetics 64

3.3.6 Model Superstructure 65
3.3.7 Instrumentation 68
3.3.8 Shaking Table Control System 69
3.3.9 Placement of Model Soil Deposit 70
3.3.10 Experimental Scenarios 72
3.4 Results and discussion 76
3.4.1 Free Field Response 77
3.4.2 Pile cap response 78
3.4.3 Low Frequency Structure Response 81
3.4.4 High Frequency Structure Response 83
3.4.5 Pile cap rocking response 85
3.5 Summary and conclusion 88
4. NUMERICAL STUDY ON THE DYNAMIC LATERAL BEHAVIOR OF GEOSYNTHETICS-REINFORCED PILE FOUNDATION SYSTEM 92
4.1 Introduction and problem overview 92
4.2 Shaking table test description 94
4.3 The numerical model 97
4.3.1 Problem dimensions 97
4.3.2 Interface conditions 99
4.3.3 Material models and parameters: 100
4.3.4 The numerical model elements and mesh configuration 111
4.3.5 The numerical calculation process 111
4.4 Free Field Ground Response Analysis Using Deep Soil 112
4.5 Numerical Model Calibration Results 116
4.6 Dynamic Model and Its Verification 116

4.6.1 Soil Model 117
4.6.2 Piles-cap-geogrid-foundation model 120
4.6.3 Interface model 121
4.6.4 Ground response analysis 123
4.7 Parametric Study Considering Dynamic Analysis 125
4.7.1 Effect of geogrid reinforcement on response to shaking with varying intensity 126
4.7.2 Effect of geogrid reinforcement on response of foundation subjected to shaking with different frequency 128
4.7.3 Effect of engineered backfill thickness 130
4.7.4 Effect of stiffness of geosynthetics reinforcement on the system performance 131
4.8 Parametric Study Considering Pseudo-Static Analysis 132
4.8.1 Building, pile cap model and geogrid 132
4.8.2 Pseudo-static seismic lateral loading calculation 136
4.8.3 Summary of numerical pseudo-static analyses 138
4.9 Results and Discussion 139
4.9.1 Effect of geosynthetic material stiffness and depth 140
4.10 Summary and Conclusions 142
5. Summary and Recommendations for Further Research 149
5.1 Summary of thesis findings 149
5.2 Recommendations for Future Research 153
Appendix A 154
Curriculum Vitae 155

List of Tables

Table 2-1: Scaling relationships for primary system variables (Meymand, 1998). 21

Table 2-2 : Soil parameters 24

Table 2-3: Model Piles calculations 26

Table 2-4: Engineering properties of Microgrid geogrid 27

Table 2-5: Summary of experimental and numerical cases 36

Table 3-1: Scaling relationships for primary system variables (Meymand, 1998). 59

Table 3-2: Model Piles calculations 64

Table 3-3: Engineering properties of geogrid 65

Table 3-4: SDOF structures model and prototype frequencies 66

Table 3-5: Summary of tests 73

Table 3-6: Summary of harmonic tests 76

Table 4-1: Granular Soil parameters 101

Table 4-2: The HSSMALL clay and aggregate parameters: 109

Table 4-3: DeepSoil input parameters; model soil column. 115

Table 4-4: The HSSMAL prototype parameters of each soil layer 119

Table 4-5: DeepSoil input parameters; prototype soil column. 124

Table 4-6: Summary of numerical model verification analyses 125

Table 4-7: HSSMALL Soil parameters of each soil layer adopted for the equivalent static study 135

Table 4-8 : Uniaxial Geogrid GG200PE specifications 136

Table 4-9: Equivalent static forces and overturning moment calculation 138

Table 4-10: Equivalent static analysis cases 139

Table 4-11: Cases 1-8 results comparison. 141

List of Figures

Figure 1-1: Aggregate interlocking with geogrid (www.windfarmbop.com)..... 1

Figure 1-2: Component parts of Reinforced Earth Wall (Holtz, 1997)..... 4

Figure 1-3 Reinforcement strips extending from a mechanically stabilized wall during construction (www.recocanada.com)..... 10

Figure 2-1: Construction sand gradation..... 22

Figure 2-2: The scaled piled cap geogrid model..... 26

Figure 2-3: Compaction of modified glyben 29

Figure 2-4: Geogrid extending between the ring and the metal disc 30

Figure 2-5: a. Schematic diagram of the testing setup, b. top view of the testing setup... 32

Figure 2-6: The Wire Line Position Sensors mounted on a frame and tied to the wires .. 33

Figure 2-7: a) Plaxis 3D numerical model of Soil and pile-cap-geogrid system b) Finite element mesh. 35

Figure 2-8: Lateral load-displacement response of model foundation and results of numerical simulations (Cases #1 and 4). 38

Figure 2-9: Lateral load-displacement response of model foundation and results of numerical simulations (Cases #2 and 5). 39

Figure 2-10: Lateral load-displacement response of model foundation and results of numerical simulations (Cases # 3 and 6) 40

Figure 2-11: experimental results comparison (cases 1-3) 41

Figure 2-12: Numerical results comparisons (cases 5-8)..... 42

Figure 2-13: Microgrid strain vs. pile cap pull load measured near to the piles face. 43

Figure 2-14: Microgrid strain vs. pile cap pull load measured far from the piles face 44

Figure 2-15: Global Microgrid deformation measured near and far from the pile face ... 45

Figure 2-16: Bending moment at pile head vs. pile cap lateral deflection 46

Figure 2-17: Shear force at pile head vs. pile cap lateral deflection 46

Figure 2-18: Pile cap deflections for microgrid lengths of 90 cm and 20 cm. 47

Figure 2-19: Maximum bending moments for microgrid lengths of 90 cm and 20 cm. ... 48

Figure 2-20: Maximum shear forces for microgrid lengths of 90 cm and 20 cm 49

Figure 3-1: Laminar soil container covered with latex membrane and aligned with corner profiles 60

Figure 3-2: Construction sand gradation 61

Figure 3-3: The scaled piled cap geogrid model 63

Figure 3-4: a) The SDOF High system b) SDOF Medium system, c) ADXL 203 Accelerometer 67

Figure 3-5: Instruments distribution diagram 69

Figure 3-6: The shaking table and control system 70

Figure 3-7: Compaction of Modified Glyben 72

Figure 3-8: The earthquake acceleration time history 74

Figure 3-9: Fourier spectrum of model scale Upland EQ (a) input signal (b) signal at table top 75

Figure 3-10: Free field response comparison (SAMP-1 to SAMP-4). 78

Figure 3-11: The dynamic response comparison of the piled cap foundation (SLNF-1 to SLNF-3). 79

Figure 3-12: Dynamic response of pile foundation with and without reinforcement (UPEQ-L). 80

Figure 3-13: The dynamic response comparison of the piled cap foundation (SHNF 1-3) 81

Figure 3-14: The dynamic response comparison of the low frequency SDOF superstructure (SLNF-1 to SLNF-3). 82

Figure 3-15: The dynamic response comparison of the low frequency SDOF superstructure (UPEQ-L). 83

Figure 3-16: The dynamic response comparison of the high frequency SDOF (SHNF-1 to SHNF-3). 84

Figure 3-17: The dynamic response comparison of the high frequency SDOF structure (UPEQ-H). 85

Figure 3-18: The dynamic vertical response comparison measured at the pile tip (SLNF-1 to SLNF-3). 86

Figure 3-19: Vertical response at the pile tip comparison (SAMP-4) 87

Figure 4-1: The schematic of the shaking table test setup 94

Figure 4-2: Input motion acceleration time history used in the shaking table test 95

Figure 4-3: Fourier spectrum of the input motion used in the shaking table test 96

Figure 4-4: Pile cap acceleration response 96

Figure 4-5 : Model pile foundation and microgrid connectivity.....98

Figure 4-6: 3D FE model of geosynthetic reinforced pile-cap system 99

Figure 4-7: Typical sand shear stress-strain loop (calculated from the shaking table tests). 102

Figure 4-8: Typical aggregate shear stress-strain loop (calculated from the shaking table tests). 103

Figure 4-9: Glyben shear stress-strain loop (calculated from the the shaking table tests). 104

Figure 4-10 : Hyperbolic stress-strain relationship in primary loading for a slandered drained triaxial test (Schanz et al., 1999).....106

Figure 4-11: Stiffness degradation for modified glyben (Turan et al., 2009a) 108

Figure 4-12 : Mean curves defining G/G_{max} versus γ relationships for gravelly soils at various confining pressures along with standard deviation boundaries for reduced data set (Rollins et al. ,1998).....113

Figure 4-13 : Mean Curves Defining D versus γ relationships for gravelly soils at various confining pressures along with standard deviation boundaries for entire data set (Rollins et al. ,1998). 114

Figure 4-14: Measured vs. calculated acceleration using DeepSoil. 115

Figure 4-15: Calculated vs. measured responses of pile cap reinforced with geogrid....116

Figure 4-16 : Soil model general view.....117

Figure 4-17 : a) Soil column stratigraphy without geogrid, b) Soil column stratigraphy after adding geogrid 118

Figure 4-18: Pile-Cap–geogrid finite element mesh. 120

Figure 4-19: Pile cap translation, Static pull test vs. 35% improved interface modulus 123

Figure 4-20: Ground response analysis, 3D finite element model vs. DeepSoil. 124

Figure 4-21: Cap motion comparison, Cases of 2 m backfill with and without geogrid (0.1 g, 3 Hz). 126

Figure 4-22: Cap motion comparison, Cases of 2 m backfill with and without geogrid (0.2 g, 3 Hz). 127

Figure 4-23: Cap motion comparison, Cases of 2 m backfill with and without geogrid (0.3 g, 3 Hz). 128

Figure 4-24: Cap motion comparison, Cases of 2 m backfill with and without geogrid (0.2 g, 2 Hz). 129

Figure 4-25: Cap motion comparison, Cases of 2 m backfill with and without geogrid (0.2 g, 5 Hz). 129

Figure 4-26: Pile cap acceleration time history comparison , (cases of 1.6 m with geogrid, 1.6m without geogrid and 6 m backfill without geogrid). 130

Figure 4-27: Effectiveness of conventional geogrid vs. polymer strips in reducing pile cap response 131

Figure 4-28 : Pile, cap, geogrid and superstructure model 133

Figure 4-29 : Plaxis model 3D view 134

Figure 4-30: Deformed model shape 140

NOMENCLATURE

c	cohesive strength
c_u	undrained shear strength
Dr	relative density
γ	soil unit weight
G/G_{max}	shear modulus reduction factor
G	dynamic shear modulus
G_{max}	maximum shear modulus
G_s	secant shear modulus
gw/c	ratio of fluids to solids by mass
M	mass matrix
K	stiffness matrix
C	damping matrix
$\overrightarrow{F}$	force matrix
Δt	time interval
T	fundamental period of superstructure
M_v	higher mode factor
R_d , R_o	Ductility factors

V	seismic base shear force
S(T)	design spectral acceleration
I_E	seismic importance factor
W	seismic dead load
$(Vs)_m$	shear wave velocities for the prototype
$(Vs)_p$	shear wave velocities for the model
w	water content
w/gw	ratio of water to water plus glycerin by mass
ε_1	axial strain
ϕ	friction angle
ψ	dilatancy angle
γ	shear strain
γ_r	threshold shear strain
$\gamma_{0.7}$	shear strain at $G_s = 0.70\ G_0$
λ	geometric scaling factor
ν	Poisson's ratio
ν_{ur}	Unloading reloading poisson's ratio

ω_n	fundamental angular frequency
ρ	mass density
σ_v	overburden stress
σ_x	confining stress
σ'_3	minor principle stress
P^{ref}	reference pressure
E	Young's modulus
E_i	initial stiffness
E_p	Young's modulus of pile material
E_{50}	secant stiffness modulus at 50% strength
E_{50}^{ref}	reference secant stiffness modulus at 50 % strength
E_{oed}	oedometer loading modulus
E_{oed}^{ref}	reference oedometer loading modulus
E_{ur}	elastic unloading reloading modulus
E_{ur}^{ref}	reference elastic unloading reloading modulus
m	amount of stress dependency power
J_p	prototype stiffness
J_m	model stiffness

q	the deviatoric current shear stress
q_a	the deviatoric asymptotic value of the shear stress
q_f	the ultimate diviatoric stress
$R_{interface}$	structure/ soil interface strength ratio
τ	shear stress
τ_{max}	maximum shear stress
D	damping ratio
K_{2max}	shear modulus number for the soil = 50 for loose sand and 75 for dense sand
σ'_m	mean effective confining stress of the soil in psf

Chapter 1

1.1 Introduction and problem overview

Geogrids are polymeric material consisting of tensile ribs with openings of sufficient size to allow interlock with the surrounding soil. This geogrid-soil interlock mechanism allows the geogrid mesh to work as a reinforcement element, which enhances the soil shear strength. Therefore, geogrids have been widely used in modern construction technology. Several application examples include: geogrid reinforced earth retaining walls (GRS); highway construction and expansion over soft soils; geogrid-reinforced pile-supported highway embankments; and geogrid reinforced slopes. The use of geogrids in flexible pavement construction is widely popular and demonstrates its advantageous interaction with the aggregate used. The geogrid mesh is laid within the aggregate base course and provides increased modulus and lateral confinement for the crushed stones intruding the apertures of the geogrid (figure 1-1).

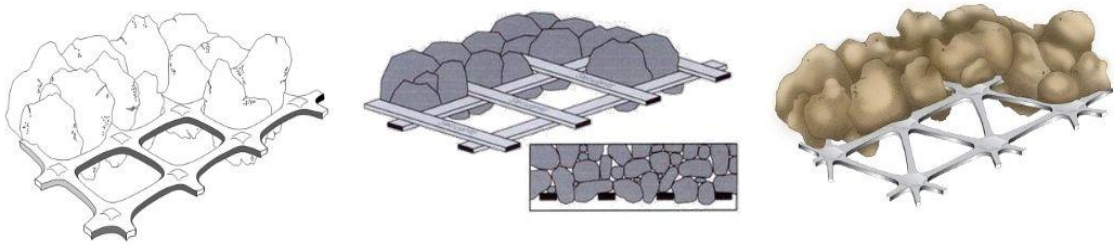

Figure 1-1: Aggregate interlocking with geogrid (www.windfarmbop.com)

This confinement system prevents the base course stones from dispersing apart under the cyclic traffic loads (Koerner, 2005).

In other applications, geogrids have been implemented to reduce lateral wall deflections arising from dynamic loads and uneven settlement of the supporting sub grades and embankments. Due to the rising concern in the construction industry with regards to mitigating the destructive effects of cyclic earthquake loads, this thesis explores the

development of a novel pile foundation system that incorporates the benefits of geosynthetics reinforcement to enhance the lateral performance of pile foundation systems.

1.2 Problem Definition and Methodology

Meeting serviceability limits in strong earthquake events has become the driving force in the design for seismic safe structures. Therefore, researchers and engineers developed several means to enhance the dynamic lateral stability of civil engineering structures. For example, Geosynthetic reinforced earth retaining structures were constructed to sustain high earthquake shaking. Therefore, this thesis investigates the effect of geosynthetics reinforcement on the lateral response of low frequency and relatively higher frequency superstructures supported by pile foundations. The investigation is carried out on two model superstructures mounted on a model pile foundation and subjected to 1-G shaking on a shaking table. The model geogrid and piles are embedded in a layered soil system that includes a synthetic soft clay layer sandwiched between a granular backfill from top and well graded sand from bottom. This composite system is subjected to three kinds of 1-D base excitation including, i) sine sweep, ii) harmonic iii) and scaled earthquake motions. The research also investigates the static lateral response of the geogrid pile composite system through subjecting the foundation cap to a static lateral pull mechanism. The results derived from the composite system are compared with the base case where the model pile foundation is not reinforced and another case with thicker granular backfill layer simulating conventional ground replacement solution to improve lateral response of piles. In addition, static and dynamic numerical models of the pile-geogrid reinforcement composite system were developed and were verified using the experimental results. The numerical models were then used to conduct a parametric study to further examine the effects of different parameters on the lateral performance of the pile-geogrid reinforcement composite system.

1.3 Research Objectives and plan

To the best of the author's knowledge, the use of geosynthetics to improve the seismic performance of pile foundations and to reduce intolerable pile lateral deflections have not been investigated. The primary focus of this thesis is to prove that geosynthetic reinforcement can enhance the lateral stability of pile foundation. Therefore, the following plan was carried out:

- To carry out static lateral pull tests to investigate the static behavior of the geogrid reinforced piled cap system.

- To carry out 1-G shaking table tests to investigate the dynamic behavior of the geogrid reinforced piled cap system.

- To develop numerical static and dynamic models for the composite pile-geogrid reinforcement system and calibrate/verify this model with the experimental results.

- To carry out a parametric study to investigate the favorable effect of geosynthetics enhanced pile foundation over a range of base excitation amplitudes and frequencies. Also, to study the effect of changing the geogrid stiffness on the lateral performance of the geosynthetics-reinforced pile foundation system.

1.4 Literature Review on Related Studies

This thesis covers several research fields related to the individual components of the geogrid reinforced pile foundation system investigated. Extensive research has been carried out to investigate the soil-pile-superstructure interaction problem using 1-G shaking. Also, the nonlinear soil-pile interaction problem has been widely studied both experimentally and numerically. On the other hand, several researches have investigated the performance of geogrid reinforced earth retaining structures and embankments subjected to dynamic loading. This research was conducted employing finite element

numerical models that were calibrated against experimental results. The following sections present some of the studies related to the studied problems.

1.4.1 Dynamic performance of geogrid reinforced retaining walls

The first Geosynthetic reinforced retaining wall was built in France in 1971. Geosynthetic reinforced walls include reinforcing geogrids or geotextile as reinforcing elements embedded in the engineered fill to counteract against the lateral earth pressure. Compared to the conventional earth retaining walls, they are more flexible and can support higher earth fills. Therefore, they suit seismic active sites (Holtz, 1997) (figure 1-2).

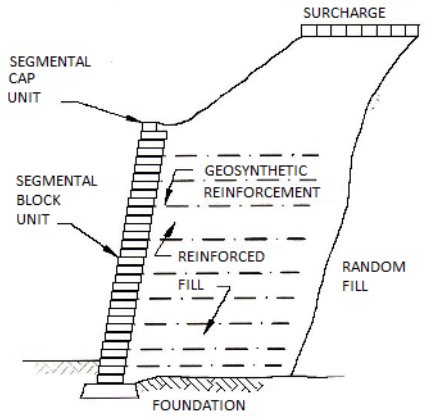

Figure 1-2: Component parts of Reinforced Earth Wall (Holtz, 1997)

Geogrid-reinforced retaining walls performed very well in major seismic events in the US and Taiwan. Sandri (1997) surveyed three geosynthetic-reinforced walls and four geosynthetic-reinforced slopes that showed no visual evidence of distress. Also, 11 geogird-reinforced segmental retaining walls and slopes exceeding 4.6 m in height survived the North Ridge earthquake in 1994, which had a magnitude of 6.7 (Sandri, 1997). Ling et al. (2001) evaluated several geosynthetic-reinforced soil retaining walls and slopes during a major earthquake event in Taiwan. Their investigation revealed that the geosynthetic-reinforced structures performed better than the unreinforced structures.

Moreover, his investigation emphasized the importance of proper seismic design of geosynthetic-reinforced soil retaining structures.

Several other researchers investigated the performance of geosynthetic-reinforced walls and arrived at the same conclusion in which several GRS walls were observed to survive major earthquake events (e.g. White and Holtz (1996), Eliahu and Watt 1991, Collin et al. (1992) and Nishimura et, al. (1996)). Additionally, several researches have been undertaken to analyze and design geosynthetic-reinforced walls for satisfactory seismic performance. A broad review of the techniques used for seismic analysis of geosynthetic-reinforced walls, slopes and embankments was carried out by Bathurst and Alfaro (1996). Bathurst and Alfaro (1996) argued that these design and analysis techniques are based on approximated analytical solutions. They recommended using the enhanced abilities of existing geotechnical finite element models, calibrated using experimental simulation procedures, for tackling the complex geosynthetic-reinforced soil structures problems with greater accuracy.

1.4.2 Numerical modeling of seismic behavior of geogrid reinforced earth retaining structures

Several researchers investigated the seismic performance of geogrid-reinforced walls using finite element and finite difference models. Bathrust and Hatami (1998) studied the influence of reinforcement length, stiffness and layers spacing on the response of reinforced walls to seismic loads using numerical modeling. Their study indicated that the static and dynamic wall lateral displacement can be altered depending on the reinforcement length, stiffness and distribution. Helwany et al. (2001) executed a finite-element model to study the seismic behavior of a 0.9 m model segmental wall subjected to EQ loading generated by a shaking table using the finite element program DYNA3D. In their finite element simulation, they used a soil model that accounted for the nonlinear hysteretic behavior of the backfill soil. They concluded that the results obtained from the finite element simulation were consistent with the experimental results. Burke et al. (2004) analyzed the seismic response of a full-scaled reinforced retaining wall using a 2-D finite element model. Ling et al. (2004) carried out a dynamic finite element procedure

to analyze the behavior of geosynthetic-reinforced soil retaining wall. El-Emam and Bathrust (2007) formulated a dynamic finite difference model to study the influence of reinforcement parameters on the seismic response of a reduced-scale reinforced soil retaining wall. Fakharian and Attar (2007) also used a dynamic finite difference model to investigate the seismic behavior of a block-faced geogrid reinforced soil bridge abutment. Liu (2009) investigated the reinforcement loads of a GRS wall subjected to seismic loading during the service life using a finite element procedure. Anastasopulos et al. (2010) used a numerical model to analyze the seismic performance of a bar–mat retaining wall at model scale employing the finite element program ABAQUS. The aforementioned research proved that both finite difference and finite element numerical models are powerful tools for prediction of the performance and nonlinear behavior of soils and earth retaining structures.

1.4.3 Nonlinear seismic performance of piles

Several researches have been undertaken to model the nonlinear seismic response of pile foundations (e.g. El Naggar and Novak, 1996; El Naggar and Bentley, 2000; El Naggar et al., 2005).

El Naggar and Novak 1996 developed an analytical model for the lateral response of single piles and pile groups. This model include: 1) soil reaction elements that account for the state of stress and gapping and slippage at both sides of the pile; 2) inner field zone elements to model the nonlinear soil behavior by nonlinear spring that represent the stiffness and a dashpot to simulate the soil hysteretic damping; 3) far field zone elements that simulate the linear stiffness and damping and account for the propagation of waves and energy dissipation; 4) pile modeled as conventional two node beam elements .

El Naggar and Bentley (2000) simulated the soil seismic nonlinearity and energy dissipation using a spring with dynamic p-y curve model and a dashpot. The soil stiffness in this simulation is derived from the dynamic p-y curve and is equivalent to the combined inner and outer zones stifnesses. The dashpot is connected in parallel to the unified spring and has a constant equivalent to the far field dashpot constant. The

computed lateral pile response from the dynamic p-y curve was in good agreement with the measured results of a Statnamic load test (El Naggar, 1998). Moreover, El Naggar and Bentley (2000) established an equation from regression analysis that relates the dynamic soil resistance with the loading frequency and the static soil reaction. This equation is used to generate dynamic p-y curves from the static curves in order to get better estimation of the response of the structures-soil system to dynamic loading. Dynamic p-y curves were implemented in the finite element program ANSYS. The ANSYS simulation showed good agreement between the analytical and dynamic p-y lateral models results.

El Naggar et al. (2005) developed a simplified Beam on Nonlinear Winkler Foundation (BNWF) model for nonlinear seismic response analysis of offshore piles. The (BNWF) is a simplified approach that accounts for nonlinear seismic-soil-pile-structure and is commonly used in engineering practice. The (BNWF) uses spring based on the p-y curve approach to represent soil resistance and dashpots to account for energy dissipation and the hysteretic behavior of the soil. The pile was modeled as discrete beam column elements. The damping of the pile segments was determined using the Rayleigh approach. The discontinuity and gapping conditions at pile-soil interface were modeled using special interface elements that account for relative movements of the pile against soil. The displacement-time or acceleration time histories at different soil layers were computed using Iwan-Mroz model for stress-strain and tangential shear modulus relation. The result of this free field analysis was then used as the input motion at BNWF support nodes. The comparison of El Naggar et al. (2005) finite element model results and the experimental centrifuge test carried out by Wilson et al (1997) indicated a good agreement when the pile damping ratio is between 3% and 5%.

1.4.4 Geogrid reinforced soils and piled supported systems.

Little research has been carried out to study the combined effect of piled geogrid systems. Liu et al. (2007) presented a case history of a geogrid-reinforced and pile-supported (GRPS) highway embankment. In this case history, ABAQUS finite-element software was used to back analyze a (3D) fully coupled model. The horizontal length of

the finite-element mesh was three times the width of half the embankment base in order to minimize the boundary effects. The piles were modeled by a 20-node quadratic brick without pore pressure degrees of freedom. The interface soils and other soils were modeled by 20-node quadratic displacement, with eight more excess pore pressure degrees of freedom. The geogrid were modeled by eight-node quadrilateral that have a capacity to resist only tensile force. The model of the pile was chosen as an isotropic linear elastic material. The embankment fill, gravel and the surface coarse-grained fill, was modeled using as linear elastic-perfectly plastic with Mohr–Coulomb failure criterion. The four foundation soils were modeled as modified cam clay materials. The comparison of the numerical model and field observation results showed that for embankment higher than 2.5 m, the computed stress reduction ratio was consistent with the measured values.

Another system that combines the favorable effect of the geosynthetic-reinforcement and piles is geosynthetic-reinforced and pile-supported earth platforms. This system is constructed over soft soils to build superstructures, such as tanks and embankments in a single stage without long-standing waiting times. Also, building this foundation system can significantly reduce total and differential settlements. Furthermore, geosynthetic-reinforced and pile-supported earth platforms can reduce earth pressures and avoid expensive excavation and refill engaged in typical situations. Compared with unreinforced pile supported earth platforms, the geosynthetic-reinforcement can reduce the settlement between pile caps. Han and Gabr (2002) carried out a numerical study on the behaviour of geosynthetic-reinforced and pile-supported earth platforms over soft foundations using the finite difference program FLAC 2D. They investigated the influencing factors related to the height of embankments, tensile stiffness of geosynthetic, and elastic modulus of pile material. The results were presented in terms of settlement, stress concentration, and soil arching. The material constitutive model adopted in this research was the nonlinear hyperbolic elastic model developed by Duncan and Chang (1970). The results of this research verified that inclusion of geosynthetic in earth platforms can reduce the total and differential settlements above the pile heads and at the ground surfaces. The research also found that increasing the stiffness of the

geosynthetic reinforcement had a favourable effect in reducing soil arching. Han and Gabr (2002) indicated that increasing the stiffness of the geosynthetic reinforcement increased the stress concentration ratio and improved the stress transfer from the soft soil to the pile. The study results also indicated that the maximum tension in geosynthetic increases with increasing the stiffness of geosynthetic, increasing the height of embankment fill and increasing the elastic modulus of the pile material.

1.4.5 Background on polymer strips

French architect/engineer Henri Vidal patented Reinforced Earth technology in 1963. Simply, it involves combining layer of earthworks and tensile reinforcements to develop a new and strong composite earth retaining structure. This technology is now commonly used globally. Polymer strips are geosynthetic material developed to provide earth reinforcement for earth retaining structures. Polymer strips to enhance the lateral stability if an earth retaining structures known as mechanically stabilized wall. The mechanically stabilized wall are built from modular blocks of various shapes and dimensions (figure 1-2), and stacked together in the vertical direction. The polymer strips are embedded between the modular blocks and extended into the soil. High frictional resistance develop between the strips and soil and provide lateral stiffness to these kind of walls (figure 1-3) (www.recocanada.com).

Figure 1-3 Reinforcement strips extending from a mechanically stabilized wall during construction (www.recocanada.com).

1.5 Contributions

This thesis explored a novel means of enhancing the lateral performance of pile foundations using geogrid reinforcement embedded in granular backfill. Before this novel system, the use of geogrid reinforcement was limited to earth structures, pavements and embankments applications. The static and dynamic results derived from this thesis may encourage researchers to carry out further field investigations to examine the quantitative performance of this novel system. Moreover, the dynamic and static tests revealed the importance of using a well-designed backfill thickness in reducing the lateral response of superstructures supported on piled foundations. The findings of this thesis together with full scale tests may present an economical alternative to using thick pile caps or large ground replacement efforts. The numerical models used in this thesis can be used as the basis for studying this foundation system at the field scale.

1.6 Scope of work

This thesis encompasses static and dynamic experiments to investigate the lateral performance of the geogrid-pile foundation system. The experimental testing results are

used to calibrate and verify static and dynamic finite element models. These numerical models are then used to perform a comprehensive parametric study to evaluate the important design parameters of the developed foundation system. To carry out these tasks, the following steps are required:

1- Preparing synthetic soft clay (modified glyben) through mixing bentonite, water and glycerin.

2- Construction of layered soil beds in the lamina container. These soil beds included: a soil bed representing the base case (soft clay overlying sand layer); a soil model representing the conventional ground replacement solution (the glyben layer sandwiched between an aggregate layer from top and a sand layer from bottom) and a soil model representing the proposed novel geosynthetic-reinforced backfill (the glyben layer sandwiched between a geosynthetic-reinforced aggregate layer from top and a sand layer from bottom).

3- Installing a geogrid mesh within the top granular backfill layer for the case of geosynthetic-reinforced backfill.

4- Installing a 2X2 model pile group in the layered soil.

5- Fabricating then fixing the model low frequency and relatively high frequency single degree of freedom structures on top of the pile cap foundation.

6- Performing lateral static pull tests on the pile foundation system with and without geogrid reinforcement and comparing its response with both the base case and the pile foundation system embedded in the backfill layer.

7- Subjecting the geogrid-reinforced pile foundation system to harmonic, sine sweep and scaled earthquake 1-D base motions using a shaking table.

8- Subjecting the same pile foundation system without the geogrid mesh to the same harmonic, sine sweep and scaled earthquake base motions using the shaking table.

9- Subjecting the same pile foundation system without reinforcement within the backfill layer to the same base excitation.

10- Employing the finite element program Plaxis 3D (Brinkgreve et. al, 2012) to develop the static and dynamic numerical models and validating these models with the experimental results.

11- Carrying out static numerical parametric study to investigate the effect of the length and stiffness of the geogrid reinforcement on the lateral performance of the geogrid pile foundation system.

12- Carrying out dynamic numerical parametric study to investigate the effect of the input ground motion amplitudes and frequency on the geogrid pile foundation system.

13- Carrying out a parametric study to investigate the effect of the depth and stiffness of geogrid on the lateral performance of the geogrid pile foundation system through the analysis of the response of a building subjected to pseudo-static seismic lateral loading.

1.7 Thesis Layout

This thesis is organized in the following chapters:

Chapter 1 presents the objectives, the literature review, the original contributions of this thesis, the scope of work and the organization of this thesis.

Chapter 2 presents the experimental work carried out to investigate the static lateral behavior of the geogrid-reinforced pile foundation system. It describes the methodology undertaken to apply a static lateral load on the pile cap and the extension behavior of the geogrid mesh. Chapter 2 also describes the finite element model developed to simulate the static lateral pull test. The results collected from the static test were used to verify this numerical model. Also, a parametric study is carried out to investigate the effect of

length and stiffness of the geogrid reinforcement on the static lateral performance of the geogrid pile foundation system.

Chapter 3 presents the experimental work carried out to investigate the dynamic lateral behavior of the geogrid-reinforced pile foundation system. Chapter 3 explains the methodology employed to construct the elements of the experimental work and the details of the shaking table tests. Then, results of the shaking table tests are presented and discussed, and conclusions are presented.

Chapter 4 presents a finite element model that is established to simulate the dynamic behavior of the geogrid-reinforced pile foundation system. Chapter 4 also include an investigation carried out to study the dynamic lateral behavior of the new foundation system on a prototype scale. Chapter 4 describes the elements of the numerical model and the soil constitutive models used to build the dynamic finite element model. The results derived from Chapter 3 were used to verify this numerical model. In addition, a parametric study is carried out to investigate the effect of the frequency of the base motion and amplitude, and the soil reinforcement stiffness on the dynamic lateral performance of the geogrid pile foundation system. Finally, a parallel seismic parametric study was carried out to investigate the effect of geogrid stiffness and depth on the lateral performance of the geogrid pile foundation system.

Chapter 5 presents the summary of the thesis and provides recommendations for future research that can be carried out benefiting from the methodology and results of this thesis.

References:

[1] Anastasopoulos, I., Georgarakos, T., Drosos, V., and Kourkoulis R. 2010. Seismic performance of bar-mat reinforced-soil retaining wall: Shaking table testing versus numerical analysis with modified kinematic hardening constitutive model. Soil Dynamics and Earthquake Engineering, **13** ,1089-1105.

[2] Bathurst, R.J.and Alfaro, M.C.1996. Review of seismic design, analysis and performance of geosynthetic rein- forced walls, slopes and embankments. International Symposium on Earth Reinforcement, keynote lecture, Kyushu, 23-52.

[3] Bathurst, R.J.and Hatami, K., 1998. Seismic response analysis of a geosynthetic reinforced soil retaining wall. Geosynthetics International, **5** (1–2), 127–166.

[4] Brinkgreve, R., Egin, E. and Swolfs, W. User's Manual for Plaxis 3D 2012 , Delft University of Technology & PLAXIS bv, The Netherlands.

[5] Collin, J. G., Chouery-Curtis, V. E., and Berg, R. R. 1992. Field observations of reinforced soil structures under seismic loading. Proceedings of the International. Symposium on Earth Reinforcement practice, H. Ochiai, N. Yasufuku, and K. Omine, eds., Vol. 1, Balkema, Rotterdam, The Netherlands, 223–228.

[6] Cai, Z. and Bathurst, R.J. 1995. Seismic response analysis of geosynthetic reinforced soil segmental retaining walls by finite element method. Computers and Geotechnics, **17** (4), 523-546.

[7] El-Emam, M.M. and Bathurst, R.J. 2007. Influence of reinforcement parameters on the seismic response of reduced-scale reinforced soil retaining walls. Geotextiles and Geomembranes, **25** (1), 33-49.

[8] Eliahu, U. and Watt, S. 1991. Geogrid-reinforced wall withstands earthquake. Geotechnical Fabrics Report, **9** (2), 8–13.

[9] El Naggar, M.H., 1998. Interpretation of Lateral Statnamic Load Test Results. Geotechnical Testing Journal, ASTM, Vol. 21, No. 3, pp. 169-179.

[10] El Naggar, M.H. and Novak M. 1996. Influence of foundation nonlinearity on offshore towers response. Journal of Geotechnical Engineering, **122** (9), 717-721.

[11] El Naggar, M.H. and Bentley, K.J. 2000. Dynamic analysis for laterally loaded piles and dynamic p-y curves. Canadian Geotechnical Journal, **37** (6), 1166-1183.

[12] El Naggar, M.H., Shayanfar, A.S., Kimiaei, M. and Aghakouchak, A.A. 2005. Simplified BNWF model for nonlinear seismic response analysis of offshore piles with nonlinear input ground motion analysis. Canadian Geotechnical Journal. **42** (2), 365-380.

[13] Fakharian, K. and Attar, I.H. 2007. Static and seismic numerical modeling of geosynthetic-reinforced soil segmental bridge abutments. Geosynthetics International, **14** (4), 228-243.

[14] Han, J. and Gabr M. A. 2002. Numerical Analysis of Geosynthetic-Reinforced and Pile-Supported Earth Platforms over Soft Soil. Journal of Geotechnical and Geoenvironmental Engineering, **128** (1), 44-53.

[15] Helwany, S.M.B., Budhu, M., McCallen, D. 2001. Seismic analysis of segmental retaining walls. I: Model verification. Journal of Geotechnical and Geoenvironmental Engineering, **127** (9), 741-749.

[16] Holtz, R. D., Christorpher, B, R., and Berg, R. R., Geosynthetic Engineering 1st ed, BiTech Publishers Ltd, BC, Canada.

[17] Koerner, R. M., 2005, Designing With Geosynthetics 4th ed, Pearson Education Ltd., New Jersey, USA.

[18] Ling, H.I., Liu, H.B., Mohri, Y., and Kawabata, T. 2001. A Bounding Surface Model for Goegrid. Journal of Engineering Mechanics, ASCE, **127** (9), 963-967.

[19] Liu, H. 2009 .Analyzing the reinforcement loads of geosynthetic-reinforced soil walls subject to seismic loading during the service life. Journal of Performance of Constructed Facilities, **23** (5), pp. 292-302.

[20] Liu, H.L., Ng, C.W.W., and Fei, K. 2007. Performance of a geogrid-reinforced and pile-supported highway embankment over soft clay: Case study, Journal of Geotechnical and Geoenvironmental Engineering, **133** (12), pp. 1483-1493.

[21] Nishimura, J., Hirai, T., Iwasaki, K., Saito, Y., and Morikshima, M. 1996. ‘‘Earthquake resistance of geogrid reinforced soil walls based on a study conducted following the southern Hyogo earthquake.’’ Proceedings., International. Symposium. on Earth Reinforcement Practice ., IS-Kyushu ’96, Earth Reinforcement Practice., H. Ochiai, N. Yasufuku, and K. Omine, eds., Balkema, Rotterdam, The Netherlands.

[22] Sandri, D. 1997. A performance summary of reinforced soil structures in the greater Los Angeles area after the Northridge earthquake, Geotextiles and Geomembranes, **15** (4-6), pp. 235-253

[23] White, D. M., and Holtz, R. D. (1996). ‘‘Performance of geosynthetic reinforced slopes and walls during the Northridge, California earthquake of January 17, 1994.’’ Proceedings. International. Symposium. on Earth Reinforcement Practice., IS-Kyushu ’96, Earth Reinforcement Practice., H. Ochiai, N. Yasufuku, and K. Omine, eds., Balkema, Rotterdam, The Netherlands,Vol. 2, 965–972.

Chapter 2

2. EXPERIMENTAL AND NUMERICAL STUDY ON LATERAL BEHAVIOR OF MODEL GEOSYNTHETIC-REINFORCED PILE-FOUNDATION SYSTEMS SUBJECTED TO STATIC HORIZONTAL LOADING

This chapter introduces an innovative use of polymer strips as part of a novel foundation concept, polymer strips reinforced pile foundation system, where polymer strips are used to enhance the lateral static resistance of the pile foundation system. The lateral static behavior of this foundation system was evaluated using a series of reduced scale physical model test performed on the model foundation installed in different soil beds contained in a small size soil container. These soil beds included: a soil bed representing the base case (soft clay overlying sand layer); a soil model representing the conventional ground replacement solution (the glyben layer sandwiched between an aggregate layer from top and a sand layer from bottom) and a soil model representing the proposed novel geosynthetic-reinforced backfill (the glyben layer sandwiched between a geosynthetic-reinforced aggregate layer from top and a sand layer from bottom).

A one directional loading system was attached to the soil container containing a three layer model soil deposit, which included a layer of synthetic clay (Modified Glyben) sandwiched between a lower and a surficial granular layers, was used. The model pile-cap system was installed through the surficial granular layer, which was reinforced using a microgrid mesh and underlying clay and sand layers. A series of lateral static pull tests have been conducted to investigate the influence of the polymer strips reinforcement on the foundation system behavior. This study also presents the results of a 3D finite element model calibrated against the physical test results. The experimental results and numerical analyses showed that the lateral resistance of a pile cap system was enhanced by the microgrid mesh embedded in the surficial granular layer. The results also showed

that the lateral resistance of the pile cap system was significantly influenced by the thickness of engineered backfill.

2.1 Introduction

Piles are used to transfer vertical and lateral loads to competent soil layers along the pile shaft and at its toe. Pile foundations are designed to provide a certain level of lateral resistance while maintaining the lateral deformation within limits required by the structural engineer. Examples of structures that are required to resist significant lateral loads include (i) high rise buildings subjected to wind and/or earthquake loads, (ii) marine structures subjected to horizontal forces due to the impact of vessels during mooring and wave action, (iii) offshore structures subjected to wind and wave loads. Pile foundations designed based on the serviceability limit offers a more cogent approach because it accounts for the displacement limit of the structure (Zhang, 2009).

A significant number of full scale lateral pile load tests have been performed in accordance with well-established standard procedures (e.g. ASTM D3966, ASTM D7383). However, only a limited number of experimental studies using reduced scale models were conducted to examine the static lateral behavior of piles. For example, Maymand (1998) applied incremental lateral static loads on single model piles and 3X3 model pile group and recorded the pile cap deflection and pile bending moments. Matsumoto (2004) executed a series of static horizontal load tests on a model piled raft in 1-g field. His research considered two variables: the height of the pulling force; and the rigidity of the pile head connection.

Numerous analytical studies were also performed. Kimura et al. (1995) performed 3D elasto-plastic finite element analysis to study the ultimate lateral behavior of pile groups in layered soil. The soil's constitutive behaviour was modeled using a Druker-Prager Model and the piles were modeled using nonlinear beam elements. Wakai et al. (1999) also used 3D elasto-plastic finite element analysis to simulate a number of model tests of free and rigid head pile groups subjected to lateral loading in homogeneous soil profiles. Zhang et al. (1999) developed a finite element code that implemented p-y curves (Reese

et al., 1974), Brown's p-multiplier approach (Brown et al., 1998) and the p-multiplier factors proposed by McVay et al. (1998) to predict the response of laterally loaded pile groups. Yang and Jeremic (2002) investigated the pile behavior under lateral loads in layered elasto-plastic soils and demonstrated good agreement between the numerical and experimental results.

Several researchers investigated the use of geosynthetics with geotechnical structures. Piles and geogrids were used together as part of a hybrid system, denoted as the geogrid reinforced and pile-supported (GRPS), to limit total and differential settlements observed in embankments (Liu et al., 2007). Several researchers investigated the (GRPS) system (e.g. Maddison et al., 1996; Han and Akins, 2002; Han and Gabr, 2002; and Liu et al., 2007) and demonstrated its advantages with regard to improving stability of embankments and reducing their settlements. On the other hand, Bathurst and Alfaro (1996), Zhenqi and Bathurst (1995), Sandri (1997), EL-Emam and Bathurst (2004) conducted experimental and numerical studies and showed that the geogrid reinforcement improved the seismic behaviour of earth retaining structures. This is attributed to the increased shear resistance due to the friction and interlocking mechanisms at the soil-reinforcement interfaces. These studies collectively demonstrate the utility of geosynthetics to improving the static and seismic lateral performance of geotechnical structures.

In this study, experimental and numerical investigations were conducted to evaluate the enhancement of the lateral performance of pile foundations reinforced using polymer strips. The physical model of the polymer strips reinforced pile foundation system comprised a model pile group that included 4 piles rigidly connected to a rigid pile cap. The model pile group was installed in a multi-layer soil deposit that included a cohesive layer underlain by a sand layer. The model soil bed included a granular top layer representing engineered granular material typically used to replace weak surficial cohesive soils. The cohesive soil layer was modeled using synthetic clay, Modified Glyben, which consists of bentonite mixed with water and glycerin. A microgrid mesh was embedded within the top granular fill layer and connected to the piles to evaluate the

static performance of a polymer strips-reinforced pile foundation system. The pile cap was loaded laterally using a pulling mechanism and fixed on the soil container. The results of the static tests were used to calibrate/verify finite element model constructed using commercial finite element software Plaxis 3D. The calibrated/verified model was used for further parametric analyses in order to investigate various aspects of interaction between the foundation, soil and polymer strips.

2.2 Background

Reduced scale model tests offer the advantage of studying the response of pile-soil-superstructure systems in a controlled environment. If they carried out properly, scaled model tests are also advantageous in seismic studies because they are able to give economic and realistic information about ground amplification, pore water pressure variations, non-linear soil behavior and soil structure interaction. Also, reduced scale model tests offer an economical alternative for full scale tests to run parametric studies (Turan et al., 2008). Rocha (1957) pioneered developing scale model similitude relationships for soil mechanics problems. The stress-strain behavior of soils was scaled assuming that they are linearly proportional in models and prototypes. Rocha's linear scaling concept was set to account for the changes in the stress system present in a 1-g environment. Iai (1989) continued Rocha's research and derived similitude relationships assuming that the constitutive stress-strain relationship was independent of the confining stress if a proper scaling factor is used. Iai (1989) validated this assumption using plane strain compression tests under varying confining stresses. He derived his similitude relations based on the geometric and density scaling factors, (λ) and (λP), respectively. Meymand (1998) successfully used this modeling approach to study soil, pile and superstructure interaction in a 1-g environment. The present study followed the same modeling approach. Table 2-1 shows the scaling relations for the variables contributing to the primary modes of system response.

Table 2-1: Scaling relationships for primary system variables (Meymand, 1998).

Parameter	Scaling factor	Parameter	Scaling factor	Parameter	Scaling factor
Length	λ	Acceleration	1	Mass density	1
Force	λ^3	Shear wave velocity	$\lambda^{1/2}$	Stress	λ
Stiffness	λ^2	Time	$\lambda^{1/2}$	Strain	1
Modulus	λ	Frequency	$\lambda^{-1/2}$	EI	λ^5

* λ: geometric scaling factor

2.3 Methodology

2.3.1 Model soil

The model soil stratigraphy comprised three layers of soils: i) a layer of silty sand overlain by, ii) a layer of synthetic clay (modified glyben) to represent the cohesive soil layer and iii) a surfacial layer of engineered granular backfill. The bottom granular layer was modeled using the fine granular material with a grain size distribution depicted in Figure 2-1. The overlying cohesive layer was modeled using Modified Glyben. Modified Glyben provides favorable characteristics for scaled physical model tests. The primary advantages of modified glyben for reduced scale model tests are: i) it consolidates at a very slow rate after application of confining pressure, and thus it can be used in 1-g and N-g tests without observing a consolidation stage; ii) it resists desiccation due to drying, and iii) its mechanical properties do not significantly change with time, which facilitates the multiple use in physical tests (Turan et al. 2009a). The laboratory results showed that

modified glyben have a normalized shear modulus versus shear strain amplitude response that is independent on the confining stress, and glycerin to water ratio (Turan et al. 2008). The modified glyben was prepared by mixing bentonite with glycerin and water. The fluid to dry bentonite ratio was 85% and the water to glycerine ratio was 50%. These ratios were chosen to simulate prototype soft clay. Hand vane shear tests (Pilcon) were used to measure the undrained shear strength of modified glyben mixture after preparation and placement in soil container. After a light compaction, one drop of a sliding hummer, the undrained shear strength of the model clay was about 19 kPa at the bottom of the clay layer and 8 kPa near the top with a density of 1406 kg/m^3. The surficial granular layer used to model engineered granular fill had an average particle size of 5 mm.

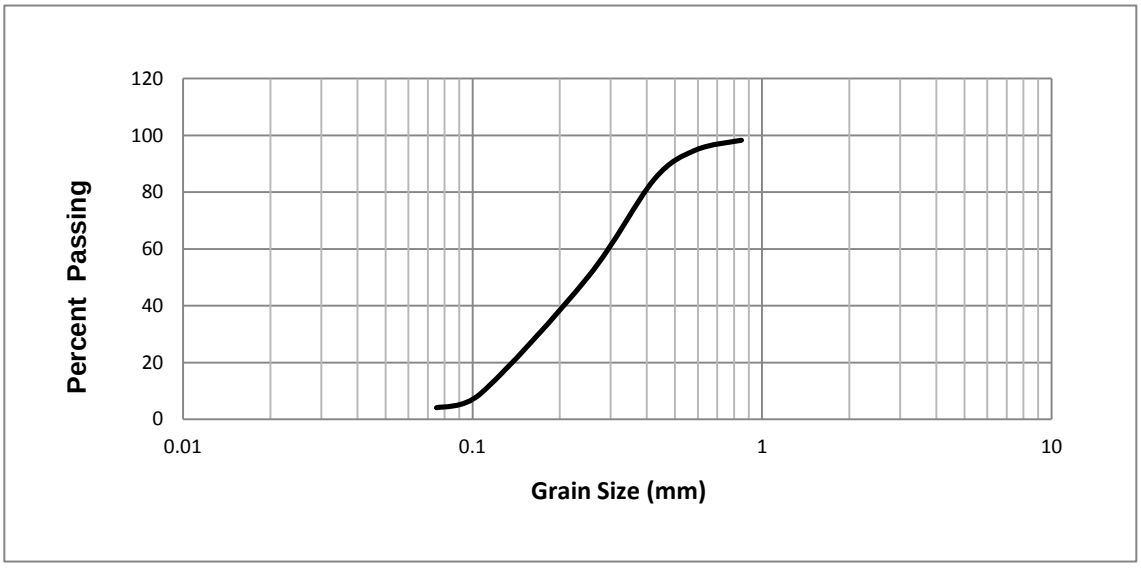

Figure 2-1: Construction sand gradation

2.3.2 Soil parameters

The geotechnical parameters of the three soil layers are summarized in this section. The strength properties of soils were obtained from direct shear tests and hand vane apparatus. In the absence of any stiffness measurements, the static soil stiffness was

estimated using empirical correlations for granular layers. The static soil stiffness for granular layers were estimated from the following relations derived by Vermeer and Schanz (1998) that estimated the Young's soil modulus based on the confining stress, i.e.:

$$\frac{E_{50}}{P^{ref}} \approx 150\sqrt{\frac{\sigma'_x}{P^{ref}}} \qquad \text{loose or silty sand} \qquad [1]$$

$$\frac{E_{50}}{P^{ref}} \approx 500\sqrt{\frac{\sigma'_x}{P^{ref}}} \qquad \text{dense and clean sand} \qquad [2]$$

Where σ_x is the confining stress, P^{ref} =100 kPa, $E \approx E_{50}$.; and shear modulus G = E/(2(1+ν) and ν is Poisson's ratio.

The elastic modulus values for the aggregate (surficial layer) and sand (bottom layer) used in the tests were derived from Equations 1 and 2, i.e.:

$$E_{aggregate} = 50000\sqrt{\frac{\sigma'_x}{P^{ref}}} \qquad [3]$$

$$E_{sand} = 40000\sqrt{\frac{\sigma'_x}{P^{ref}}} \qquad [4]$$

The elastic modulus values of aggregate and sand were evaluated from Equations 3 and 4 considering the low confinement stresses at the mid depth of each granular layer. For the cohesive layer comprising of modified glyben, the stiffness was estimated based on the correlation shown in equation [5] and presented in Turan et al. (2009a). The shear wave velocity (V_s) of the glyben layer was estimated based on the undrained shear strength determined using the hand (lab) vane apparatus and (V_s) value was estimated using the undrained shear strength (c_u) of glyben using the empirical equation given below.

$$V_s = 26.52\ \mathrm{Ln}\ (c_u) - 33 \qquad [5]$$

The dynamic shear modulus of the glyben is calculated as:

$$G_{max} = \rho V_s^2 \quad [6]$$

Where ρ is soil density = unit weight/gravity acceleration.

The calibrated finite element numerical model showed that some of the clay elements was deformed by the applied lateral load up to a shear strain level amounted to 0.1 %. This level of shear strain corresponds to 60 % G/G_{max} taken from the glyben degradation curve (Turan et al. 2009a). Therefore, the static shear modulus of glyben, G_{static}, was assumed to be 60 % of the dynamic shear modulus obtained from an average clay Vs of 36 m/s. Also, the measured undrained shear strength (using lab shear vane) of glyben near the backfill interface was less than that at the bottom by around 56 % due to the overburden stress buildup. Therefore, a layer of weak clay was induced near the backfill surface, which has been replaced with strong granular layer when the depth of backfill was increased. The structure-glyben interface strength was assumed in the analysis to be 10 % of the glyben strength due to using a smooth cap and acrylic piles. Table 2.2 shows the soil parameters used in the numerical analysis.

Table 2-2 : Soil parameters

	Aggregate	Glyben	Sand
Unit weight, (kN/m^3)	16.1	13.8	17.35
C (kPa)	0	10	0
ϕ_{peak} (degrees)	50	0	40

(Appendix A)			
G_{static} (kPa)	1194	1093	3222
Poisson's ratio, ν	0.15	0.2	0.3

The model foundation system

The reduced scale model foundation comprised four 600 mm long and 19 mm diameter acrylic tubes. These model piles were rigidly connected to an aluminum cap with 200 mm X 200 mm plan dimensions and 6 mm thickness which correspond to a concrete cap of 0.7 m thickness. Four plastic rings were fabricated and clamped on the piles to facilitate the load transfer between the microgrid and the piles. The microgrid mesh was extended and pressed inside two halves of rings using four steel bolts. The rings were fixed in their vertical position using a plastic bolt. Figure 2-2 shows the details of the foundation model. Table 2-3 provides a summary of the scaled model corresponding prototype dimensions evaluated using the scaling relationships presented in Table 2-1.

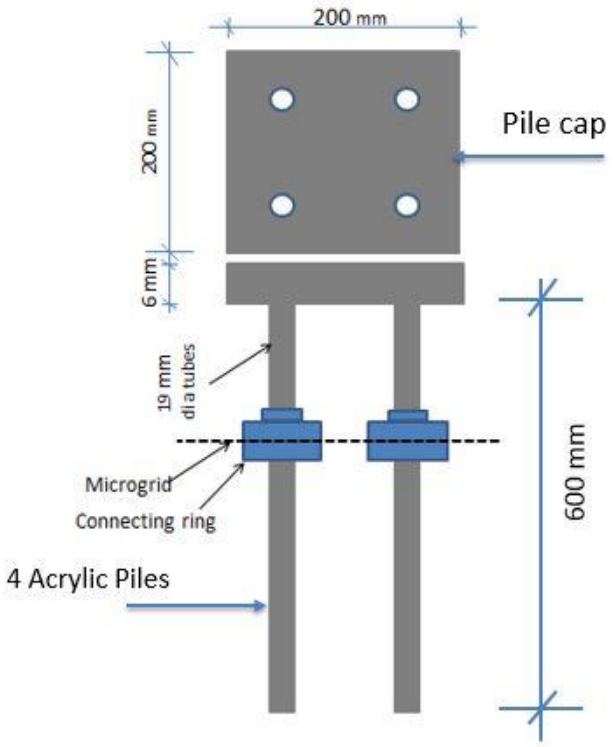

Figure 2-2: The scaled piled cap geogrid model

Table 2-3: Model Piles calculations, λ = 20.

Parameter	Model pile (Acrylic)	Calculated Prototype pile (Steel)
Outer diameter (mm)	19	380
Length (mm)	600	12000
Young's modulus (kPa)	3.2×10^6	200×10^6
Flexural rigidity, E_pI (kN.m^2)	1.82×10^{-2}	5.81×10^4
Axial rigidity, E_pA (kN)	6.03×10^5	3.5×10^6

2.3.3 The Model geogrid

The microgrid mesh was introduced within the aggregate layer at a depth of 3.5 times the pile diameter (i.e 66 mm). The geosynthetic mesh used in the model tests was a bi-axial knitted Microgrid manufactured by STRATAGRID. STRATAGRID Microgrid is manufactured utilizing a complex knitting process and polymer coatings to provide desired engineering properties and constructed of high molecular weight and high tenacity polyester yarns. The yarns provide significant tensile capacity through precision knitting into a dimensionally firm, uniform network of apertures. The model stiffness value of the microgrid at 2% was J_m = 110 kN/m. With a geometrical scale factor $\lambda = 20$, the prototype stiffness $J_p = J_m \lambda^2 = 110 \times 20^2 = 44000$ kN/m (El Emam and Bathurst, 2004). Table 2-4 shows the main engineering properties of the STRATAGRID microgrid. STRATAGRID microgrid was considered as model size polymer strips in this study.

Table 2-4: Engineering properties of Microgrid geogrid

Index Properties	Test Method	Value
Ultimate Strength	ASTM D-6637 Method A	29.2 kN/m
Creep Limited Strength	ASTM D-5262/D-6992	16.8 kN/m
Strength @ 2% Strain	ASTM D4595	2.2 kN/m
Strength @ 5% Strain	ASTM D4595 (MD)	7.3 kN/m
Strength @ 5% Strain ASTM	ASTM D4595 (CMD)	4.4 kN/m
Aperture Size	Measured	2.54 x 6.35 mm

2.3.4 Model Stratigraphy

The testing program was commenced by assembling the soil container (Turan et al. 2009b). A wood board covered with fine steel grits was then bolted to the bottom of soil container. The steel grits was glued to the wood board using epoxy and installed on the bottom of container. Prior to soil placement, the sides of the soil container were covered with latex membrane to prevent soil particles from migrating out of the soil container through the openings between the lamina. The initial granular layer of the model soil was placed inside the container in lifts of 20 mm. Each lift of sand was compacted by tamping until an 80 % relative density had been achieved. Subsequently, the pile-cap system was installed. To eliminate excessive settlement during the testing program, the lumped mass representing the superstructure was placed and maintained on the cap for 24 hours to expedite the piles immediate settlement. Subsequently, sand backfilling proceeded in lifts until a total layer thickness of 36 cm was reached.

Blocks of soft modified glyben were prepared by pressing weighed quantities into a small box with dimensions of 70x70x50 mm. These blocks were then placed over the sand layer, positioned side by side and compacted using a drop hammer until the target total layer thickness was reached. Each layer of clay had 40 mm thickness. Figure 3 depicts the compaction process of modified glyben. Subsequently, a granular layer was placed on top of the modified glyben layer to simulate a situation where the soft cohesive layer is over-excavated and replaced with engineered granular fill. The details of placement of this layer are presented in the following subsection. In field applications, when soft cohesive soils exist at or near the ground surface, the soft clay is typically excavated and replaced with engineered backfill.

Figure 2-3: Compaction of modified glyben

2.3.5 Placement of geogrid-reinforced engineered granular fill

The granular layer was placed on top of cohesive soil layer to represent typical excavation and replacement with engineered granular fill. This is a common practice where shallow layers of compressible soils are encountered. Once the granular soil was placed in lifts, the microgrid mesh was laid within the granular layer at the specified depth. The mesh was connected to four model piles using the clamps (rings). To measure the global microgrid extension during the static pull test, two thin wires were hocked on two 50 mm diameter smooth metal discs extending out of the soil container towards two wire position sensors. The discs were glued at the surface of the microgrid and aligned at the two centerlines of the 2x2 pile group. The two discs were attached at 55 and 300 mm

from the face of the microgrid ring to examine the strain behavior of the microgrid mesh near and far from the pile face (see Figure 2-4).

Figure 2-4: Geogrid extending between the ring and the metal disc

2.3.6 Loading System and Instrumentation

The horizontal static load was applied to the pile cap directly through a tension wire connected to a pulling mechanism which was fixed at the side of soil container. The pulling mechanism comprised of a hand-operated winch and rollers that allow the cable to run smoothly and horizontally to the pile cap top (Figure 2-5 a and b).

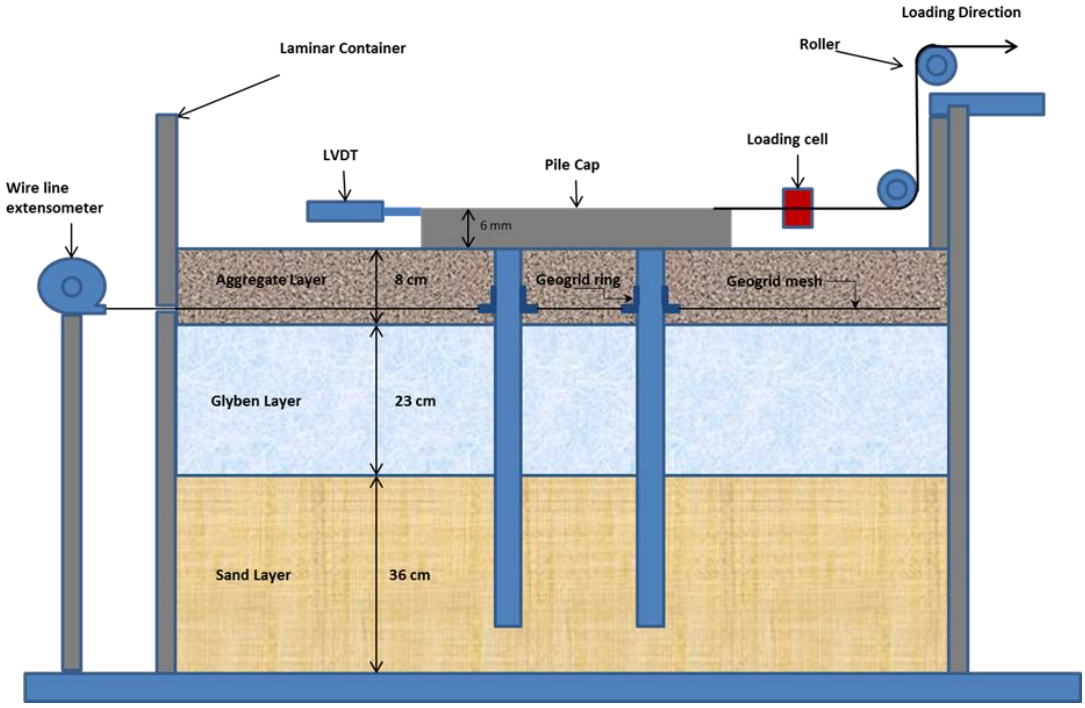
Loading Direction
Laminar Container
Roller
LVDT
Loading cell
Pile Cap
Wire line
extensometer
6 mm
Aggregate Layer
8 cm
Geogrid ring
Geogrid mesh
Glyben Layer
23 cm
Sand Layer
36 cm

(a)

(b)

Figure 2-5: a. Schematic diagram of the testing setup, b. top view of the testing setup.

The pull load applied to the pile cap was measured using an OMEGA 500 N load cell connected to the pulling wire. The pile cap horizontal translation was measured using a 25 mm linear variable displacement transducer (LVDT) made by Hoskin Scientific Ltd. The LVDT sensor has a measuring range of 25 mm with a sensitivity of 7.3/7.5 mv/v. Figures 5a and b show the LVDT and the load cell, which were used to record displacements and loads while the pile cap was being pulled slowly. The global strain of the microgrid mesh was measured by two 100 mm range Penny & Giles Draw Wire Position Sensors (Figure 2-6). The Wire Position sensors has a resolution of ± 0.07 mm. The clamps of the wire sensors were tied to two thin wires extending out of the soil container towards the two 50 mm diameter smooth metal discs. The position sensors were mounted on the frame supporting the soil container. The output signals from LVDT, load cell and position sensors were recorded at a computer station that housed the data acquisition system panels and data logging software.

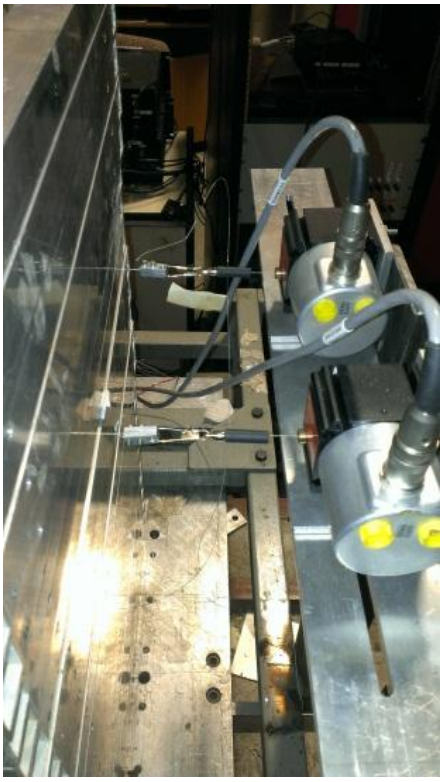

Figure 2-6: The Wire Line Position Sensors mounted on a frame and tied to the wires

2.3.7 Numerical model

The numerical model was established using the commercial finite element software Plaxis 3D. The numerical model comprised ten-node tetrahedron elements to simulate the soil volume, six-node plate elements to simulate the pile cap, shell elements to simulate the microgrid mesh and three-node beam elements to simulate piles. The rings that connected the piles to the microgrid mesh were simulated using larger pile tube elements. Interface elements were used at pile-soil interfaces. Figure 2-7 depicts the three dimensional view of the numerical model.

The pile-soil interfaces were modeled as embedded interface elements having their strength equivalent to a percentage of the adjacent soil shear strength, denoted as Rinterface. The pile-soil interface elements are three nodes elements connecting both sides of pile nodes and soil nodes within the soil's tetrahedron elements. These interface surfaces allow relative movement between piles and soil elements (Brinkgreve et al., 2012). Within the backfill layer, the Pile-Soil $R_{interface}$ strength is assumed to be 90 % of the adjacent soil strength for the total depth of 8 cm to account for minor slippage associated with the relatively small static loading. . In order to simulate the Microgrid/soil interlock at the geogrid mesh level, the geogrid-soil element deformation is assumed continuous along the common edge between geogrid and soil elements.

The constitutive behavior of the soil and interface was modeled using elastic-perfectly plastic stress-strain relationship and Mohr-Coulomb failure criterion. Around the soil volume, general boundary conditions were automatically imposed around the soil volume according to the following rules (Plaxis manual, 2011).

- Vertical model boundaries with their normal in x-direction (i.e. parallel to the yz-plane) are fixed in x-direction (Ux =0) and free in y- and z-direction.
- Vertical model boundaries with their normal in y-direction (i.e parallel to the xz-plane) are fixed in y-direction (Uy =0) and free in x- and z-direction.
- Vertical model boundaries with their normal neither in x- nor in y-direction are fixed in x- and y- direction (Uy =Ux=0) and free in z-direction.
- The model bottom boundary is translational fixed in all directions (Ux=Uy=Uz=0).
- The ground surface is translational free in all directions.

Plaxis allows users to execute the finite element model in phases. The numerical calculations were executed in 18 phases to simulate the geostatic equilibrium, construction sequence as well as incremental application of lateral loads. The pull load was applied on a node at the center of the model pile cap in increments starting from 100 N and increased by 100 N increments at each loading stage until a maximum load of 800

N was reached. Other numerical models that included a microgrid-reinforced granular layer with different microgrid embedment depths were developed and analyzed. The results of these analyses were compared with the results of the base case where no microgrid reinforcement was present.

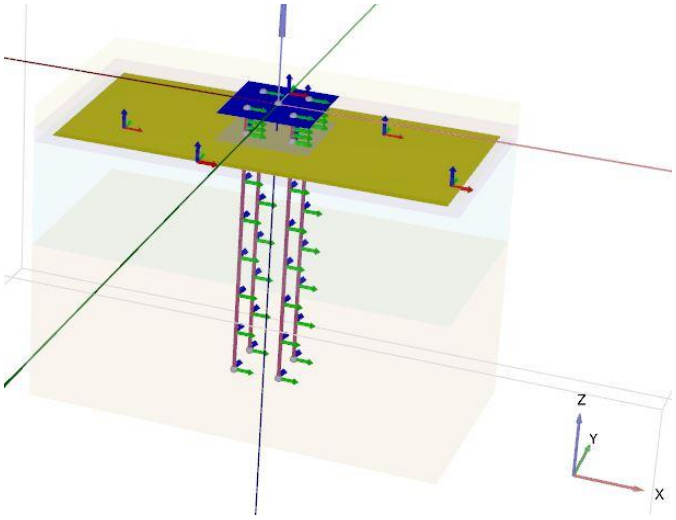

(a)

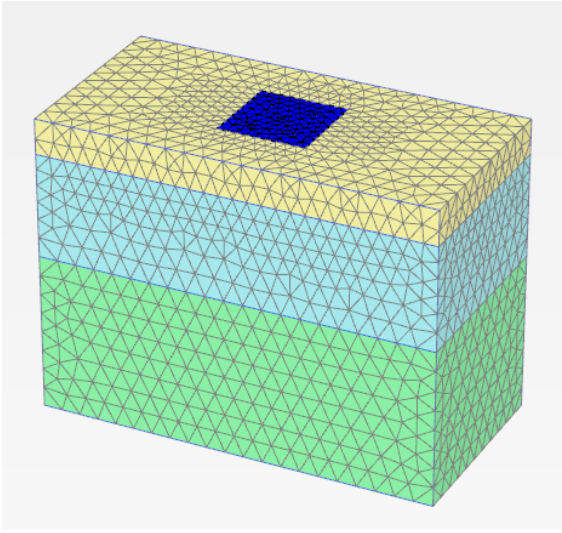

(b)

Figure 2-7: a) Plaxis 3D numerical model of Soil and pile-cap-geogrid system b) Finite element mesh.

2.3.8 Experimental and numerical test cases

Table 2-5 shows the summary of the experimental and numerical test cases. As shown in Table 2-5, three physical modeling cases and their corresponding numerical models were considered and analyzed: (i) foundation with thin and thick engineered backfill with microgrid; (ii) foundation with thin and thick engineered backfill without microgrid; and (iii) the base case of foundation in soft clay without backfill and without microgrid. Table 2-6 provides the thickness of each of the three layers considered in the different test cases.

Table 2-5: Summary of experimental and numerical cases

Test No.	Test case description
1	Static pull test , foundation in deep backfill with Microgrid
2	Static pull test , foundation in deep backfill without Microgrid
3	Static pull test , foundation in shallow backfill without Microgrid
4	Plaxis model of static pull, foundation in deep backfill with Microgrid.
5	Plaxis model of static pull, foundation in deep backfill without Microgrid.
6	Plaxis model of static pull, foundation in shallow backfill without Microgrid.
7	Plaxis model of static pull, foundation in shallow backfill with Microgrid.
8	Plaxis model of static pull, foundation in soft clay without backfill (base case).

Table 2-6 : Thickness of different soil layers considered in different test cases

Test Case No	Surficial backfill layer Thickness (m)	Soft clay layer Thickness (m)	Bottom sand layer Thickness (m)
1,2,4,5	0.08	0.23	0.36
3,6,7	0.03	0.28	0.36
8	0	0.31	0.36

2.4 Results and discussion

The results are presented in terms of the load-displacement response of the model foundation, shear forces and bending moments of the piles as well as strain in the microgrid material. The results from the different cases are compared to evaluate the effects of using the microgrid material on the foundation response and the possibility for reducing the requirements for engineered backfill.

2.4.1 Pile cap translation

The measured load-displacement response curves of the model foundations were compared with the responses simulated using the numerical models and results were depicted in Figures 2.8 and 2.9. Figure 2.8 shows the experimental static pull test results and the numerical simulation of the static test for the deep backfill case with microgrid (Cases 1 and 4). Figure 2.9 shows the experimental and numerical static pull test results for the deep backfill case without the embedment of the microgrid mesh (Cases 2 and 5). The experimental and numerical results shown in Figures 2.8 and 2.9 demonstrate good agreement between the two sets. Comparing the results in Figures 2.8 and 2.9 indicates that the addition of the microgrid mesh increased the lateral stiffness of the foundation and reduced its lateral displacement. For example, a 3 mm displacement was caused by 700 N loads in Case 2, where no microgrid reinforcement was used, while the same

amount of displacement was caused by 800 N when the microgrid reinforcement was applied (Case 1). This indicates about 15 % improvement in lateral resistance.

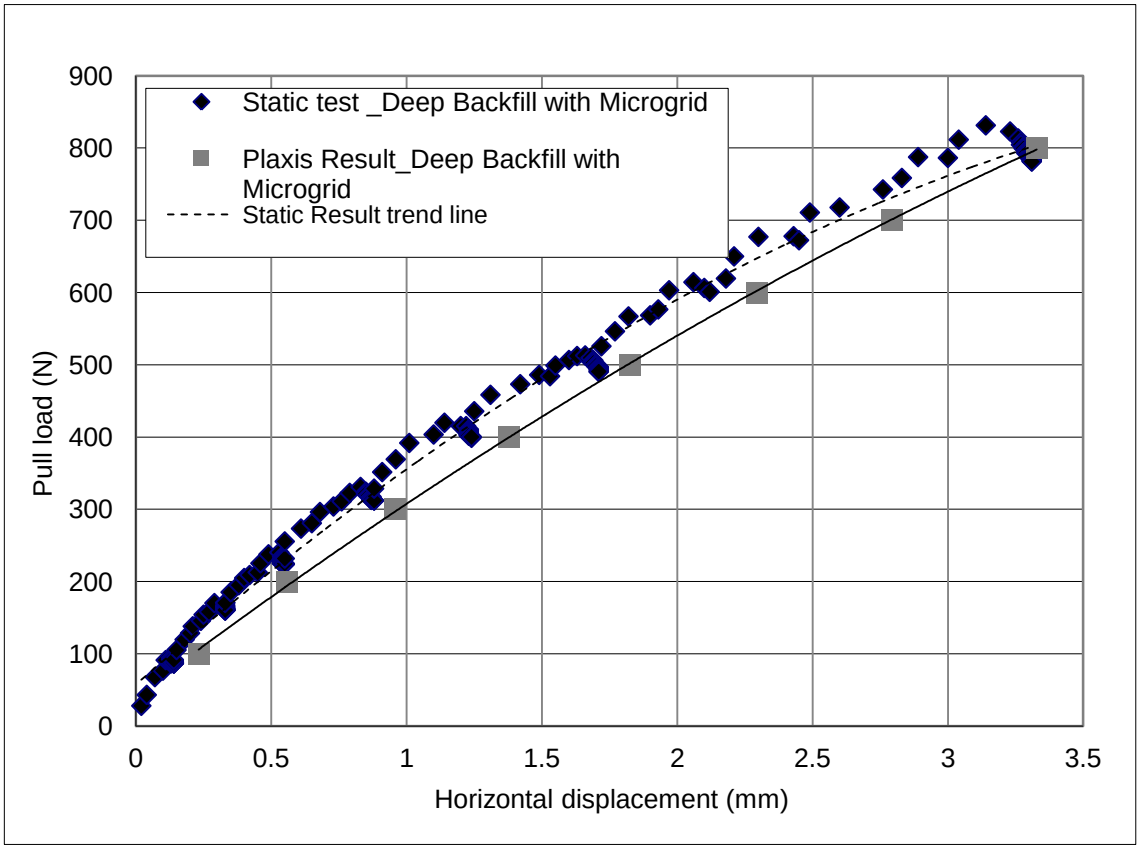

Figure 2-8: Lateral load-displacement response of model foundation and results of numerical simulations (Cases #1 and 4).

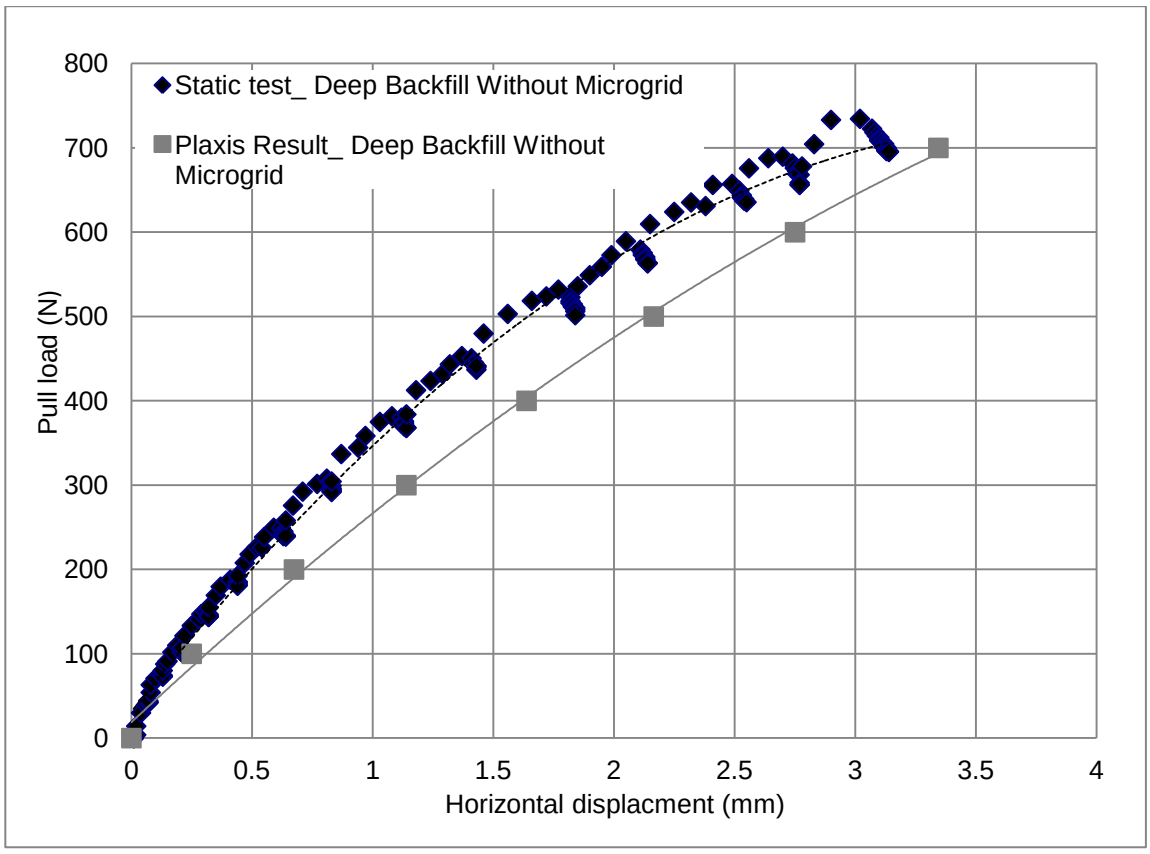

Figure 2-9: Lateral load-displacement response of model foundation and results of numerical simulations (Cases #2 and 5).

Figure 2-10 compares the experimental and numerical results for Cases 3 and 6, where no microgrid was used and a shallow layer of aggregate backfill was considered. Figure 2-10 indicates a good agreement between the experimental and numerical result. Also, the comparison between Case 3 (thin aggregate backfill layer) and Cases 2 (thick aggregate backfill layer) revealed that reducing the backfill layer reduced the lateral stiffness of the pile group and resulted in larger lateral displacement of the pile foundation.

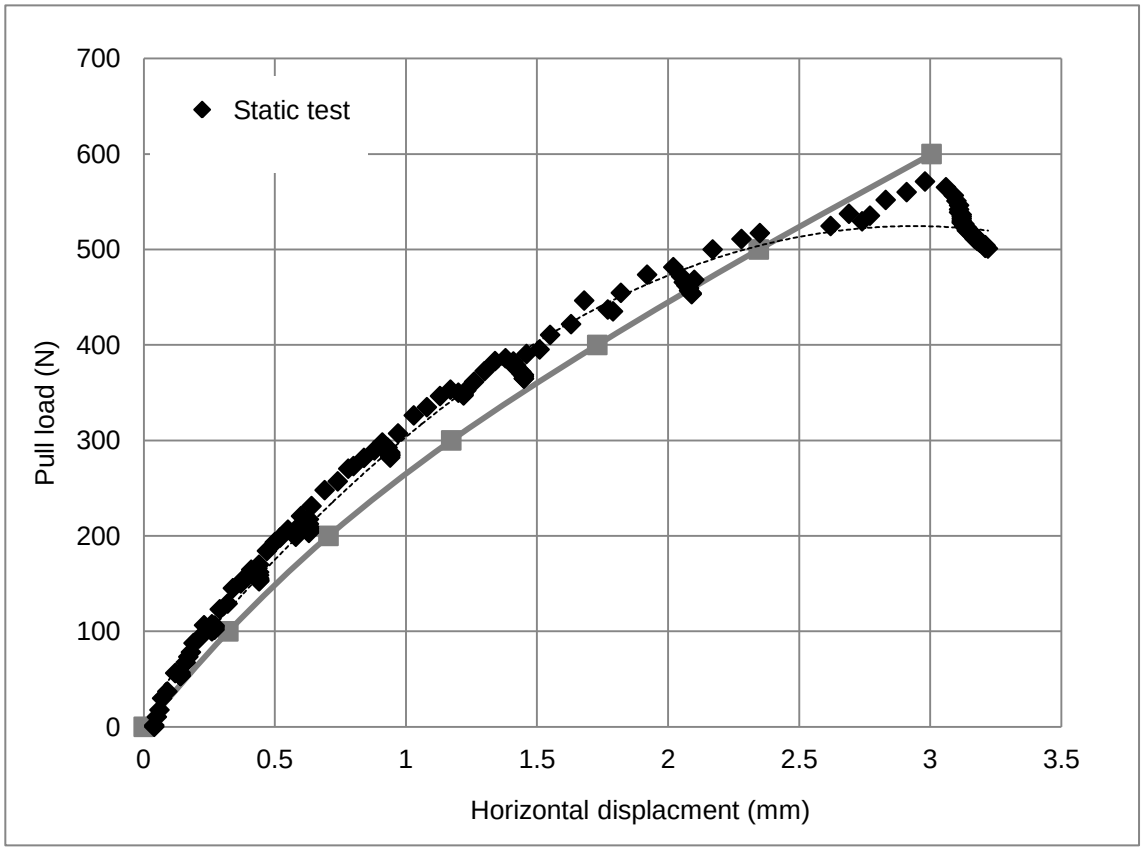

Figure 2-10: Lateral load-displacement response of model foundation and results of numerical simulations (Cases # 3 and 6)

Figure 2-11 compares the experimental Cases 1 to 3. The results indicate that the pile cap foundation resistance to lateral deformation improved by 15 % at 3 mm displacement due to the addition of microgrid. Also, the data trend shows that the resistance of the pile cap foundation system to lateral loading was degraded by 20 % due to reducing the thickness of granular backfill to half.

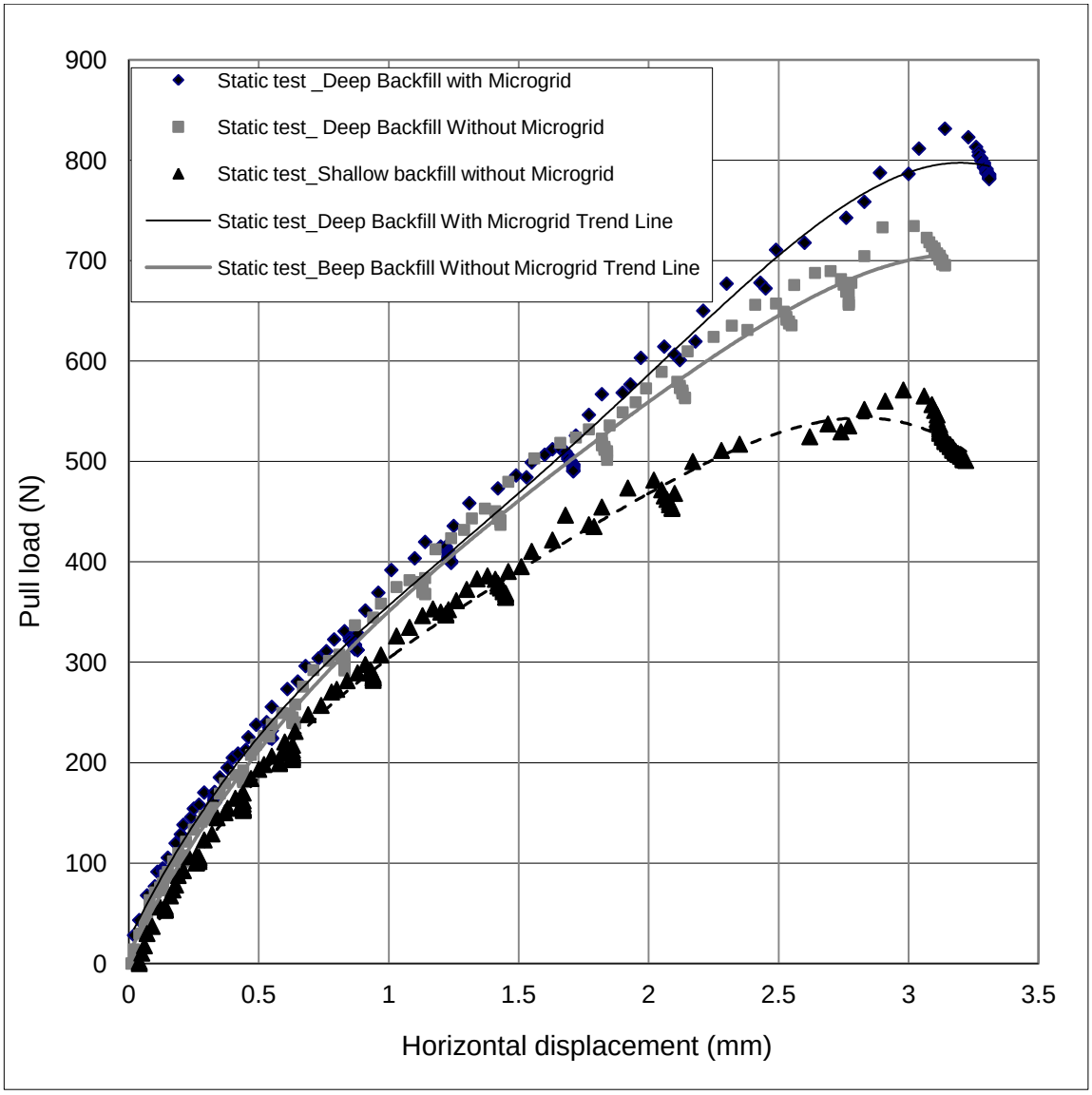

Figure 2-11: experimental results comparison (cases 1-3)

Figure 2-12 compares the results of the numerical analysis for cases 5 to 8. It can be noted from Figures 2-12 that the pile foundation performance has been improved due to increasing the granular backfill. Also, it shows the superiority of the polymer strips solution as the shallow backfill with microgrid resulted in the least lateral displacement. The results show that using the microgrid reinforcement can allow smaller backfill and yet improved response. This can represent an effective solution and significant saving in

cost and construction time in sites where deep backfill be required following conventional ground replacement design.

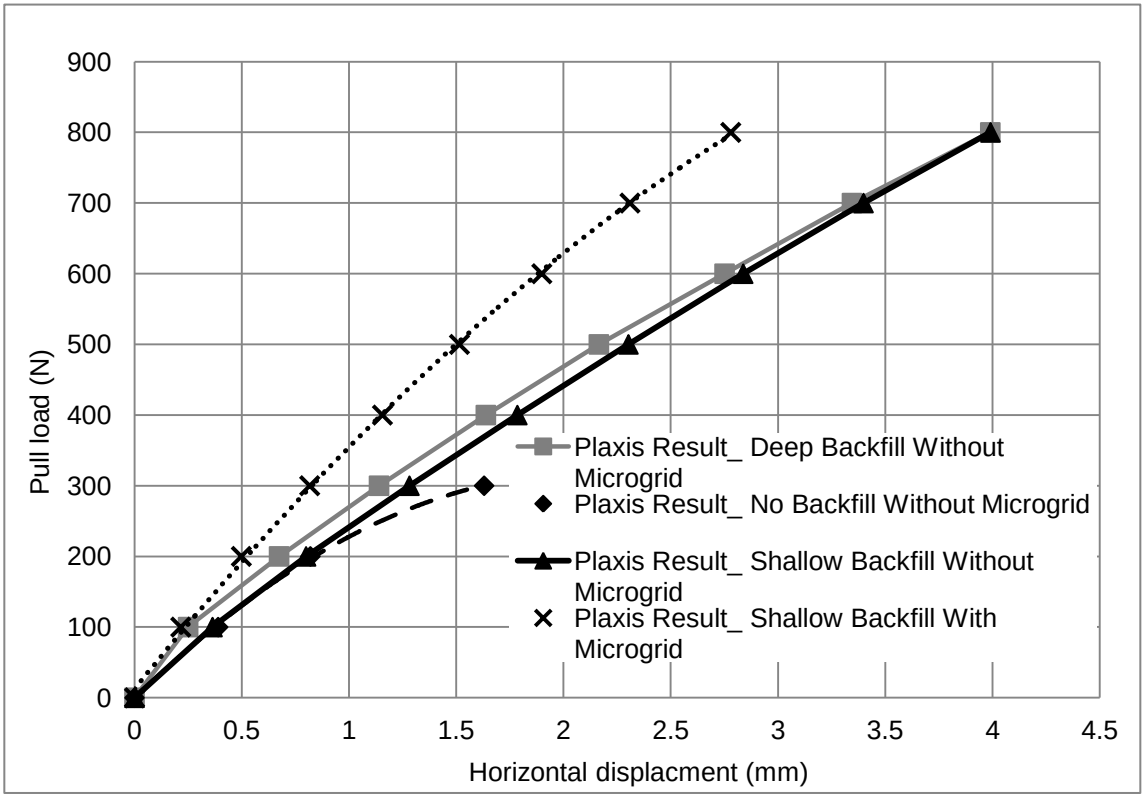

Figure 2-12: Numerical results comparisons (cases 5-8)

2.4.2 Extension of microgrid (in Deep backfill case)

Figure 2-13 shows the measured microgrid extension near the piles during the static pull test. The microgrid lateral deflection, at a distance of 56 mm from the pile ring was subtracted from the pile deflection at the microgrid level to obtain the magnitude of microgrid extension. This value was divided by the microgrid length of interest to obtain the microgrid strain. Figure 2-13 shows the stiffness behavior of the microgrid and indicates an increasing stiffness as a result of increase in deflection (i.e. hyper-elastic stiffness). Figure 2-14 shows the variation of foundation lateral resistance with the microgrid strain far from the piles. It can be noticed from Figure 2-14 that the microgrid strain increases as the pile cap pull load increases. This behavior indicates stiffening in the lateral behavior of the foundation system due to the hyper-elastic behavior of the

microgrid mesh. Thus, it can be expected that with increasing lateral loads, the efficiency of the polymer strips reinforcement will increase. Comparing the results in Figure 2-13 shows that the microgrid strain near the pile (only the first 5 mm) was in the range of 5 to 25%. However, Figure 2-14 shows that the rest of the microgrid mesh experienced strain in the range of 0.5 to 2%. It may be inferred that the average strain for the microgrid mesh up to the maximum load applied was about 2 to 2.5%. Therefore, the strength and stiffness parameters of the microgrid used in the numerical models would be evaluated at 2% strain.

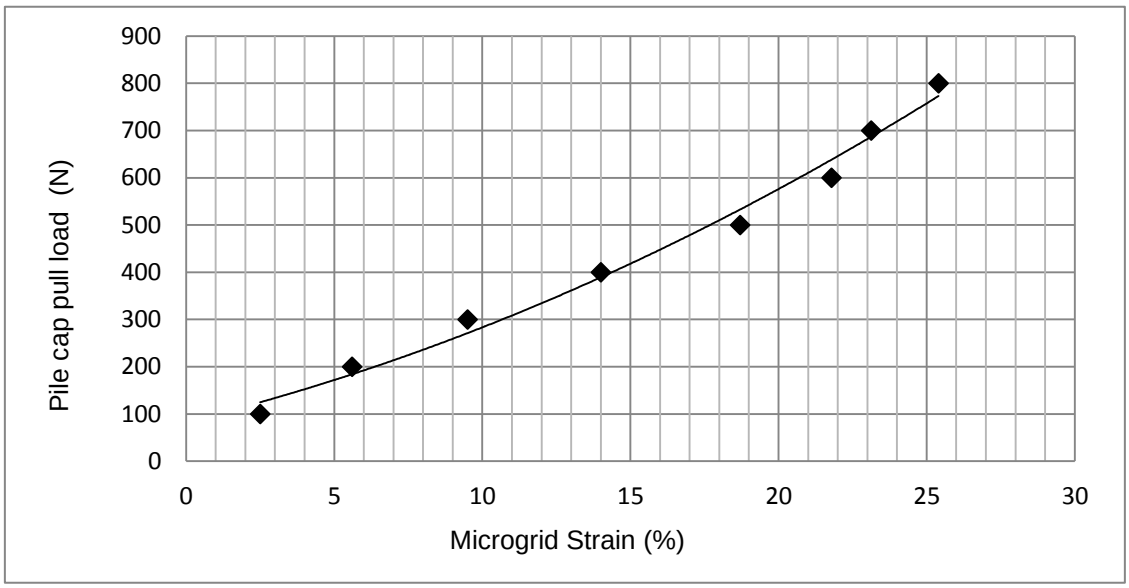

Figure 2-13: Microgrid strain vs. pile cap pull load measured near to the piles face.

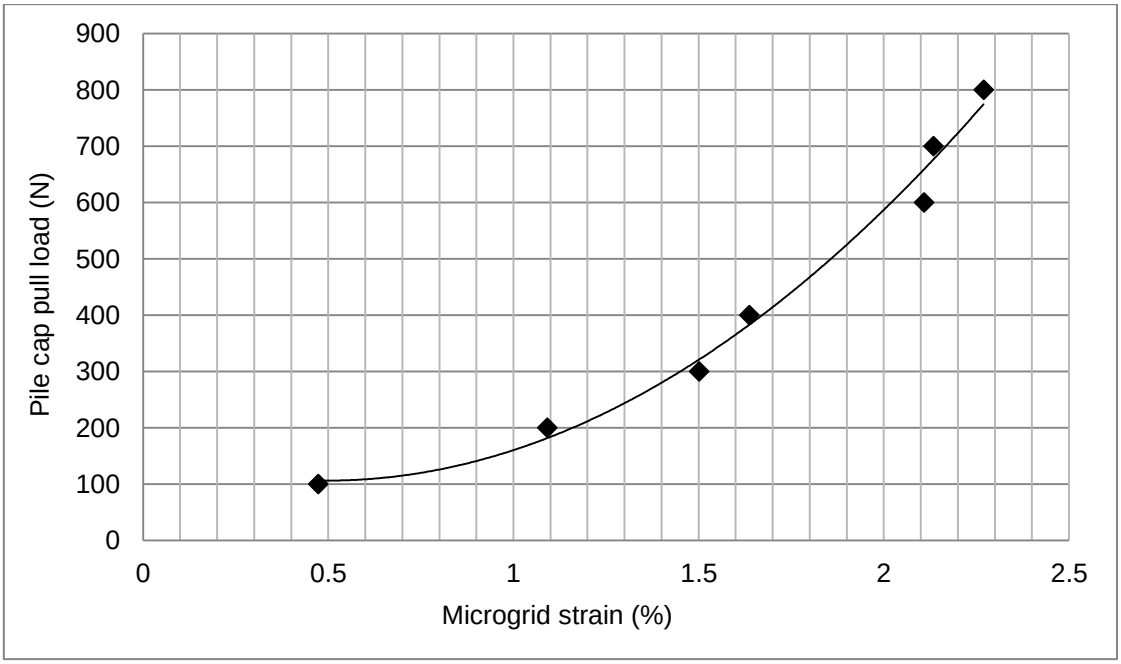

Figure 2-14: Microgrid strain vs. pile cap pull load measured far from the piles face

Figure 2-15 displays the microgrid extension near and far from the piles measured at WIRE1 and WIRE2, respectively. The results show that in the initial loading phase, the microgrid reinforcement was not engaged. However, as the lateral load increased, the microgrid reinforcement was engaged due to the interlocking of the granular material within the microgrid, which increased the shearing resistance of the aggregate in the vicinity of the microgrid. It can also be noticed that the microgrid (and the interlocked aggregates) stiffness increased as the lateral load increased due to further mobilization of the interlocking mechanism. In addition, Figure 15 indicates that the extension that the polymer strips experiences under a given lateral load dissipated along the microgrid mesh away from the foundation.

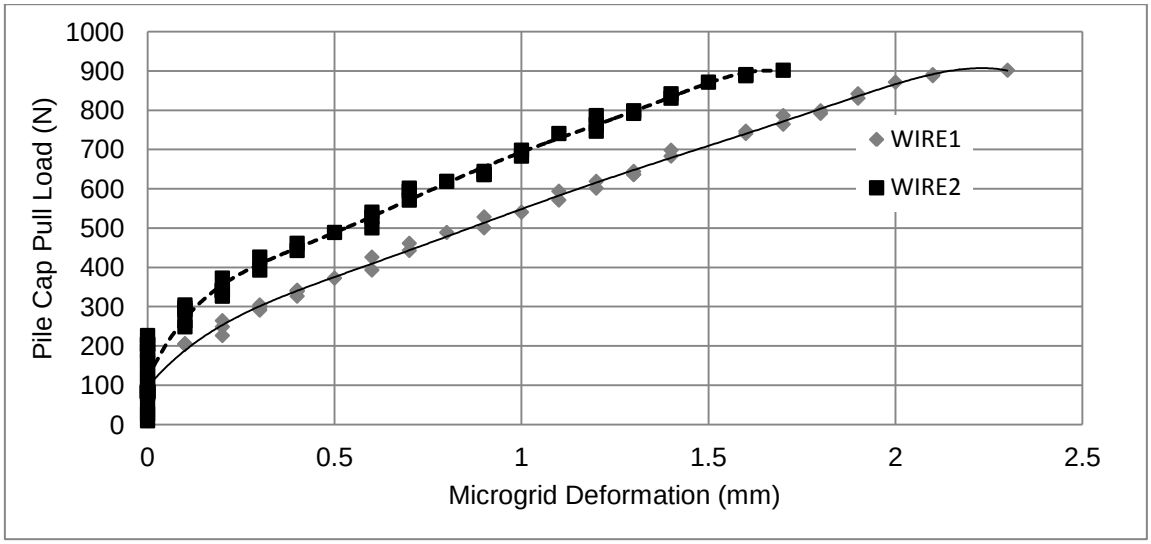

Figure 2-15: Global Microgrid deformation measured near and far from the pile face

2.4.3 Results of Numerical Analysis

The results of the numerical parametric study that was conducted to investigate various aspects of the mechanical interaction between the foundation, soil and microgrid reinforcement are presented in this section.

Bending Moment and Shear Forces and in Piles

The piles section-forces and moments calculated employing the numerical models that were calibrated using the results of the physical tests are presented herein. Figure 2-16 demonstrates the effect of microgrid reinforcement on the maximum bending moment of the piles as the static lateral load increased. It can be noted that the bending moment decreased due to the addition of the microgrid mesh by approximately 8%. However, the reduction in shear force was marginal (only 2%) compared to the reduction in the bending moment as noted from Figure 2-17.

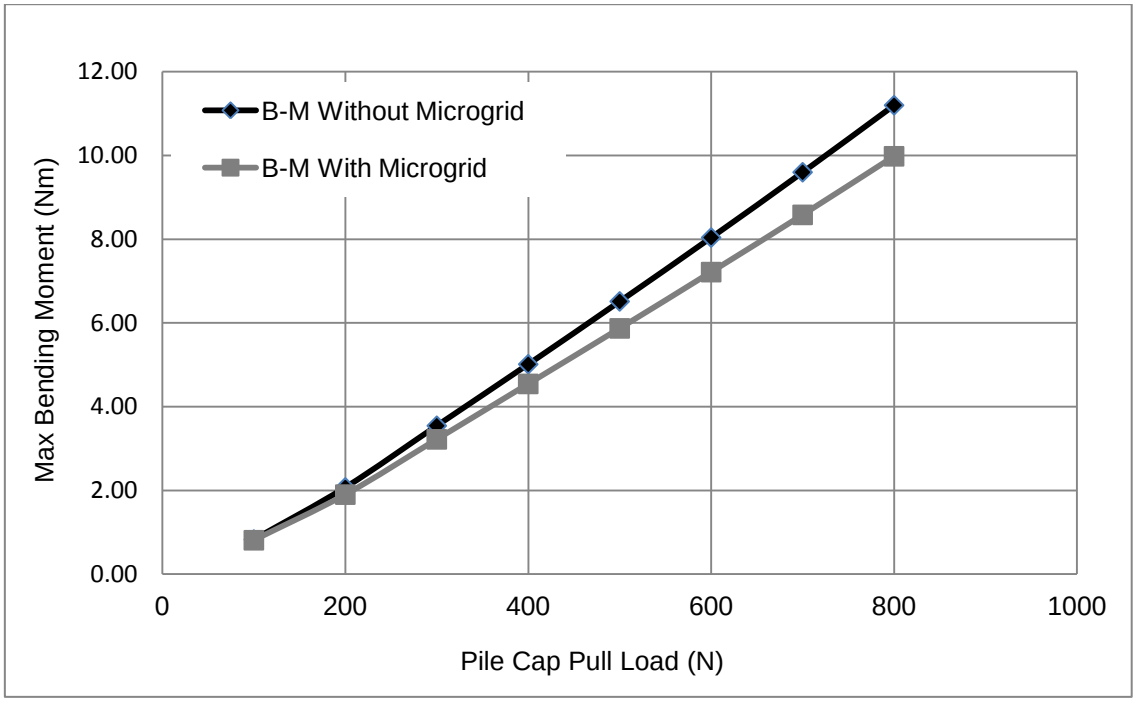

Figure 2-16: Bending moment at pile head vs. pile cap lateral deflection

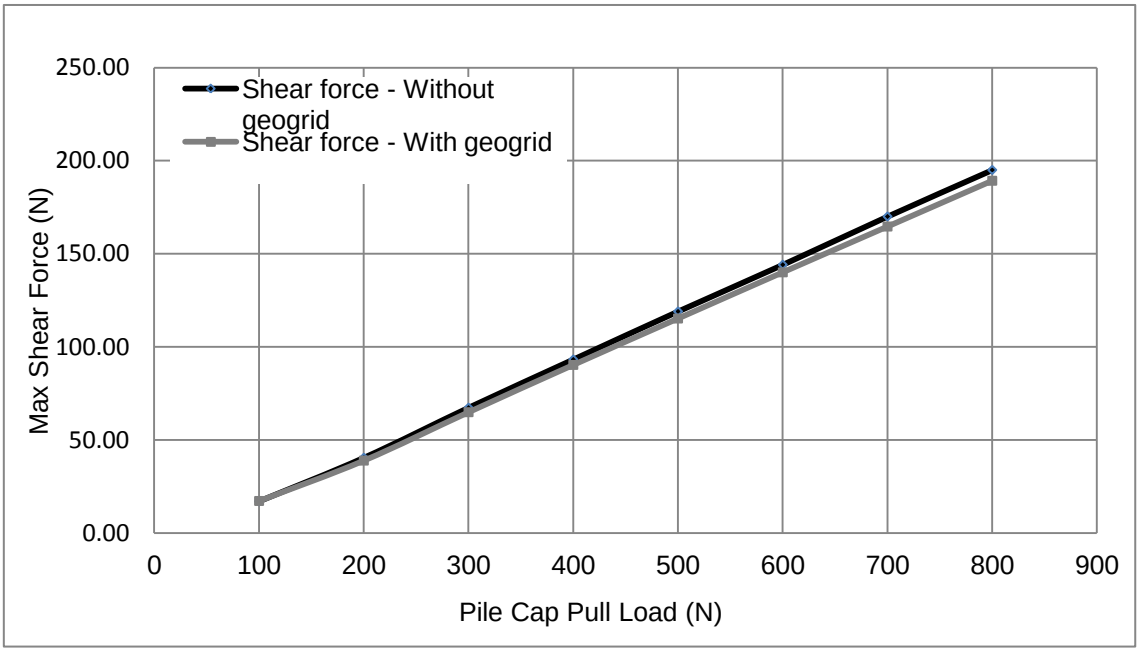

Figure 2-17: Shear force at pile head vs. pile cap lateral deflection

Effect of Microgrid Length

Figure 2-18 compares the pile cap deflections calculated for two microgrid lengths. The microgrid lengths considered in the parametric analyses were, 90 cm and 20 m. The results shows that increasing the microgrid mesh length reduced the lateral pile cap deflection by around 12%. Moreover, Figures 2-19 and 2-20 demonstrate the effect of microgrid length on the maximum bending moment and shear forces on the piles. It can be noted from Figures 2-19 and 2-20 that as the microgrid mesh extent from the pile foundation increased, the bending moment decreased by around 5%. Also, it can be noticed that this reduction in shear force was marginal compared to the reduction in the bending moment.

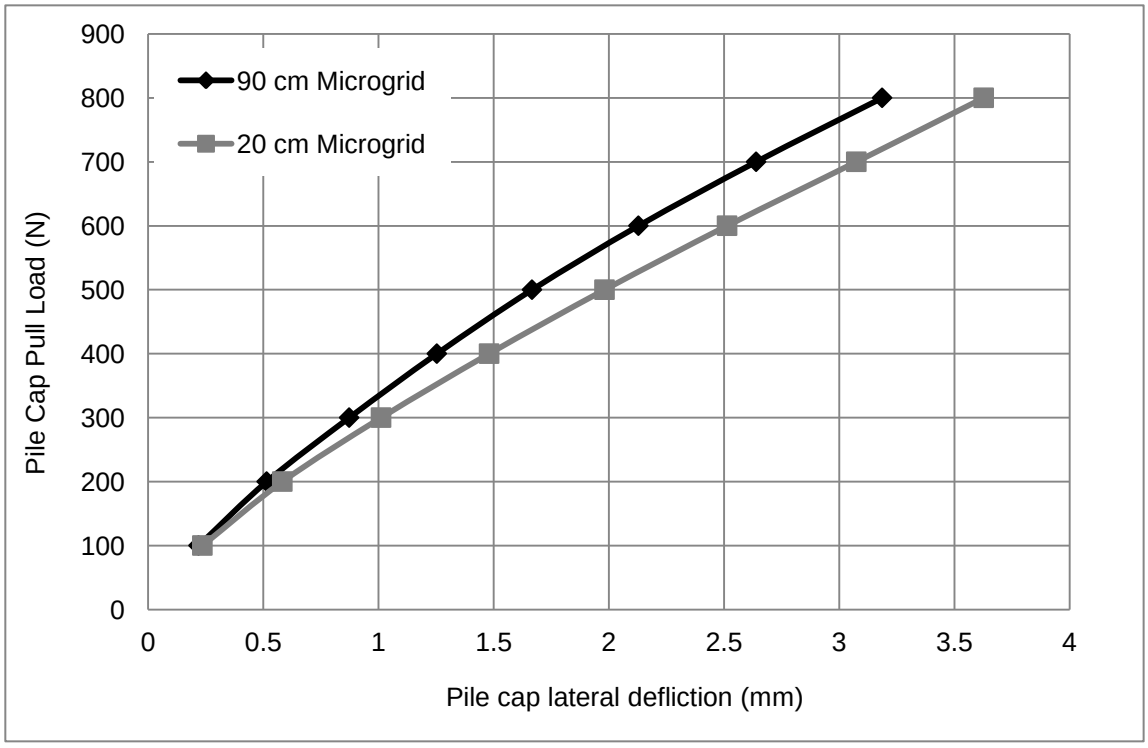

Figure 2-18: Pile cap deflections for microgrid lengths of 90 cm and 20 cm.

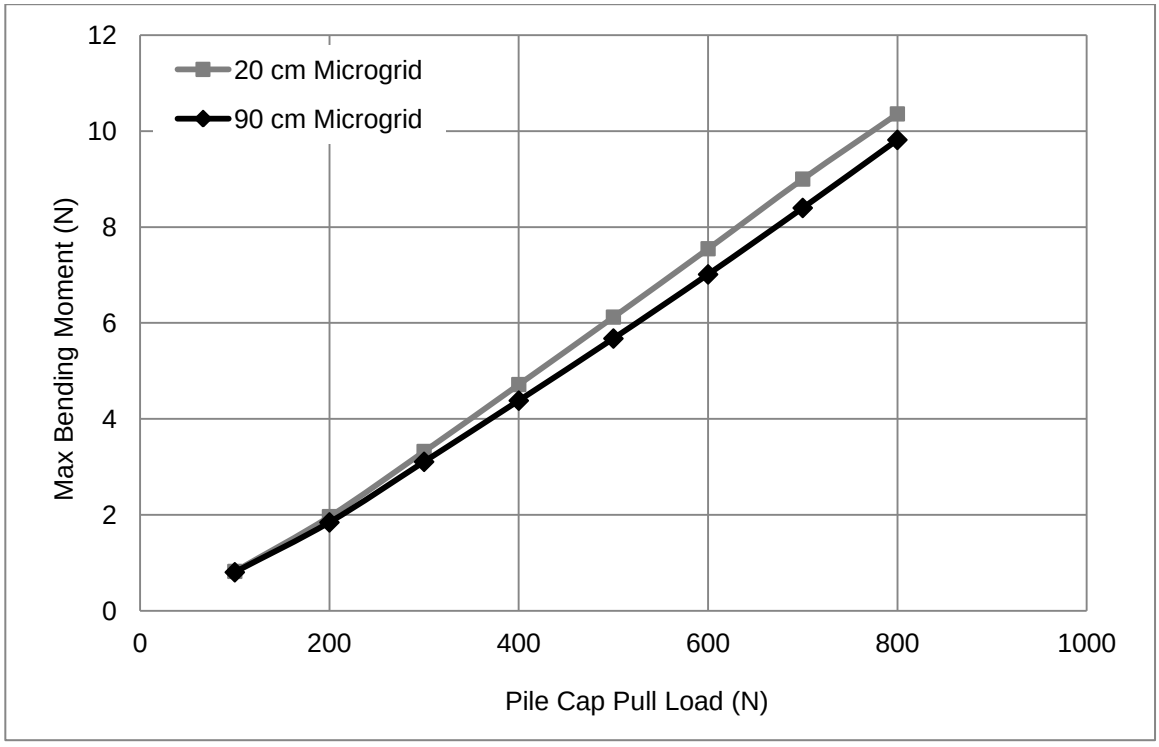

Figure 2-19: Maximum bending moments for microgrid lengths of 90 cm and 20 cm.

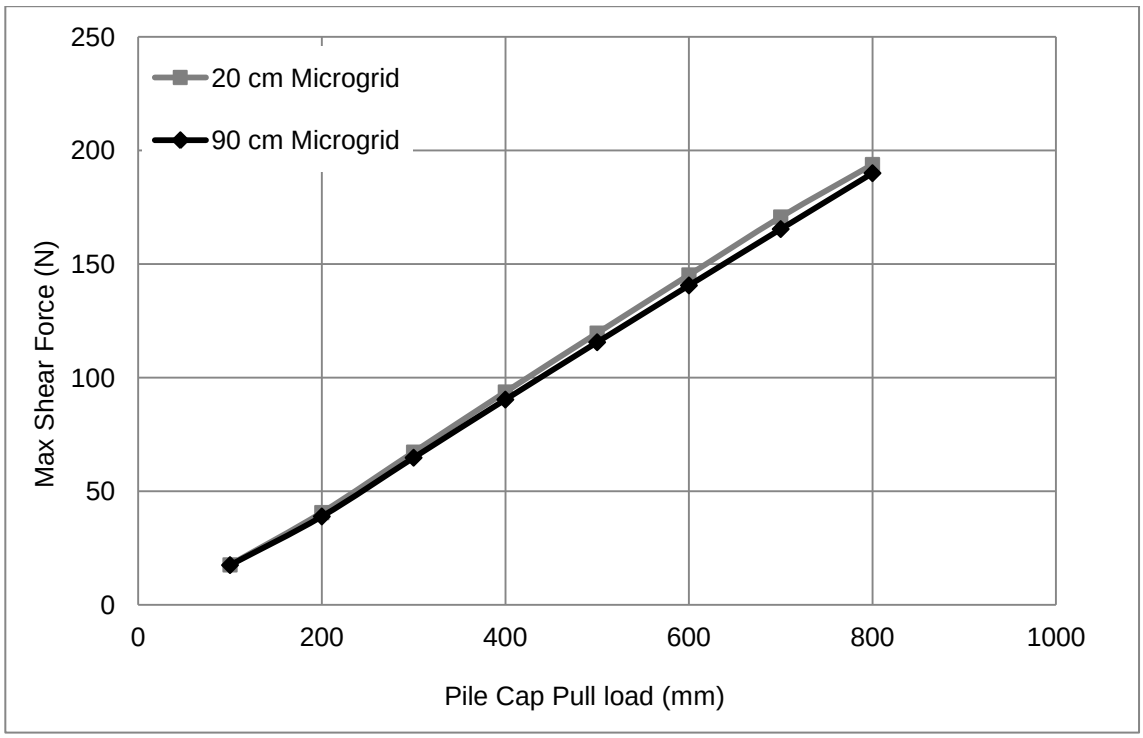

Figure 2-20: Maximum shear forces for microgrid lengths of 90 cm and 20 cm

2.5 Summary and Conclusions

This chapter presented static model tests and numerical simulations to investigate the lateral behavior of a model polymer strip reinforced pile foundation system. The following conclusions were derived from the results of reduced scale physical tests and corresponding numerical analyses:

- The lateral resistance of the foundation system was increased by 15 % due to the addition of the model microgrid mesh and extending it near the boundary of the soil container.
- The peak lateral resistance of the foundation system decreased by 20 % due to reducing the thickness of the surficial granular backfill layer.

- The numerical results show that the addition of the polymer strips would allow reducing the required soft ground replacement by 50%, while providing improved lateral performance.
- The numerical results showed that the addition of the geosynthetic reinforcement reduced the bending moment by 8% and reduced the shear force by 2%.
- The numerical results also showed that extending the geosynthetic reinforcement increased the lateral stiffness of the foundation system and reduced the lateral displacement by 12 %.
- The numerical results indicated that extending the microgrid mesh farther from the pile foundation bending decreased the bending moment by around 5%.
- The parametric study indicated that the extent of the geosynthetic reinforcement influences the level of enhancement it provides. Thus, the length of the reinforcement should be optimized for the specific case considered.
- Overall, the model scale experimental and numerical results showed that the beneficial effects of the geosynthetic reinforcement increased as the applied load increased. Thus, further improvement of the lateral performance of the geosynthetic-reinforced foundation is expected if the foundation is allowed to experience larger displacement.

References:

[1] Bathurst, R.J. and Alfaro, M.C. 1996. Review of seismic design, analysis and performance of geosynthetic rein- forced walls, slopes and embankments. International Symposium on Earth Reinforcement, keynote lecture, Kyushu, 23-52.

[2] Brown, D. A., Morrison, C., and Reese, L. C. 1 988. Lateral load behavior of pile group in sand. Journal of Geotechnical. Engineering. ASCE, **114** (11), 1261–1276.

[3] Cai, Z., and Bathurst, R.J. 1995. Seismic response analysis of geosynthetic reinforced soil segmental retaining walls by finite element method. Computers and Geotechnics, **17** (4), 523-546.

[4] El-Emam, M. M., and Bathurst, R.J. 2007 .Influence of reinforcement parameters on the seismic response of reduced-scale reinforced soil retaining walls. Geotextiles and Geomembranes, **25** (1), 33-49.

[5] El-Emam, M. M., and Bathurst, R.J. 2004. Experimental design, instrumentation and interpretation of reinforced soil wall response using a shaking table. International Journal of Physical Modelling in Geotechnics, 4, 13-32.

[6] Han, J., and Akins, K. 2002. Use of geogrid-reinforced and pile supported earth structures. Proceedings. Deep Foundations 2002: An International Perspective on Theory, Design, Construction, and Performance, ASCE, Reston, Va.,pp. 668–679.

[7] Han, J., and Gab, M. A. 2002. Numerical analysis of geosynthetic reinforced and pile-supported earth platforms over soft soil. Journal of Geotechnical and Geoenvironmental. Engineering, **128** (1) , 44–53.

[8] Meymand, P. J. 1998. Shaking table scale model tests of nonlinear soil-pile-superstructure interaction in soft clay. Ph.D. Dissertation, University. of California, Berkeley, CA.

[9] Iai, S. 1989. Similitude for shaking table tests on soil-structure-fluid models in 1g gravitational field. Soils and Foundations, **29** (1), 105–118.

[10] Kimura, M., Adachi, T., Kamei, H., and Zhang, F. 1995. 3-D Finite element analyses of the ultimate behavior of laterally loaded cast-in-place concrete piles. In G. N. Pande and S. Pietruszczak, editors, Proceedings of the Fifth International Symposium on Numerical Models in Geomechanics, NUMOG V,. A. A. Balkema, September 1995. pp. 589-594.

[11] Maddison, J. D., Jones, D. B., Bell, A. L., and Jenner, C. G. 1996. Design and performance of an embankment supported using low strength geogrids and vibro concrete columns. Geosynthetics: Applications, design and construction, De Groot, Den Hoedt, and Termaat, eds., Balkema, Rotterdam, The Netherlands, 325–332.

[12] Matsumoto, T., Fukumura, K., Pastsakorn, K., and Horikoshi, K. 2004. Experimental and analytical study on behavior of model piled rafts in sand subjected to horizontal and moment loading. International Journal of Physical Modeling in Geotechnics, **4** (3), 2042-6550.

[13] McVay, M. C., Zhang, L. M., Molnit, T., and Lai, P. 1998. Centrifuge testing of large laterally loaded pile groups in sands. Journal of Geotechnical and Geoenvironmental Engineering, ASCE, **124** (10), 1016–1026.

[14] Reese, L. C., Cox, W. R., and Koop, F. D. 1974. Analysis of laterally loaded piles in sand. Proceedings. 6th Annual. Offshore Technology. Conference. Offshore Technol. Conference., Richardson, Tex., 473–483.

[15] Rocha, M. 1957. The possibility of solving soil mechanics problems by the use of models, Proceedingd.4th Int. Conference. Soil Mechanical. Foundation. Engineering, 1, 183-188.

[16] Schanz, T. and Vermeer, P. A. 1998. On the stiffness of Sands, Getechnique, 48, 383-387.

[17] Sandri, D. 1997. A performance summary of reinforced soil structures in the greater Los Angeles area after the Northridge earthquake, Geotextiles and Geomembranes, **15** (4-6), pp. 235-253.

[18] Tatsuoka, F., Sakamoto, M., Kawamura, T., and Fukushima, S. 1986. Strength and deformation characteristics of sand in plane strain compression at extremely low pressures, soils and foundations, **26** (1), 65-84.

[19] Turan, A., Hinchberger, S.D., and El Naggar, M.H. 2009a .Mechanical characterization of an artificial clay. Journal of Geotechnical and Geoenvironmental Engineering, **135** (2), 280-290.

[20] Turan, A., Hinchberger, S.D., and El Naggar, M.H. 2009b. Design and commissioning of a laminar soil container for use on small shaking tables. Soil Dynamics and Earthquake Engineering, **29** (2), 404-414.

[21] Turan, A., Hinchberger, S.D., and El Naggar, M.H. 2008 Investigation of dynamic performance of bentonite-glycerin-water based artifitial caly. GRC Research Report No: GEOT-08-01, The University of Western Ontario, London, ON, Canada.

[22] Wakai, A., Gose, S., and Ugai, K. 1999. 3-D Elasto-Plastic finite element analysis of pile foundations subjected to lateral loading. Soil and Foundations, **39** (1), 97-111.

[23] Yang, Z and Jeremic, B. 2005. Study of soil layering effects on lateral loading behavior of piles. Journal of Geotechnical and Geoenvironmental Engineering, ASCE, **131**(6), 1090-0241.

[24] Zhang, M. M. Limin and Lai, P. 1999. Numerical analysis of laterally loaded 3x3 to 7x3 pile groups in sands. Journal of Geotechnical and Geoenvironmental Engineering, **125** (11), 936-946.

Chapter 3

3. EXPIRMENTAL STUDY ON THE DYNAMIC LATERAL BEHAVIOR OF GEOGRID REINFORCED PILE FOUNDATION SYSTEM

The use of geosynthetic reinforcement in earth structures have increased significantly over the last two decades. The advantages associated with the use of geosynthetics have been well documented. Some of the typical applications include slopes reinforcement, improvement of embankments foundations, mechanically stabilized retaining structures and subgrade improvement for roads.

Certain subsurface conditions may dictate special foundation solutions such as piled foundation systems. Such foundations are widely used in seismically active areas, where they are expected to resist significant lateral loads. However, the weak subsurface conditions that dictate the use of pile foundation systems result in low lateral foundation resistances. This chapter introduces an innovative use of geosynthetics as part of a novel foundation concept called geosynthetics-reinforced pile foundation, where polymer strips are used to enhance the lateral resistance of the pile foundation system.

The seismic pile-soil-geosynthetics interaction of this system was evaluated using a series of reduced scale physical model tests performed on a shaking table in 1G environment. A uni-directional laminar shear box containing a three layer soil stratigraphy, which included a layer of synthetic clay known as modified glyben (Turan et al. 2009a) sandwiched between lower and upper layers of granular materials, was used in the physical model tests. The model pile-cap system that supported a single degree of freedom structure was installed and a series of tests were performed using dynamic loadings in the form of sine sweep, harmonic and scaled earthquake signals in order to identify the amplification and resonance conditions of the foundation system and to evaluate various aspects of the pile-soil-geosynthetic interaction.

3.1 Introduction

Poor ground conditions near the surface pose some foundation challenges for design engineers. In many cases, deep foundation systems (piles) are sought as the practical foundation option to address the challenges of weak foundation soils. Pile foundations are widely used in seismically active areas, where they are expected to resist significant lateral loads. However, the weak subsurface conditions near the ground surface often dictate expensive and time consuming ground replacement, pile inclination or soil stabilization practices in order to enhance the lateral resistance of the pile foundations.

This chapter introduces the results of reduced scale physical model tests of a novel geosynthetics-reinforced pile foundation system. The physical model of the pile foundation system was composed of 4 model tube piles connected with a rigid steel cap. The steel cap is connected to a model single degree of freedom structure (SDOF). The SDOF was designed and fabricated to examine the effect of model reinforcing polymer strips (microgrid mesh) on the seismic response of structures with different natural periods. The foundation system was installed in a multi-layer soil deposit that comprised a soft cohesive layer underlain by a sand layer. The model soil stratigraphy in the laminar container included a granular top layer representing the engineered granular material, which is often used to replace the weak surficial cohesive soil. The cohesive soil layer was modeled using the Modified Glyben (Turan et al. 2009a). A microgrid mesh was embedded within the top granular fill layer and was connected to the piles. The dynamic performance of the pile-cap-microgrid system has been studied using shaking table tests in 1g environment. Various forms of dynamic loads such as harmonic loads, sine sweep and scaled earthquake signals have been used to assess the performance of the microgrid reinforcement to improve lateral foundation response.

3.2 Background

Geosynthetics are polymeric materials that consist of tensile ribs with openings of sufficient size to allow interlocking with the surrounding soils. Examples of practical use of geosynthetics include geogrids, geonets, cellular confinement and polymer strips. The geosynthetics-soil interaction mechanism allows the geosynthetics to work as a reinforcing element, which provides the soil with tensile strength and enhances its shear resistance. Therefore, geosynthetics have been widely used in modern construction practices. Several researchers have investigated the use of geosynthetic-reinforced soils to enhance the resistance of the geotechnical structures. Studies such as Bathurst and Alfaro (1996), Zhenqi and Bathurst (1995), Helwany et al. (2001), El-Emam (2007) and Liu (2009) investigated the use of geogrid reinforcement to enhance the stability of earth retaining walls. Others investigated the performance of geosynthetics as part of geosynthetics reinforced embankment support systems (e.g. Liu et al., 2007).

The use of polymer strips reinforcement to improve the lateral resistance of pile foundation systems under dynamic loading conditions was studied in this chapter using a reduced scale physical modeling approach in a 1g environment. Despite the limitations of the 1g shaking table tests with regard to achieving the suitable stress fields for testing cohesionless soils, these tests have been used extensively to examine the dynamic behaviour of polymer strips reinforced earth retaining structures and the seismic soil-pile-superstructure interaction problem. Sakagutchi et al. (1992) conducted a set of reduced scale shaking table tests on a modular block soil wall. Matsumo et al. (1998) investigated the influence of increasing the length of soil reinforcement through a set of shaking table tests on six model walls. Koseki et al. (1998) investigated the dynamic lateral behaviour of a conventional and reinforced soil model walls through a series of shaking table tests. El Emam and Bathrust (2007) carried out comprehensive shaking table tests to examine the influence of geogrid reinforcement parameters such as stiffness, length and vertical spacing on the seismic response of reduced scale soil retaining wall.

Extensive research was conducted to investigate the seismic soil-pile-superstructure interaction (SSPSI) problem using 1g shaking table tests. Kubo (1969) was the first to perform shaking table model pile tests. Gohl (1991), Liu and Chen (1991), Yan et al. (1991), Sreerama (1993), Markis et al. (1997), Tao et al. (1998) are some examples of such studies. Most of these studies have investigated the seismic response of single piles and small pile groups in cohesionless soil. Although many tests have shown deviations from a specific model similitude rule, few scale model tests have been calibrated with prototype tests and been proven successful.

The use of geosynthetics to improve the seismic performance of piled foundations and to reduce intolerable pile lateral deflections is a new concept. Thus, this research is carried out to investigate the dynamic lateral performance of geosynthetics-reinforced pile foundation system using reduced scale shaking table tests.

3.3 Methodology

This section describes the testing facility, provides a brief description of the model testing laminar container, and summarizes the similarity rules used to develop the scaled models. This section also gives a detailed description of the model soils, model foundation system and the single degree of freedom system that represents the superstructures. The instrumentation and data acquisition systems as well as the testing plan and procedures followed in this study are explained.

3.3.1 Reduced scale physical model

Reduced scale model tests offer the advantage of studying the response of pile-soil-superstructure systems in a controlled environment. If they carried out properly, reduced scale model tests are also advantageous in seismic studies because they are able to give economic and realistic information about ground amplification, pore water pressure variations, non-linear soil behavior and soil structure interaction. Also, reduced scale model tests offer an economical alternative for full scale tests to run parametric studies (Turan et al., 2008). In this research, several reduced scaled model tests were carried out

on a shaking table. The main feature of shaking table tests is that they are executed in in a 1-g environment which does not induce the elevated confining stress field required for proper modeling of cohesionless soils ,as in centrifuge tests (Meymand, 1998).

Rocha (1957) started developing scale model similitude relationships for soil mechanics problems. Rocha scaled the stress-strain behavior of soils assuming that they are linearly proportional in models and prototypes. Rocha's linear scaling concept was set to account for the changes in the stress system present in a 1g environment. Iai (1989) continued Rocha's research and derived similitude relationships assuming that the constitutive stress-strain relationship is independent on the confining stress if a proper scaling factor is used. He validated this assumption using plane strain compression tests under varying confining stresses (Tatsuoka et al., 1986). The tests results showed that this assumption is valid for axial strains lower than the strains at failure peak stress. Iai (1989) derived his similitude relations based on the geometric and density scaling factors, (λ) and (λ_p), respectively. Meymand (1998) developed a modeling approach suitable for soil, pile and superstructure conditions. In his method, the primary modes of system response are defined first. Then, prototype values for the variables contributing to these modes are selected. Similarity rules are then used to verify that the calculated implied prototype response is reasonable. Table 3-1 shows the scaling relationships for the variables contributing to the primary modes of system response.

Table 3-1: Scaling relationships for primary system variables (Meymand, 1998).

Parameter	Scaling factor	Parameter	Scaling factor	Parameter	Scaling factor
Length	λ	Acceleration	1	Mass density	1
Force	λ^3	Shear wave velocity	$\lambda^{1/2}$	Stress	λ
Stiffness	λ^2	Time	$\lambda^{1/2}$	Strain	1
Modulus	λ	Frequency	$\lambda^{-1/2}$	EI	λ^5

* λ: geometric scaling factor

3.3.2 The shaking table and soil container

The model soil bed was formed in a laminar container placed on a 1.22 m x 1.22 m 1-D shaking table. The laminar container comprises of 24 rectangular shaped laminae stacked to create an 807 mm high, 900 mm long and 450 mm wide box with 2 mm clearance between laminae. The laminae are machined using solid high strength aluminum alloy section. Figure 1 shows the details of laminar container used in this study (Turan et al., 2009b). The shaking table was equipped with pneumatic and electrical actuators controlled by a digital control module that allows the generation of various types of signals. The shaking table used in this study is a one-dimensional table that can generate various types of dynamic loads, such as harmonic, sine sweep and white noise signals.

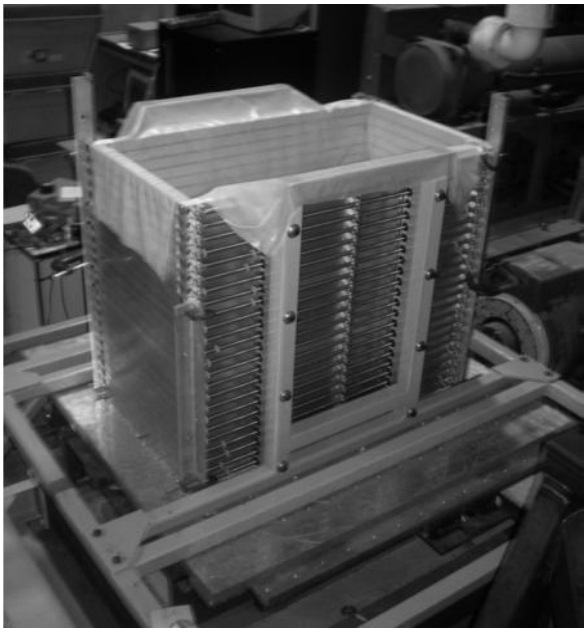

Figure 3-1: Laminar soil container covered with latex membrane and aligned with corner profiles

3.3.3 The model soil column

The model soil stratigraphy comprised three layers of soils starting from bottom to top: i) a layer of silty sand; ii) a layer of synthetic clay (modified glyben) to represent the cohesive soil layer; and iii) a surfacial layer of engineered granular backfill. The bottom granular layer was modeled using the fine granular material with grain size distribution depicted in Figure 3-2. The peak angle of internal friction of the sand was measured as 40° from direct shear tests.

Figure 3-2: Construction sand gradation

The overlying cohesive layer was modeled using modified glyben, which provides favourable characteristics for scaled physical model tests. The primary advantages of modified glyben for reduced scale model tests are: i) it consolidates at a very slow rate after application of confining pressure, thus it can be used in 1-g and N-g tests without a observing a consolidation stage; ii) it resists desiccation due to drying; and iii) its mechanical properties do not significantly change with time, which facilitates its multiple use as part of the physical testing program. Also, laboratory results showed that modified glyben have a normalized shear modulus versus shear strain amplitude response that is independent on the confining stress, and glycerin to water ratio (Turan et al. 2009a). Therefore, it is suitable for 1G environment tests.

The modified glyben was prepared by mixing bentonite with glycerine and water. The fluid to dry bentonite ratio was 85% and the water to glycerine ratio was 50%. These ratios were chosen to simulate prototype soft clay. Hand-held vane shear test (Pilcon) was used to measure the undrained shear strength of the modified glyben mixture after preparation and placement in the soil container. After light compaction, the undrained shear strength of the model clay Cu was about 19 kPa at the bottom of the clay layer and 8 kPa near the top with a density of 1406 kg/m^3.

The corresponding average shear wave velocity for an average Cu of 15 kN/m^2 was estimated to be 40 m/s using the empirical relation reported in Turan et al. (2009a), i.e.

$$V_s = 26.52 \text{ Ln } (c_u) - 33 \quad [1]$$

Using similitude relationships shown in Table 1, with a geometric scaling factor λ=20, The model clay shear wave velocity of 40 m/s correspond to a prototype clay shear wave velocity of approximately 113 m/sec. This shear wave velocity corresponds to a soft to medium consistency for prototype clay.

The main source of the shear resistance of the microgrid mesh is derived from the interlocking mechanism with the surrounding backfill. Therefore, the top engineered backfill layer was simulated using aggregates with an average particle size of 5 mm. The peak angle of internal friction of the aggregates was measured as 50˚ from direct shear tests.

3.3.4 Model Foundation System

The reduced scale foundation model was made of four acrylic tubes with a length of 60 mm and a diameter of 19 mm. These piles were rigidly connected to a steel cap of 20 X 20 mm and 6 mm thickness which correspond to a concrete cap of 0.7 m thickness. Four plastic rings were fabricated and installed to facilitate the load transfer between a microgrid mesh and the piles. The microgrid mesh was extended and pressed inside the rings using four steel bolts. Rings were fixed in their vertical position using a plastic bolt. Figure 3-3 shows the details of the model foundation. Table 3.2 provides a summary of the model scaling calculations.

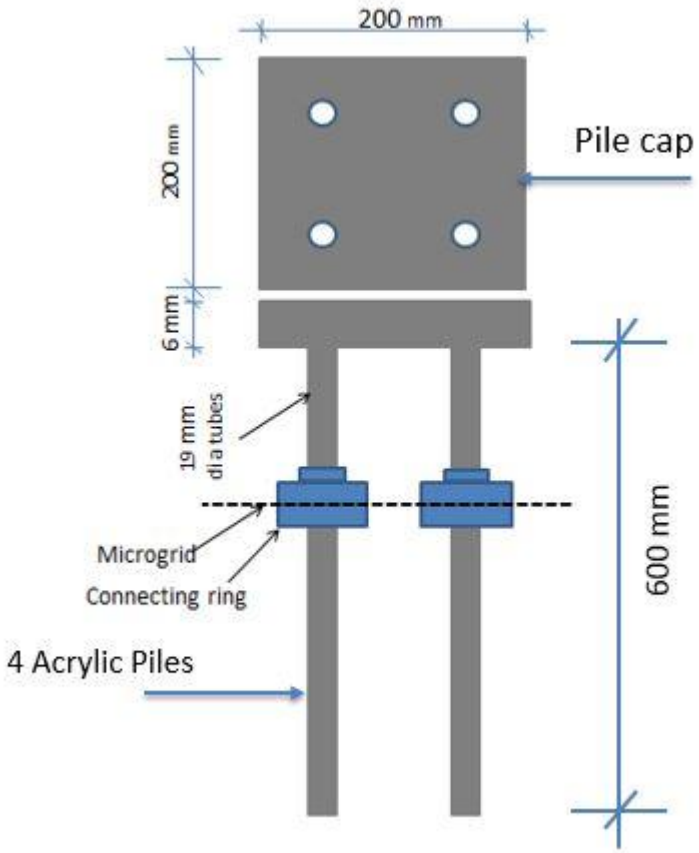

Figure 3-3: The scaled piled cap geogrid model

Table 3-2: Model Piles calculations, λ = 20

Parameter	Model pile (Acrylic)	Calculated Prototype pile (Steel)
Outer diameter (mm)	19	380
Length (mm)	600	12000
Young's modulus (kN/m^2)	3.2×10^6	200×10^6
Flexural rigidity, E_pI ($kN.m^2$)	1.82×10^{-2}	5.81×10^4
Axial rigidity, E_pA (kN)	6.03×10^5	3.5×10^6

3.3.5 Model Geosynthetics

The microgrid mesh was introduced within the aggregate layer at a depth of 3.5 times the pile diameter (i.e 66 mm). The geosynthetics were simulated in the physical model tests by using a bi-axial knitted Microgrid manufactured by STRATAGRID. STRATAGRID Microgrid was manufactured utilizing a complex knitting process and polymer coatings to provide various engineering properties and constructed of high molecular weight and high tenacity polyester yarns. The yarns provide significant tensile capacity through precision knitting into a dimensionally firm, uniform network of apertures. The model stuffiness value of the Microgrid at 2% J_m = 110 kN/m. With a geometrical scale factor λ = 20, the prototype stiffness $J_p = J_m \lambda^2 = 110 \times 20^2 = 44000$ kN/m (EL-Emam and Bathurst 2004). Table 3.3 shows the main engineering properties of the STRATAGRID Microgrid.

Table 3-3: Engineering properties of geogrid

Index Properties	Test Method	Value
Ultimate Strength	ASTM D-6637 Method A	29.2 kN/m
Creep Limited Strength	ASTM D-5262/D-6992	16.8 kN/m
Strength @ 2% Strain	ASTM D4595	2.2 kN/m
Strength @ 5% Strain	ASTM D4595 (MD)	7.3 kN/m
Strength @ 5% Strain ASTM	ASTM D4595 (CMD)	4.4 kN/m
Aperture Size	Measured	2.54 x 6.35 mm

3.3.6 Model Superstructure

The superstructure was modeled using a single degree of freedom system. The model single degree of freedom (SDOF) structure was machined using a 30 mm long steel column with a square cross-section of 25x25 mm, supporting a 9.5 kg mass. This mass was connected to the column with a 10 mm diameters bolt (see Figure 3-4). The natural frequency of the SDOF structures was determined via a sine sweep test conducted on the shaking table while the SDOF structure was rigidly clamped on top of the table. The natural periods of the SDOF structures correspond to two structures with two different natural frequencies. Table 3.4 shows the model and prototype natural frequencies of the two structures. The SDOF with lower natural frequency is denoted low frequency (LF) SDOF and the SDOF with the higher natural frequency is denoted high frequency (HF) SDOF.

Table 3-4: SDOF structures model and prototype frequencies

Simulated BLDG Type	BLDG Height (m)	BLDG Period T (sec)*	BLDG Frequency – prototype (Hz)	SDOF Frequency – model (Hz)
Steel moment frame	18.5	0.45	2.24	10.03
Steel moment frame	26.5	0.59	1.71	7.64

*$T_a = 0.05\ h^{0.75}$ (NBCC CI.4.1.8.11.3(c))

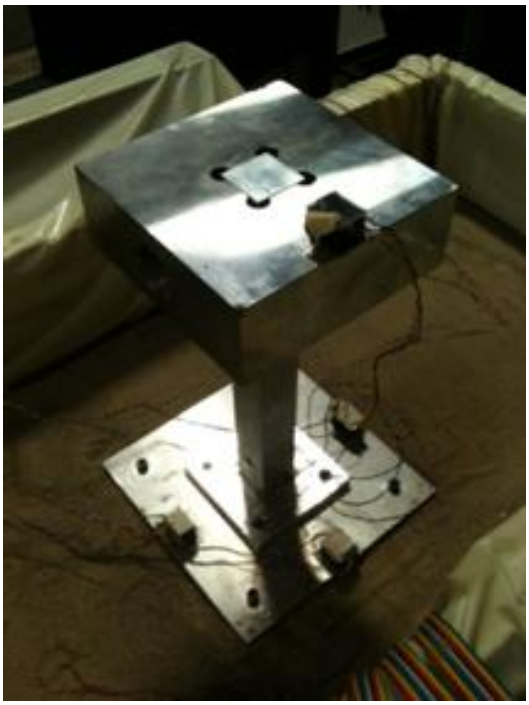

(a) SDOF Low Frequency

(b) SDOF High Frequency

(c) Accelerometer incased

Figure 3-4: a) The SDOF High system b) SDOF Medium system, c) ADXL 203 Accelerometer

3.3.7 Instrumentation

Ten accelerometers (AC1–AC10) were used to monitor the acceleration response of the shaking table, the model soil deposit, the piled cap and the SDOF model structure. The accelerometers (type ADXL203) were small size high precision devices with dual-axis. The ADXL203 accelerometers were capable of measuring accelerations for a range of ±5*g* with a sensitivity of ±0.3 % mv/g. In addition, a laser displacement transducer (DISP1) (Matsushita-KDCL) was fixed on the laminar container frame to measure the shaking table motion, which could be used to verify the base acceleration signal measured by AC1 on top of the table. The output signals were recorded as analog voltages that were proportional to acceleration and displacement. Figure 3-4 (c) shows an accelerometer containing capacitors, resistors and power supply elements and encased in a plastic box for protection against humidity and contamination due to soil contact. The signal output and power cables of each accelerometer were connected to an amplifier box, which was connected to the data acquisition system.

Figure 3-5 shows the positions of all accelerometers in/on the soil container and on the model piled-cap-structure system. AC1 was used to measure the response on the shaking table. The soil response was monitored by accelerometers AC2 to AC6 embedded in the soil column at a distance 20 cm from the edge of the pile cap as depicted in Figure 5. AC8 was fixed on top of the pile cap to monitor the pile cap lateral response. AC7 and AC9 were fixed at the edges of the pile cap with 90 degrees angle with horizon to measure the vertical response at both edges of pile cap. The response of SDOF structure was monitored using AC10, which was mounted at the top of the lumped mass model.

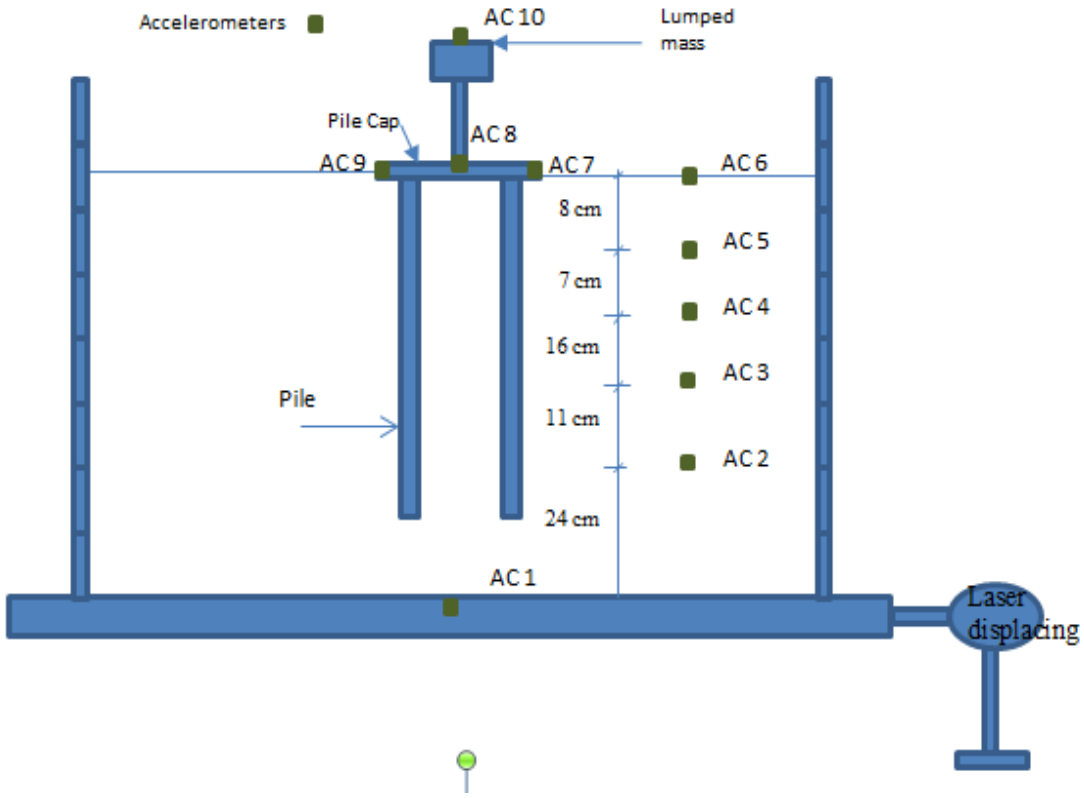

Figure 3-5: Instruments distribution diagram

3.3.8 Shaking Table Control System

The shaking table system was managed by an in-house control software (FRE) developed at the Western University BLWT (Boundary Layer Wind Tunnel). The FRE software is capable of running the table with various vibration signals such as harmonic, sine weep

and white noise. The vibration system responds to a low voltage signal by producing a corresponding displacement through the actuator of the shaking table, as shown in the schematic diagram in Figure 3-6. The FRE is also capable of simultaneously generating the control signal and recording output from displacement and acceleration sensors.

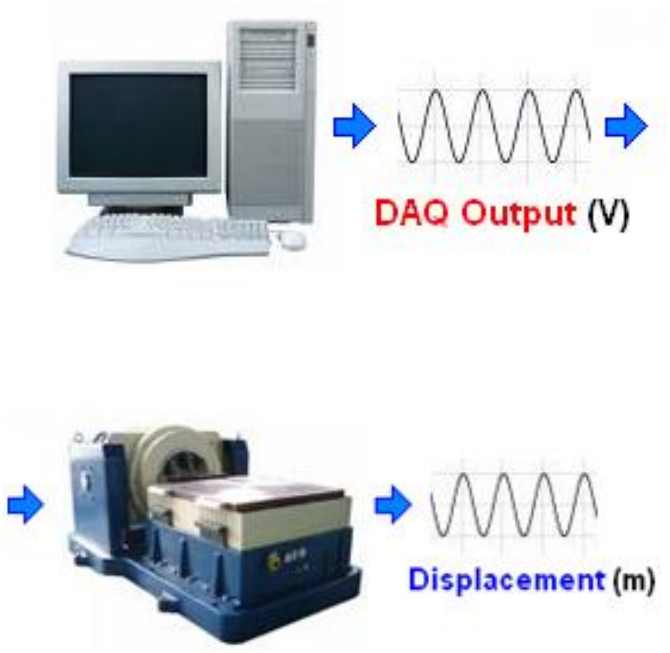

Figure 3-6: The shaking table and control system

3.3.9 Placement of Model Soil Deposit

The testing program was commenced by assembling the laminar container on top of the shaking table. A wood board covered with steel grits was then bolted to the shaking table at the bottom of the lamina container. The steel grits were glued to the wood board using epoxy and installed on the table to ensure transfer of the table motion to the soil column through friction forces at the steel grit-soil interface. Prior to soil placement, the sides of the laminar box were covered with latex membrane to prevent soil particles from migrating out of the box through the openings between the laminae. The initial bedding

layer of the model soil column was backfilled inside the box using layers of sand. Each layer of sand was compacted after applying several cycles of harmonic shaking signals until an 80 % relative density has been achieved (which was determined based on monitoring the height of the sand in the box).

Sand backfilling proceeded in layers where each layer was compacted by shaking each 20 kg of sand into a 2 cm layer until a total layer depth of 36 cm is reached. Blocks of soft modified glyben were then placed over the last sand layer. The blocks of soft modified glyben were prepared by pressing weighed quantities of clay in a small cubical acrylic box with dimensions of 70 x 70 x 50 mm. The clay blocks were positioned side by side and compacted using a drop hammer. Each layer of clay had 40 mm thickness with 1406 Kg/m^3 bulk density. Figure 3-7 depicts the compaction process of Modified Glyben.

The clay layer thickness was varied in accordance with the following scenarios studied as part of this research: i) shallow backfill case with the clay removal/aggregate backfill thickness of 30 mm, and ii) deep backfill case with the clay removal/aggregate backfill thickness of 80 mm. The aggregate backfill was compacted using the same drop hammer. Each 30 mm layer of aggregate weighed 20 kg and compacted into a density of 1650 kg/m^3. The aggregate backfill was continued in layers up to the bottom of the model cap foundation. After the compaction process, the clay undrained shear strength was measured using the hand vane shear apparatus. The average undrained shear strength c_u of the top 100 mm of clay was determined as 9 kPa. Beneath that, the clay layer had an average c_u of 19 kPa. This increase in clay strength was due to the compaction effort.

The model pile-cap system was placed into the soil bed after all layers were prepared as described. In order to eliminate excessive settlement during the testing program, the lumped mass was placed and maintained on top of the cap for 24 hours to have the piles complete the immediate settlement.

Figure 3-7: Compaction of Modified Glyben

3.3.10 Experimental Scenarios

Several shaking table tests were carried out with the objectives of i) studying the influence of the geosynthetics reinforcement on the dynamic performance of the pile foundation, ii) studying the influence of the geosynthetics reinforcement on the dynamic response of the single degree of freedom structures, and iii) exploring the potential for using geosynthetics reinforcement to reduce the thickness of the aggregate backfill. The physical model of the geosynthetics-reinforced pile-structure system was excited using three main types of signals: sine sweep signals, harmonic signals and a scaled earthquake acceleration time history. Table 3-5 presents a summary of the shaking table tests.

Table 3-5: Summary of tests

Test ID	Type of input motion	Predominant frequency (Hz)	Peak Ground Accel. (PGA), g	Purpose
SLNF-1 SLNF-2 SLNF-3	Sine Sweep	5 - 19	0.25	Response of LF SDOF system: 1) deep backfill without geogrid case, 2) deep backfill with geogrid, and 3) shallow backfill without geogrid
SHNF-1 SHNF-2 SHNF-3	Sine Sweep	5 - 19	0.25	Response of HF SDOF system: 1) deep backfill without geogrid case, 2) deep backfill with geogrid, and 3) shallow backfill without geogrid
UPEQ-L UPEQ-H	Random earthquake time history	16	0.3	Response of LF and HF SDOF systems to scaled Upland Earthquake time histories.
SAMP-1 SAMP-2 SAMP-3 SAMP-4	Harmonic signal	16	0.06 to 0.1	Ground motion amplification: shallow & deep backfill with or without geogrid (Table 3-6)

Notes: LF is Low natural frequency; HF is High natural frequency

The sine weep excitation was used to examine the response of the LF and HF SDOF structures and the pile cap model (cases SLNF and SHNF). The shaking table control

system enables users to generate various sine sweep signals with a range of frequencies at a specific maximum amplitude. The soil-structure model has been excited with a 5 minute long sine sweep signal with frequencies ranging from 5 Hz to 19 Hz. The sine sweep test was repeated after installing the microgrid mesh at a depth of 3.5 times the pile diameter within the aggregate backfill. This sine sweep test was also performed to investigate the effect of reducing the thickness of the backfill layer on the system response.

The geosynthetics-soil-foundation-structure model was also subjected to scaled earthquake time histories (cases UPEQ-L & UPEQ-H). The earthquake time history was generated from the original 1990 Upland earthquake with a peak ground acceleration of 0.25g and a predominant frequency of 3.6 Hz (see Figure 3-8). The predominant frequency of 3.6 Hz corresponded to a scaled model frequency of 16 Hz based on a geometric scaling factor of 20. The shaking table was used to simulate the scaled earthquake acceleration time history. As shown in Figures 3-9a and 3-9b, the comparison of the Fourier spectrum of scaled input signal and response measured at table top show close agreement in terms of amplitude and frequency content. The minor discrepancies could be due to the limited abilities of the actuator and the control system due to lacking a motion correction feedback system.

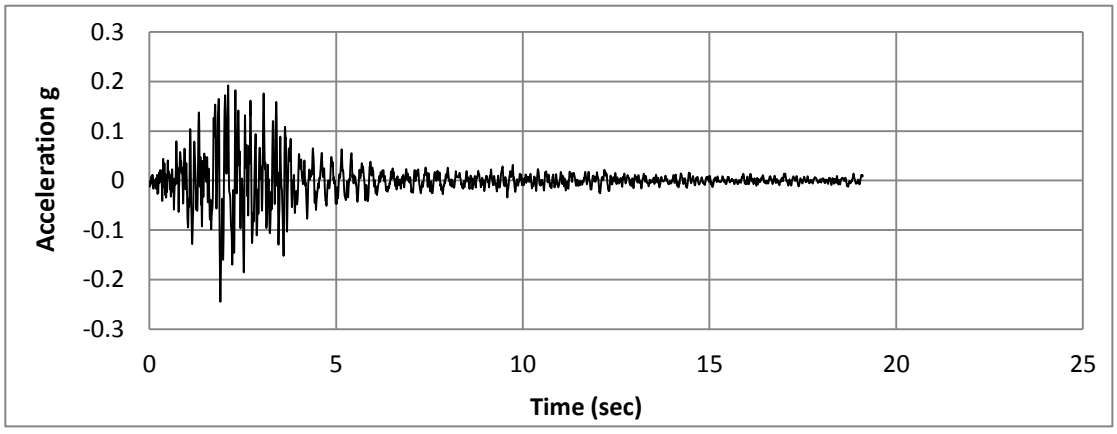

Figure 3-8: The earthquake acceleration time history

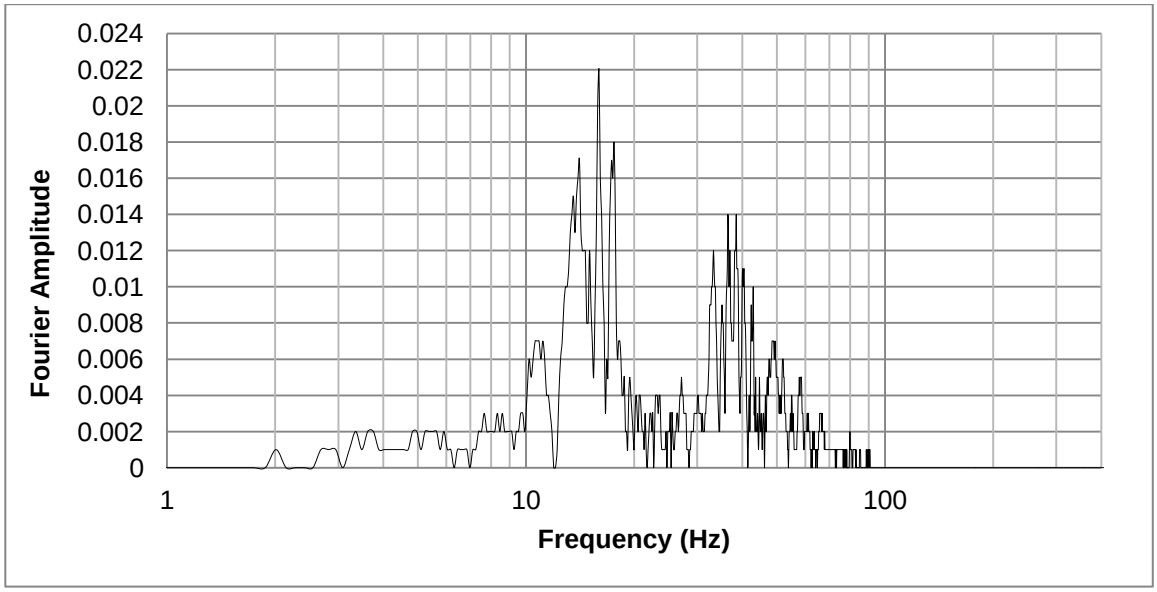

(a)

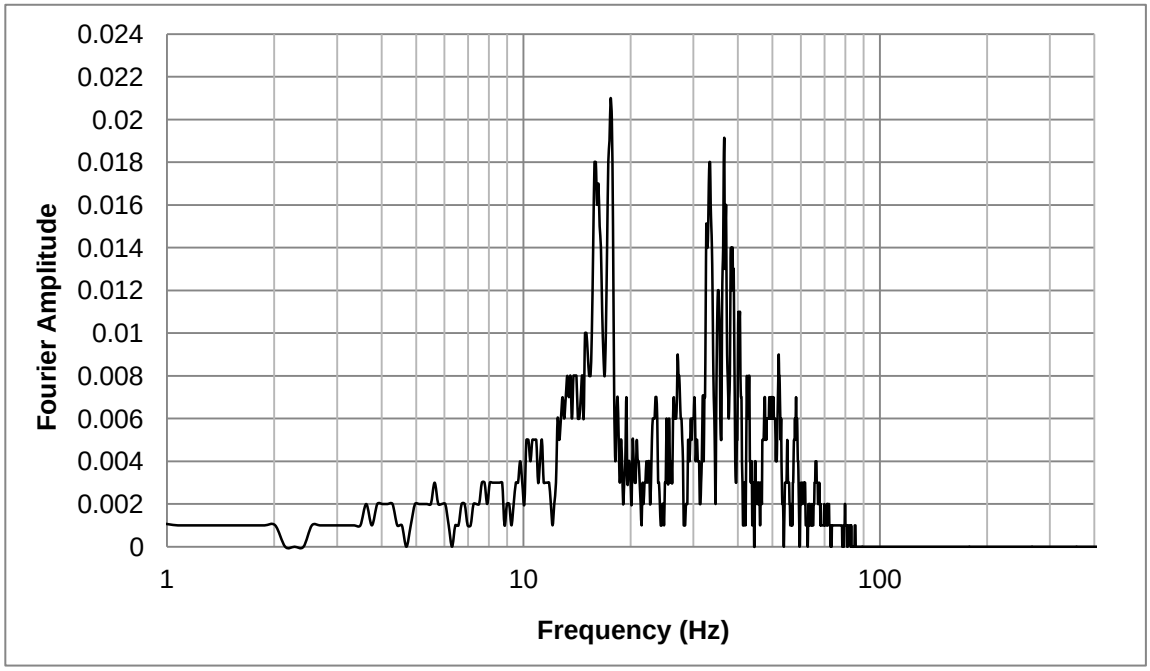

(b)

Figure 3-9: Fourier spectrum of model scale Upland EQ (a) input signal (b) signal at table top

The model was also excited with four harmonic signals with 16 Hz frequency and amplitudes ranging from 0.06g to 0.1g (cases SAMP1 to SAMP4). Table 3.6 presents a summary of these cases and the amplification factor calculated from the acceleration response of each case. The amplification factor was obtained from dividing the amplitude of soil response by the base excitation amplitude. This group of tests was performed to investigate the input motion amplification through the soil column. Similar tests were also conducted to investigate the cases where the microgrid mesh was present in the backfill. This harmonic signal was used to investigate the response of the system with reduced-thickness backfill layer.

Table 3-6: Summary of harmonic tests

Case #	Base acceleration (g)	Amplification factor		
		Deep backfill with microgrid	Deep backfill without microgrid	Shallow backfill without microgrid
SAMP-1	0.061	3.705	3.951	4.754
SAMP-2	0.090	7.444	8.889	9.778
SAMP-3	0.100	7.400	8.500	9.400
SAMP-4	0.120	6.667	8.333	10.00

3.4 Results and discussion

The results of the shaking table tests performed in this study are summarized in this section. The results include the response of free field ground response analyses, the response of the model geosynthetics-reinforced pile foundation system and the response of the SDOF superstructure models. The results are discussed comparatively considering the cases of shallow backfill and deep backfill. The feasibility of using polymer strips to enhance the dynamic induced lateral behaviour of the model pile-cap-superstructure system was also investigated.

3.4.1 Free Field Response

The results of harmonic tests that were conducted in the absence of model foundation/structure system are presented here (SAMP1 to SAMP4). The results obtained from AC6 are summarized in Figure 3-10 and Table 3.6. Figure 3-10 shows the amplification factors for lateral acceleration plotted against the input base acceleration amplitudes. It can be seen that the amplification factor showed an increasing trend with the increase of excitation amplitude due to the increased non-linearity experienced by the dynamically loaded soil. The results also indicated that this case, where aggregate backfill had the smaller thickness experienced the largest amplification. The case of deeper backfill exhibited a lower amplification factor. The lowest amplification was observed when the microgrid mesh was present within the deep backfill. Around 23 % reduction in the amplification factor from almost 8.5 to 6.5 can be observed at a base acceleration of 0.12 g. This behaviour can be attributed to the stiffening of soil column due to the combined effect of increased backfill thickness and the addition of microgrid. The large amplification factors can be attributed to the fact that the models were excited with a harmonic load, that has a frequency of 16 Hz, very close to that of the system valued at 15.4 Hz, and thus resonance conditions occurred.

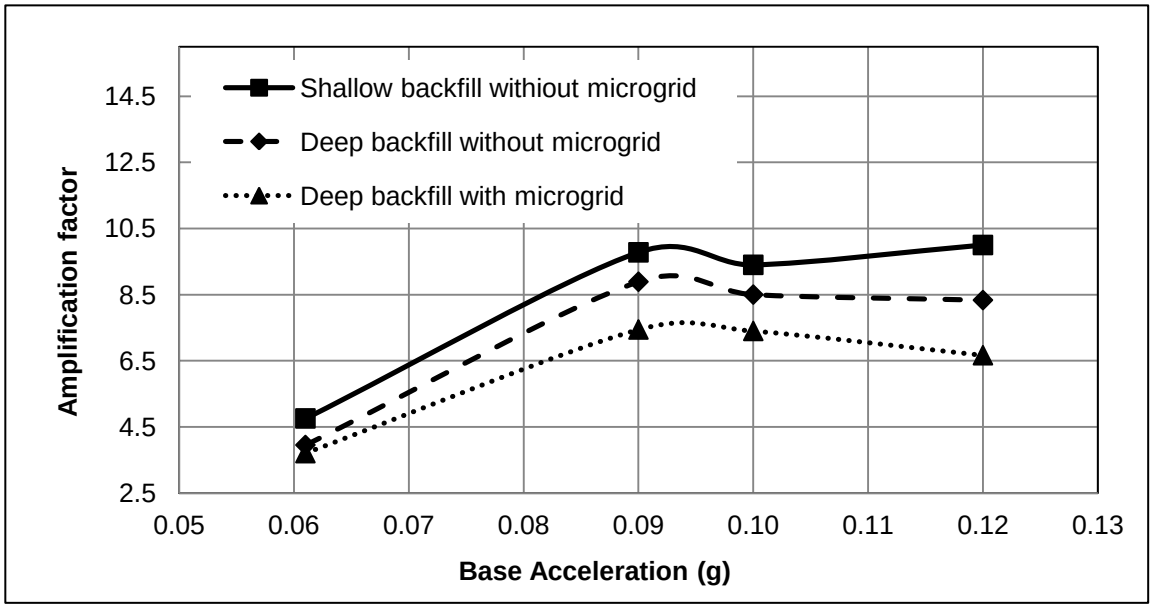

Figure 3-10: Free field response comparison (SAMP-1 to SAMP-4).

3.4.2 Pile cap response

Figure 3-11 shows the results of the sine sweep test with respect to the lateral response measured at the pile cap using AC8 (cases SLNF 1-3). This test was run while the LF SDOF structure was affixed on top of the pile cap. The response comparison shows that the presence of the microgrid mesh had a significant effect on the lateral response of the pile cap level. This could be attributed to the lateral stiffening of the foundation due to the addition of the microgrid reinforcement. When the microgrid reinforcement was present, the Fourier amplitude was reduced around 15% from 2.6 to 2.2 at a frequency of 10 Hz's.

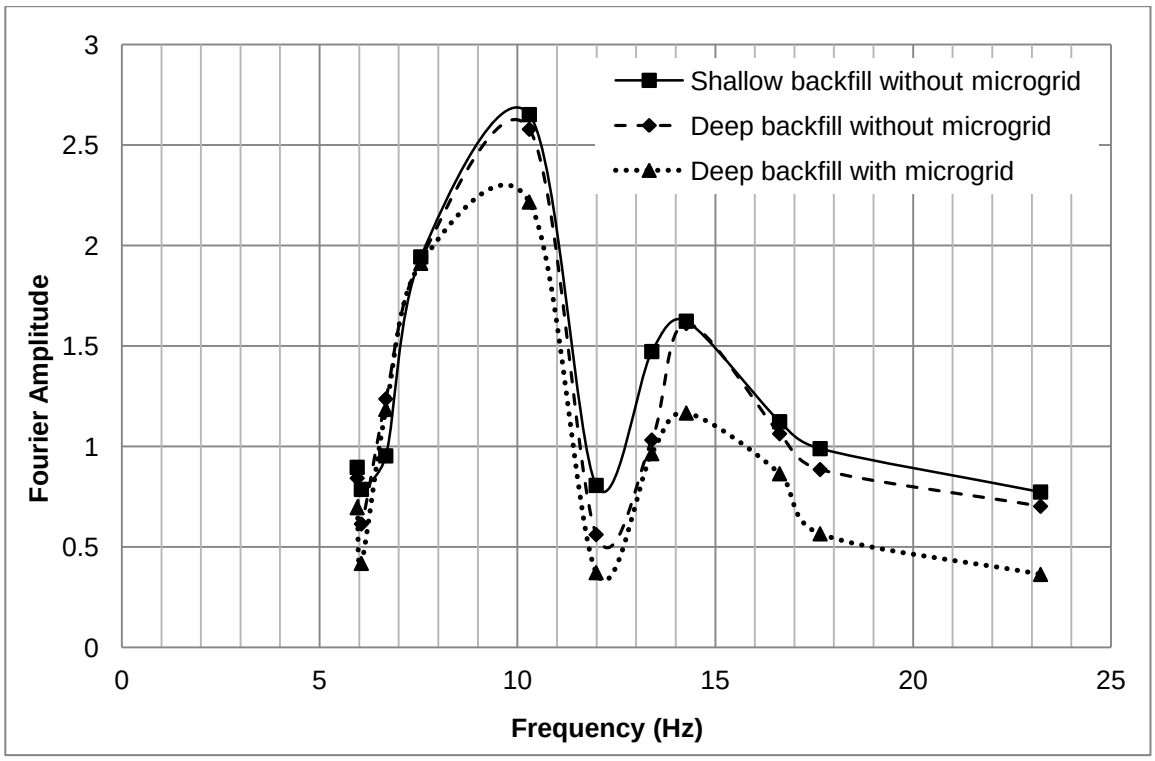

Figure 3-11: The dynamic response comparison of the piled cap foundation (SLNF-1 to SLNF-3).

Figure 3-12 depicts the Fourier amplitudes for three test cases excited using scaled earthquake excitation (cases UPEQ-L). It can be seen that increasing the backfill depth and the addition of microgrid reduced the lateral seismic response of the pile cap.

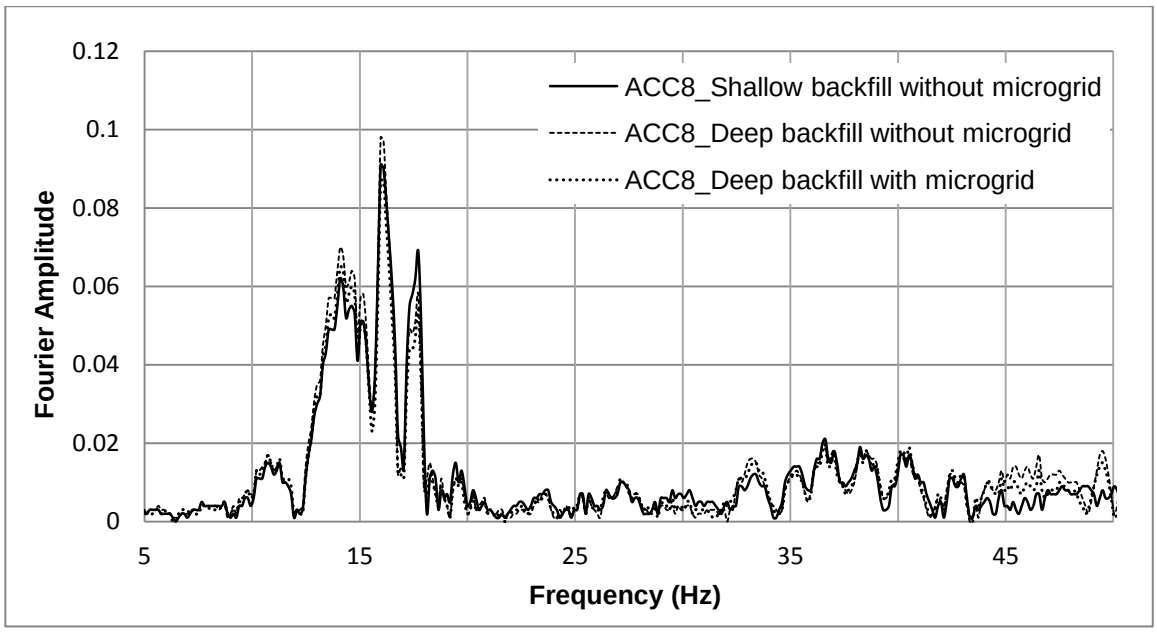

Figure 3-12: Dynamic response of pile foundation with and without reinforcement (UPEQ-L).

Figure 3-13 shows the Fourier amplitudes of the sine sweep tests for the HF SDOF structure was fixed on top of the pile cap (cases SHNF 1-3). Similar to the case of LF SDOF, the response comparison shows that the addition of the microgrid attenuated the response at the pile cap level. Also, Figure 3-13 shows that the reduction of backfill caused the lateral cap response to increase.

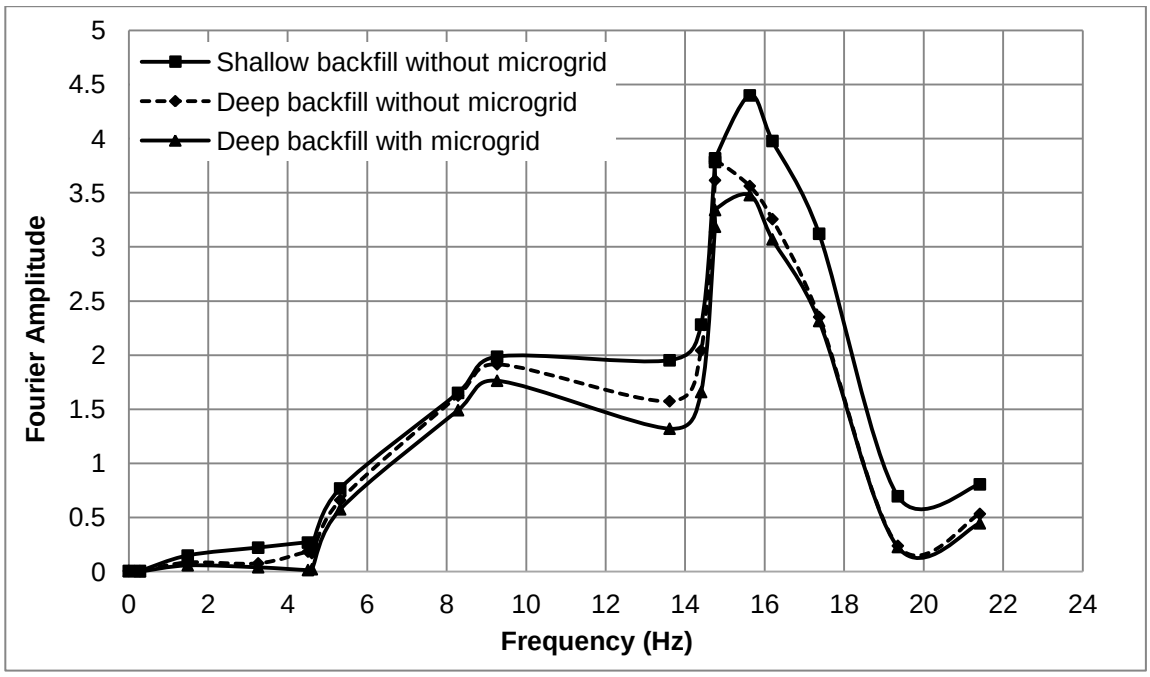

Figure 3-13: The dynamic response comparison of the piled cap foundation (SHNF 1-3)

3.4.3 Low Frequency Structure Response

The sine sweep test results of the LF SDOF structure were obtained from AC10 and are illustrated in Figure 3-14 (cases SLNF 1-3). The comparison of the Fourier amplitudes for the aforementioned test cases shows that the model with the smaller backfill thickness displayed the highest response of the SDOF superstructure at all frequencies. Increasing the backfill thickness significantly reduced the response. A further reduction in the response of the SDOF superstructure was observed for the case where the microgrid was present. This additional reduction in the structural response was small due to three reasons: the thicker backfill has already stiffened the system sufficiently; the relatively shallow embedment depth of the microgrid (i.e. low overburden), which did not allow the full mobilization of the resisting forces from microgrid; and the relatively low amplitude input motion, which resulted in small deformations (i.e. strains in the microgrid), which resulted in lower stiffness of the microgrid (because its stiffness is hyper-elastic, with higher stiffness for larger strains as shown in Chapter 2). Therefore, it can be expected

that the beneficial effect of the geosynthetics reinforcement would be more prominent for larger input motions with larger amplitudes and in situations with optimized backfill thickness.

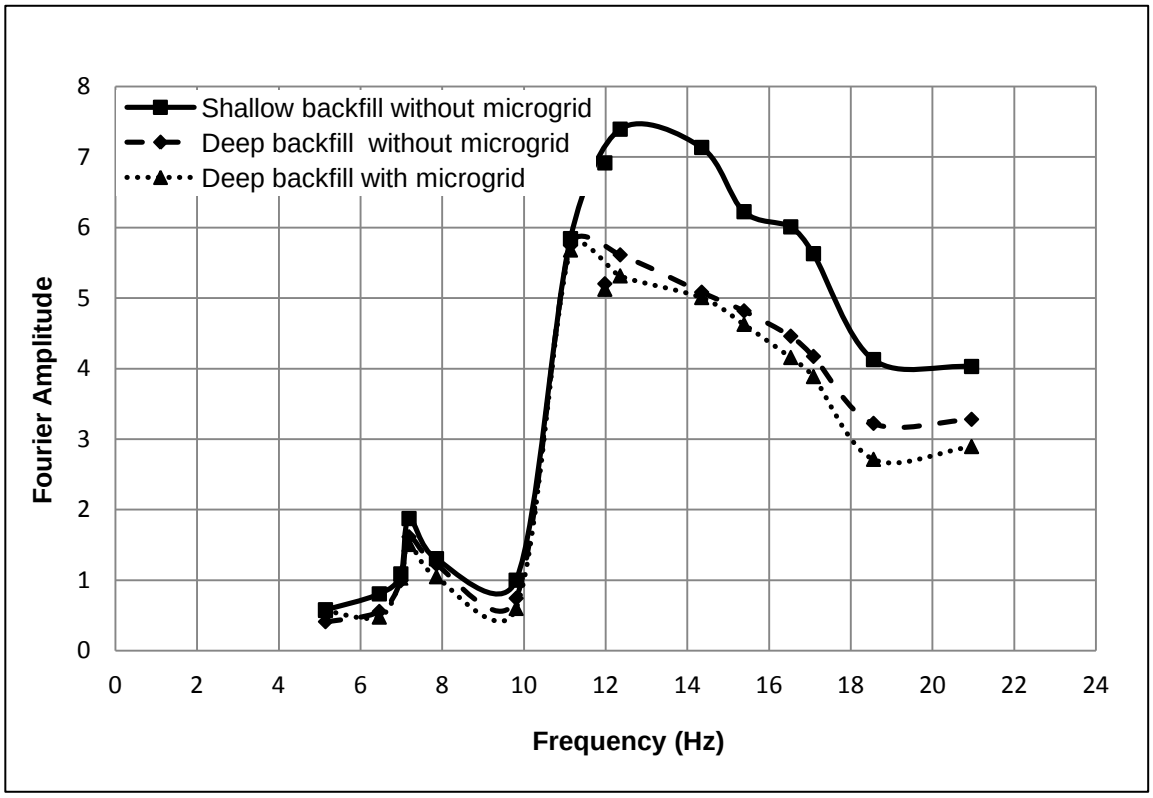

Figure 3-14: The dynamic response comparison of the low frequency SDOF superstructure (SLNF-1 to SLNF-3).

Figure 3-15 shows the Fourier amplitudes of the three test cases excited using the scaled earthquake excitation (see UPEQ-L). Despite that at low frequencies the three backfill cases contributed to almost the same response, It is can be seen that at frequencies beyond 16 Hz both increasing the backfill depth and addition of microgrid attenuated the lateral seismic response of the low frequency SDOF superstructure.

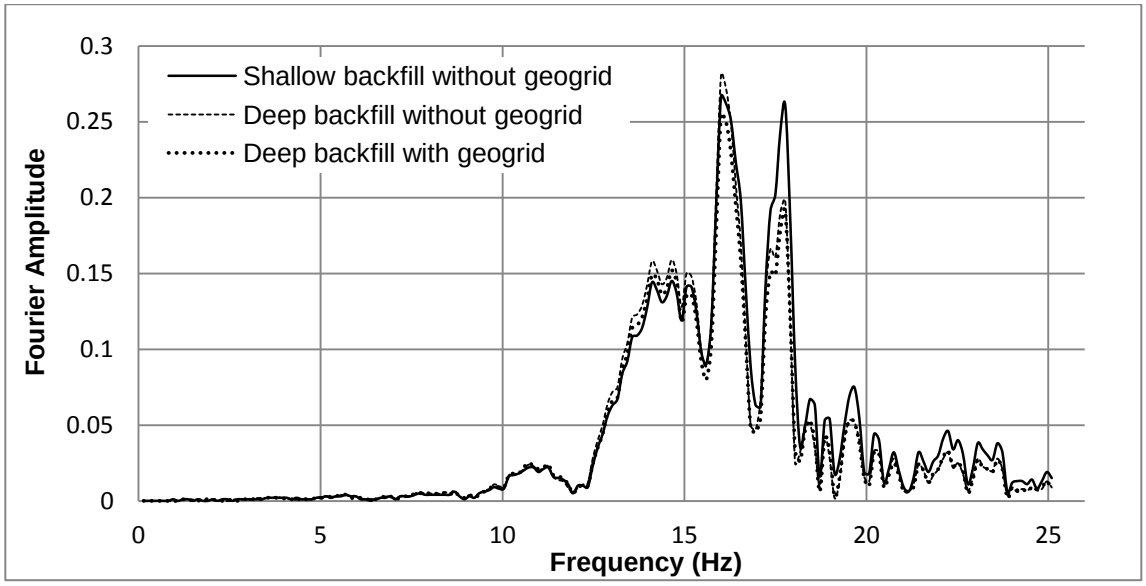

Figure 3-15: The dynamic response comparison of the low frequency SDOF superstructure (UPEQ-L).

3.4.4 High Frequency Structure Response

Figure 3-16 shows the sine sweep tests results that were carried for the HF SDOF structure system (cases SHNF-1 to 3). It can be noted from Figure 3-16 that the microgrid attenuated the response of the HF SDOF structure only slightly. The attenuation remained insignificant compared to what was achieved for the LF SDOF structure. In the sine sweep load, with constant acceleration amplitude, the lateral displacement amplitudes of the cap associated with the High frequency SDOF would be lower than the displacement amplitudes associated with the low frequency SDOF. Thus, the strains in the microgrid are lower for the high frequency SDOF structure compared to the low frequency SDOF structure. Therefore, the effect of microgrid was not noticeable in the lateral vibration of the cap connected with the high frequency SDOF structure.

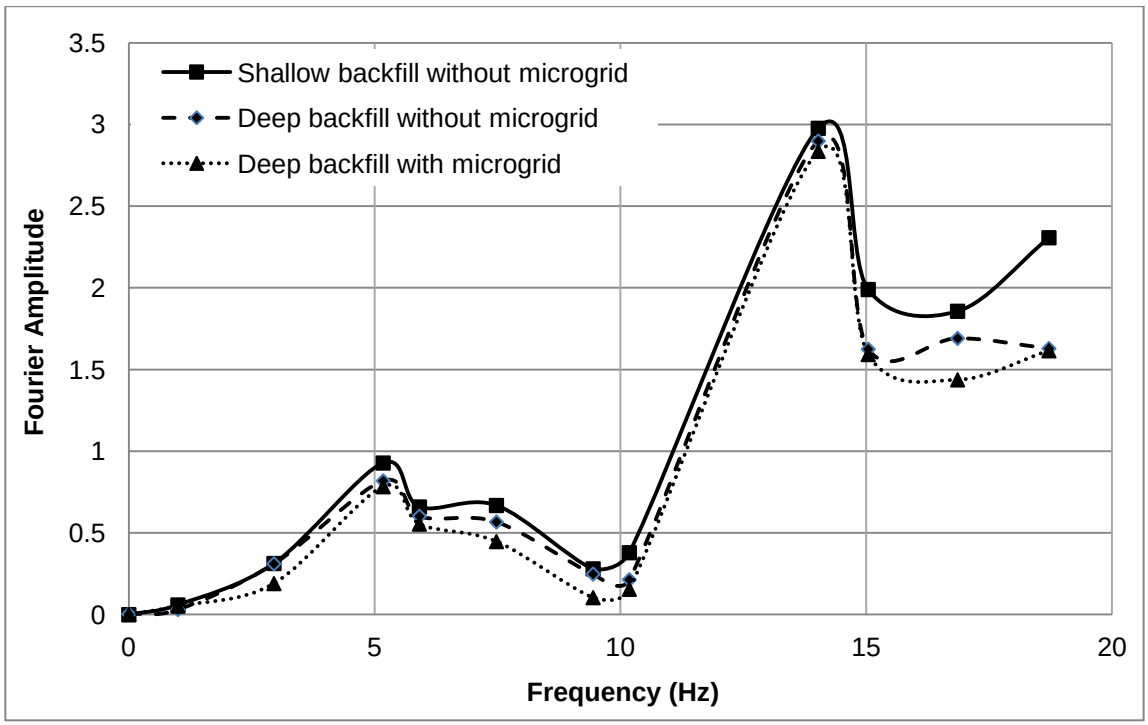

Figure 3-16: The dynamic response comparison of the high frequency SDOF (SHNF-1 to SHNF-3).

Figure 3-17 compares the Fourier amplitudes of the three backfill test cases for the scaled earthquake motion UPEQ-H. In contrast to the LF SDOF system test results, Figure 3-17 indicates that there was almost no change in the structure response due to the addition of microgrid. Comparing the results in Figures 3-15 and 3-17 indicates that the structural response of the HF SDOF structure was almost half the response of the LF SDOF system. The reduction in the response amplitudes for the HF SDOF structure resulted in reduced lateral foundation deformations, and hence reduced strains in the microgrid, i.e., it was not engaged and consequently was ineffective at this low level of lateral displacement.

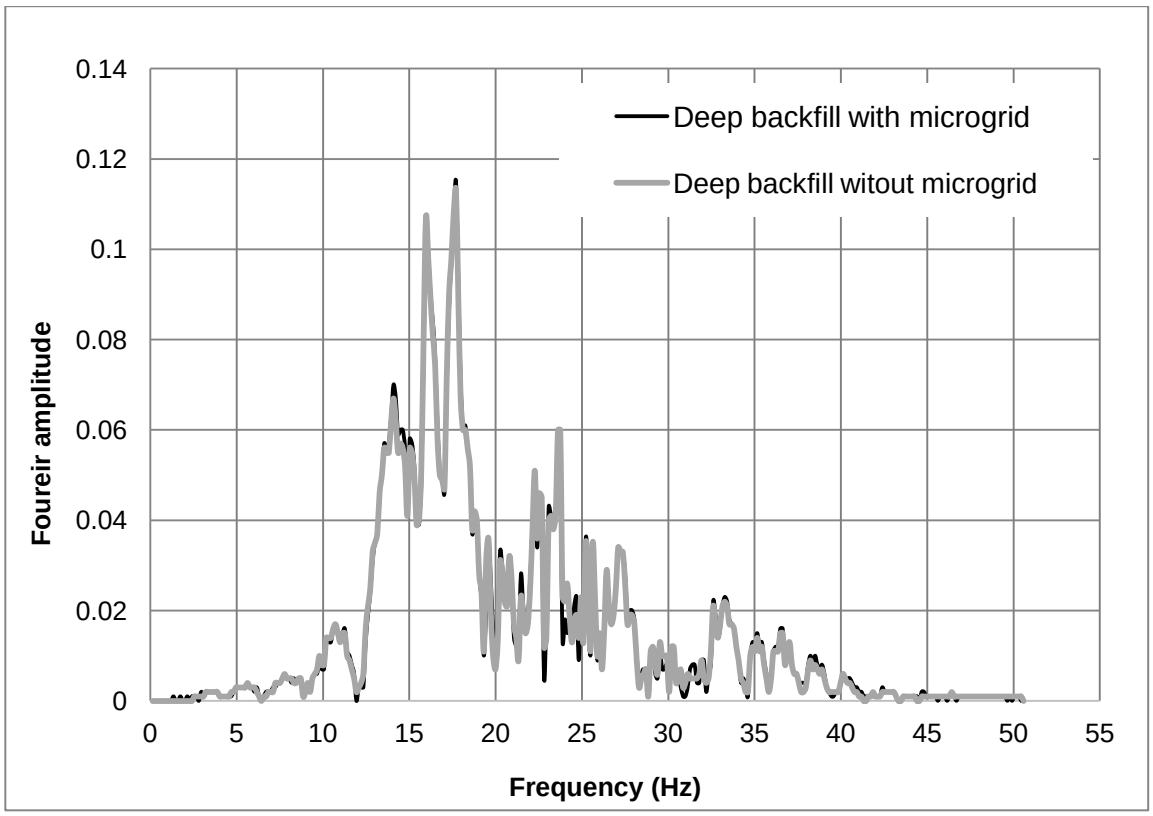

Figure 3-17: The dynamic response comparison of the high frequency SDOF structure (UPEQ-H).

3.4.5 Pile cap rocking response

Figure 3-18 shows the Fourier amplitude spectrum of the vertical acceleration response to the sine sweep signal measured at the corner of the pile cap for three test cases (SLNF-1 to 3) measured by AC9. It can be noted that the vertical acceleration amplitudes at the pile cap was attenuated as a result of adding the microgrid mesh. Figure 3-18 also shows that reducing the thickness of the backfill layer increased the response and caused lengthening in the predominant period. The sine sweep tests revealed that increasing the backfill thickness from 8 cm to 3 cm reduced the peak cap rocking motion by 15 % and the addition of microgrid reinforcement further reduced the peak rocking motion by 9 %. These results show the favourable effects of adding the microgrid mesh on the pile cap

rocking vibration mode. It also indicates that selecting a proper backfill depth is vital in controlling the rocking mode of vibration of the pile cap.

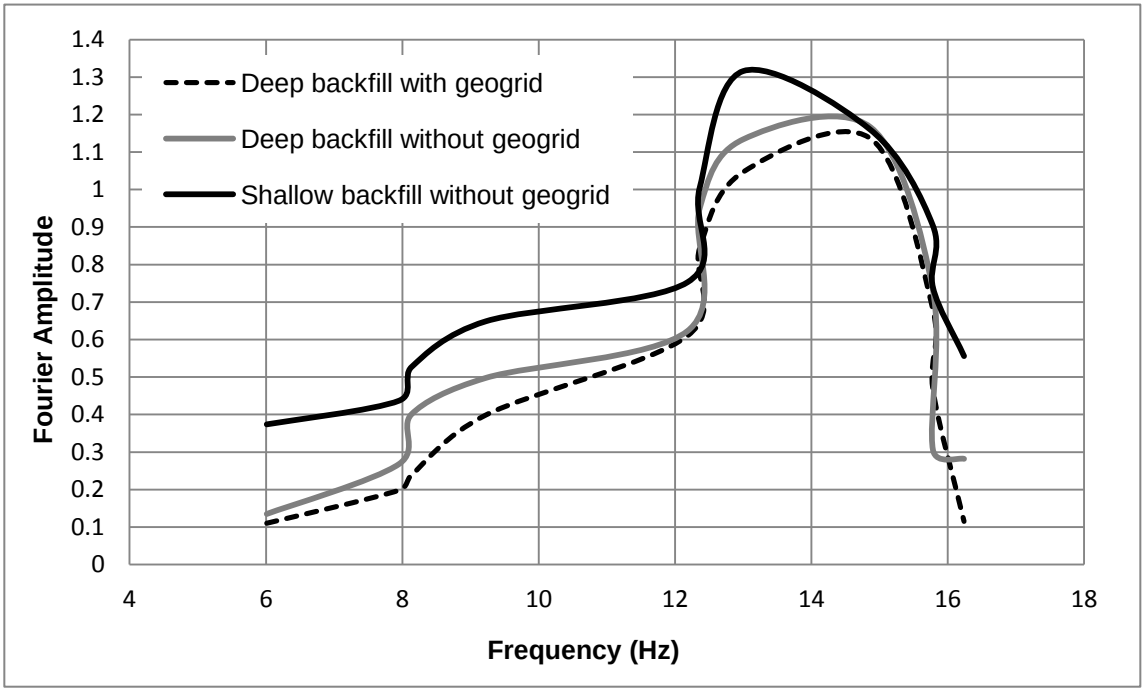

Figure 3-18: The dynamic vertical response comparison measured at the pile tip (SLNF-1 to SLNF-3).

After removing the structure, harmonic shaking tests with frequency = 16 Hz and amplitude = 0.12 g were performed (cases SAMP-1 to 4). Figure 3-19 shows the results of the harmonic signal excitation measured at the corner of the pile cap by AC9 for the cases of deep backfill with and without microgrid and the shallow backfill case. The comparison between these three cases shows that, as expected, using a thicker granular backfill attenuated the rocking vibration of the cap and hence, the vertical response. It can also be noticed that the addition of the microgrid mesh further reduced the rocking motion at the pile cap due to stiffness contribution by the microgrid mesh.

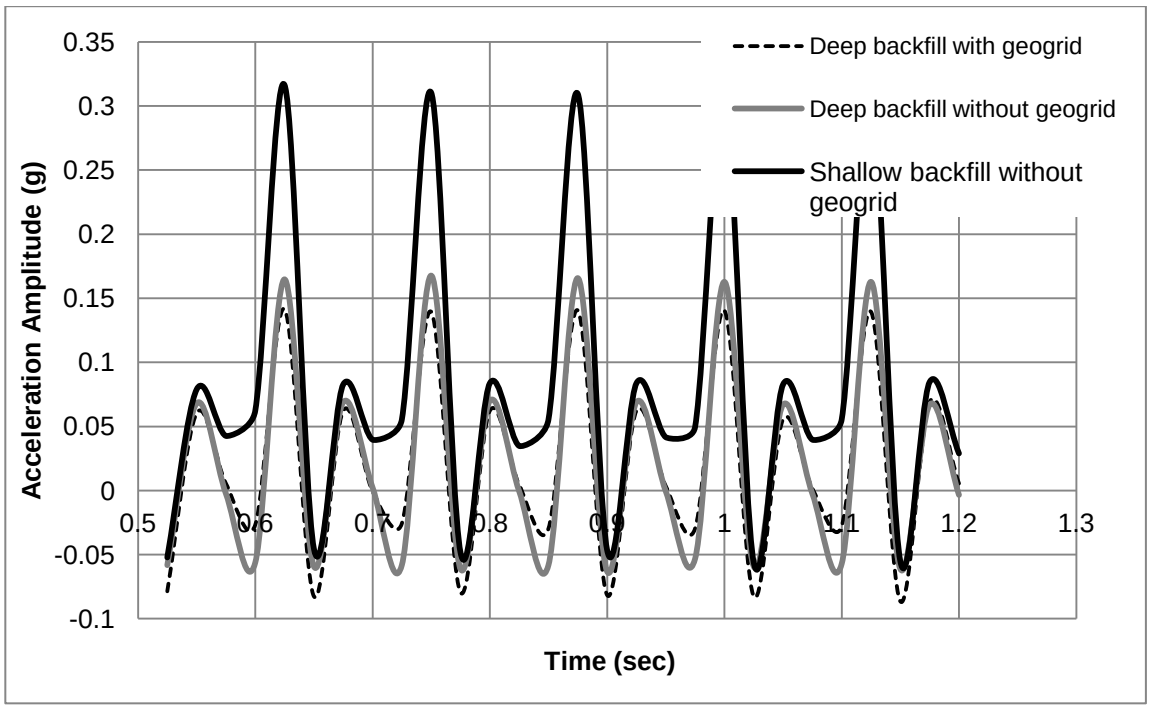

Figure 3-19: Vertical response at the pile tip comparison (SAMP-4)

3.5 Summary and conclusion

This chapter presented the results of a series of reduced scale shaking table tests performed to study the influence of geosynthetics reinforcement on the dynamic response of SDOF superstructures supported on pile foundations. The results presented here provide physical evidence to the effectiveness of the proposed foundation concept and can be used to calibrate numerical models. The following is a summary of observations made during the tests and the conclusions derived from this experimental study;

- As expected, increasing the thickness of the backfill layer reduced the ground motion amplification and the maximum dynamic response of the soil column to harmonic loading. The addition of the microgrid mesh further reduced the lateral response by 23%.
- The scaled earthquake and sine sweep tests indicated that the microgrid reinforcement resulted in reducing lateral response of the pile foundation, even for the case with thicker engineered backfill. The maximum lateral response of the pile cap decreased farther for the case of the geosynthetics-reinforced backfill.
- The lateral response of the SDOF systems to the scaled earthquake and sine sweep tests decreased for the case of microgrid-reinforced backfill. The sine sweep tests results indicated that the thick backfill reduced the maximum lateral response of the low frequency SDOF structure and the microgrid reinforcement reduced it further. The effectiveness of the microgrid reinforcement in reducing the dynamic response was more pronounced at higher inertial interaction associated with the low frequency SDOF due to the larger dynamic loads associated with larger deformations in the microgrid.
- The rocking vibrations of the pile cap due to the sine sweep tests and harmonic loading were reduced due to the geosynthetics reinforcement. The sine sweep tests revealed that increasing the backfill thickness from 3 cm to 8 cm reduced the peak cap rocking motion by 15 % and the addition of microgrid reinforcement further reduced the rocking motion by 9 %.

References

[1] Bathurst RJ, Alfaro MC. 1996. Review of seismic design, analysis and performance of geosynthetic rein- forced walls, slopes and embankments. International Symposium on Earth Reinforcement, keynote lecture, Kyushu, 1996. p. 23-52.

[2] Cai, Z., and Bathurst, R.J. 1995. Seismic response analysis of geosynthetic reinforced soil segmental retaining walls by finite element method. Computers and Geotechnics, **17** (4), 523-546.

[3] El-Emam, M.M., Bathurst, R.J. 2007. Influence of reinforcement parameters on the seismic response of reduced-scale reinforced soil retaining walls. Geotextiles and Geomembranes, **25** (1), 33-49.

[4] El-Emam, M. M., and Bathurst, R.J. 2004. Experimental design, instrumentation and interpretation of reinforced soil wall response using a shaking table. International Journal of Physical Modelling in Geotechnics, **4**, 13-32.

[5] Gohl, W. 1991. Response of pile foundations to simulated earthquake loading: experimental and analytical results, Ph.D. Dissertation, Univ. of British Columbia.

[6] Helwany, S.M.B., Budhu, M., and McCallen, D. 2001. Seismic analysis of segmental retaining walls. I: Model verification. Journal of Geotechnical and Geoenvironmental Engineering, **127** (9), 741-749.

[7] Iai, S., 1989. Similitude for shaking table tests on soil-structure-fluid models in 1 g gravitational field. Soils and Foundations, **29** (1), 105–118

[8] Koseki,J., Munaf, Y., Tatsuoka, F., Tateyama, M., Kojima, K. and Sato, T. 1998. Shaking and tilt table tests of geosynthetic-reinforced soil and conventional-type retaining walls. Geosynthetics International, **5** (1), 73-96.

[9] Kubo, K. 1965. Experimental study of the behaviour of laterally loaded piles. Proceedings of the 6th International. Conference on Soil Mechanics and Foundation Engineering, Montreal, Vol. 2, 275-279.

[10] Liu, H. and Chen, K. 1991. Test on behavior of pile foundation in liquefiable soils, Proceedings of the 2nd International Conference on Recent Advances in Geotechnical Engineering and Soil Dynamics, St. Louis, Vol.1, 233-235.

[11] Liu, H.L., Ng, C.W.W., and Fei, K. 2007. Performance of a geogrid-reinforced and pile-supported highway embankment over soft clay: Case study. Journal of Geotechnical and Geoenvironmental Engineering, **133** (12), 1483-1493.

[12] Liu, H. 2009. Analyzing the reinforcement loads of geosynthetic-reinforced soil walls subject to seismic loading during the service life. Journal of Performance of Constructed Facilities, **23** (5), 292-302.

[13] Makris, N., Tazoh, T., Yun, X., and Fill, A. 1997. Prediction of the measured response of a scaled soil-pile-superstructure system. Soil Dynamics and Earthquake Engineering, **16**, 113-124.

[14] Matsumo, O., Tsutsumi, T., Yokoyama, K. and Saito, Y. 1998. Shaking table tests and analysis of geosynthetic-reinforced soil retaining walls. Geosynthetic International, **5** (1-2), 97-126.

[15] Meymand, P. 1998. Shaking table scale model tests of nonlinear soil-pile-superstructure interaction in soft clay, Ph.D. Dissertation, University of California, Berkeley.

[16] Michalowski R L. 1998. Soil reinforcement for seismic design of geotechnical structures. Computers and Geotechnics, **23** (1-2), 1-17.

[17] Rocha, M. 1957. The possibility of solving soil mechanics problems by the use of models. Proceedings of 4th International Conference of Soil Mechanics and Foundations Engineering, Vol.1 pp, 183-188.

[18] Sakaguguchi, M., Muramatsu, M. and Nagura, K. 1992. A discussion on reinforced embankment structures having high earthquake resistance". Proceedings of the

International Symposium on Earth Reinforcement Practice, IS-Kyushu'92, Ochiai, Hayashi and Otani (Editors), Fukuoka, Japan, pp. 287-292.

[19] Sreerama, K. 1993. Dynamic pile-soil-pile interaction using model tests under simulated earthquakes. Ph.D. Dissertation, University of Missouri-Rolla, MO.

[20] Tao, X., Kagawa, T., Minowa, C., and Abe, A. 1998. Verification of dynamic soil-pile interaction". Proceedings of the 3rd Conference on Geotechnical Earthquake Engineering and Soil Dynamics, ASCE, Seattle, 1199-1210.

[21] Tatsuoka, F., Sakamoto, M., Kawamura, T., and Fukushima, S. 1986. Strength and deformation characteristics of sand in plane strain compression at extremely low Pressures. Soils and Foundations, **26** (1), 65-84.

[22] Turan, A., Hinchberger, S.D., El Naggar, M.H. (2009a). Mechanical characterization of an artificial clay. Journal of Geotechnical and Geoenvironmental Engineering, **135** (2), 280-290.

[23] Turan, A., Hinchberger, S.D., El Naggar, M.H. (2009b). Design and commissioning of a laminar soil container for use on small shaking tables. Soil Dynamics and Earthquake Engineering, **29** (2), 404-414

[24] Yan, L., Byrne, P., and Dou, H. 1991. Model studies of dynamic pile response using hydraulic gradient shaking table tests. Proceedings of the 6th Canadian Conference of Earthquake Engineering, Toronto, 335-342.

Chapter 4

4. NUMERICAL STUDY ON THE DYNAMIC LATERAL BEHAVIOR OF GEOSYNTHETICS-REINFORCED PILE FOUNDATION SYSTEM

This chapter presents the finite-element (FE) analysis for simulating the dynamic performance of geosynthetics-reinforced pile foundation system. The (FE) models were established using the program Plaxis 3D (Brinkgreve et al., 2012). The numerical models were verified against the shaking table test results of a model scale geosynthetics-reinforced pile foundation system as described in Chapter 3. A parametric study was carried out to investigate the effect of different design parameters on the effectiveness of the proposed geosynthetics-reinforced pile foundation system. These parameters included: the frequency and amplitude of ground motion; the stiffness and strength of the geosynthetic reinforcement, the location of the reinforcement within the backfill material and the thickness of the backfill material. The numerical results indicated that the geosynthetic-reinforcement greatly reduced the maximum lateral response of the pile cap connected with the low frequency single degree of freedom structural model.

4.1 Introduction and problem overview

Geosynthetics are polymeric material consisting of tensile ribs with openings of sufficient size to allow interlocking with the surrounding soil. This geosynthetics-soil interlocking mechanism allows the geosynthetics to work as a reinforcement element, which enhances the soil shear strength. The geogrid mesh is laid within the aggregate engineered fill provides increased modulus and lateral confinement for the crushed stones intruding the apertures of the geogrid. Therefore, geosynthetics have been widely used in modern construction technology. Several application examples include geogrid reinforced earth retaining walls (GRS), highway construction and expansion over soft soils, geogrid-reinforced pile-supported highway embankments and geogrid reinforced slopes. In these applications, geogrids have been widely implemented to reduce lateral

wall deflections arising from dynamic loads and uneven settlement of the supporting sub grades and embankments.

Due to the rising concerns in the construction industry with regards to mitigating the destructive effects of cyclic earthquake loads, several researches investigated the use of geogrid-reinforced soils to enhance the seismic resistance of geotechnical structures. These studies include: Bathurst and Alfaro (1996); Cai and Bathurst (1995); Michalowski (1998); Helwany et al. (2001); Ling et al. (2004); Christopher (2004); Liu (2009); El-Emam and Bathurst (2007); and Fakharian and Attar (2007). These studies collectively demonstrated the superior performance of geogrid-reinforced walls to resist lateral dynamic loading and provided verified finite element numerical models to analyze the dynamic behavior of these walls.

In parallel, several researches investigated the seismic pile-soil interaction problem through experimental and numerical studies. Several investigators such as Yegian and Wright (1973), Angelides and Roesset (1980), Randolph (1981), Faruque and Desai (1982), Trochanis at al. (1988, 1991) Wu and Finn (1997), and Bentley and El Naggar (2000) developed finite element models to analyze the dynamic response of piles. These researches proved that the finite element method is a powerful tool for analyzing the soil-pile-structure interaction (SSPSI) problem.

Pile foundations are typically used when the ground conditions near the surface cannot support the structural loads. In these situations, piles are used to transfer the loads to more competent soil layers at larger depths below the ground surface. In many cases, these foundations are subjected to significant lateral loads due to seismic or wind loading. However, the weak subsurface conditions that dictate the use of pile foundations result in low lateral foundation resistance, which poses a challenge to design engineers. Conventional solutions involve either ground improvement techniques (e.g. jet grouting, vibro compaction, etc.) or ground replacement for a substantial depth of the weak surficial soil. These solutions are typically expensive and cause significant construction delays.

This chapter introduces the dynamic analysis of an innovative use of geosynthetics, where geogrid is used to enhance the lateral resistance of pile foundations. The shaking table tests carried out to investigate the behavior of a model geogrid-pile foundation system were used to calibrate a finite element model developed using the program Plaxis-3D, which was then used to conduct a parametric study. The results of the parametric stud are presented and discussed herein.

4.2 Shaking table test description

The numerical model developed in this research was calibrated using the results of shaking table tests. Figure 4-1 shows a schematic diagram of the shaking table test setup that include: i) the soil model; ii) the laminar box (soil container); and iii) the shaking table and, iv) the geogrid-pile foundation model.

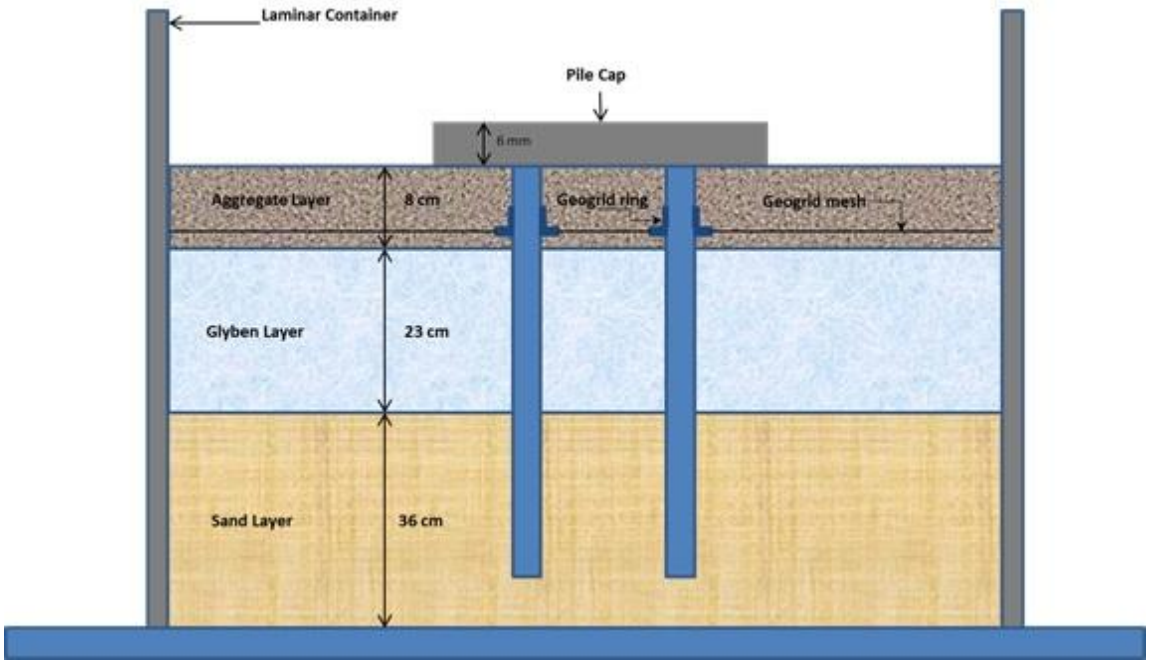

Figure 4-1: The schematic of the shaking table test setup

Figure 4-1 shows three layers of soil from bottom to top: i) a silty sand to represent underlying soil layer; ii) a synthetic soil layer (modified glyben) to simulate soft clay

soil; and iii) coarse aggregate with relatively small sizes to represent a backfill of course grained soil. Modified glyben provide favourable characteristics for scaled physical model tests (Turan et al., 2009). The initial bedding layer of the model soil column was backfilled inside the box using layers of sand. Then, blocks of soft modified glyben were placed over the last sand layer and were compacted using a drop hammer to form a uniform soft clay layer. Finally, the aggregate backfill was compacted using the same drop hammer.

The shaking table was excited using a harmonic base motion with frequency = 16 Hz and amplitude = 0.06 g. The frequency of this harmonic signal is the scaled model frequency of an excitation frequency of 3.6 Hz using a geometric scaling factor of 20. Figures 4-2 and 4-3 show the input motion time history and Fourier spectra. Figure 4-4 shows the pile cap acceleration response for the case of geogrid-reinforcement embedded in the top aggregate layer.

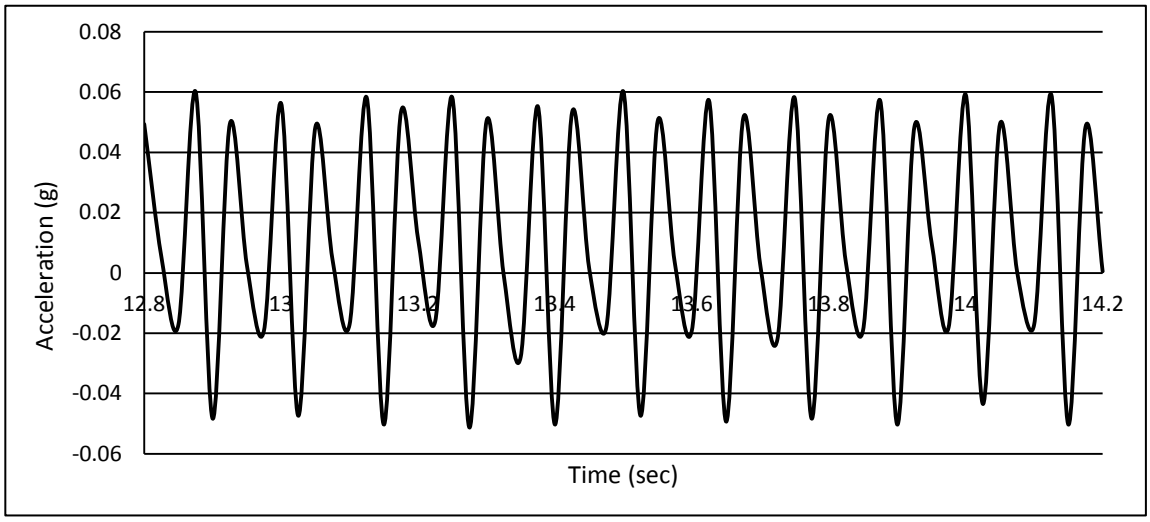

Figure 4-2: Input motion acceleration time history used in the shaking table test

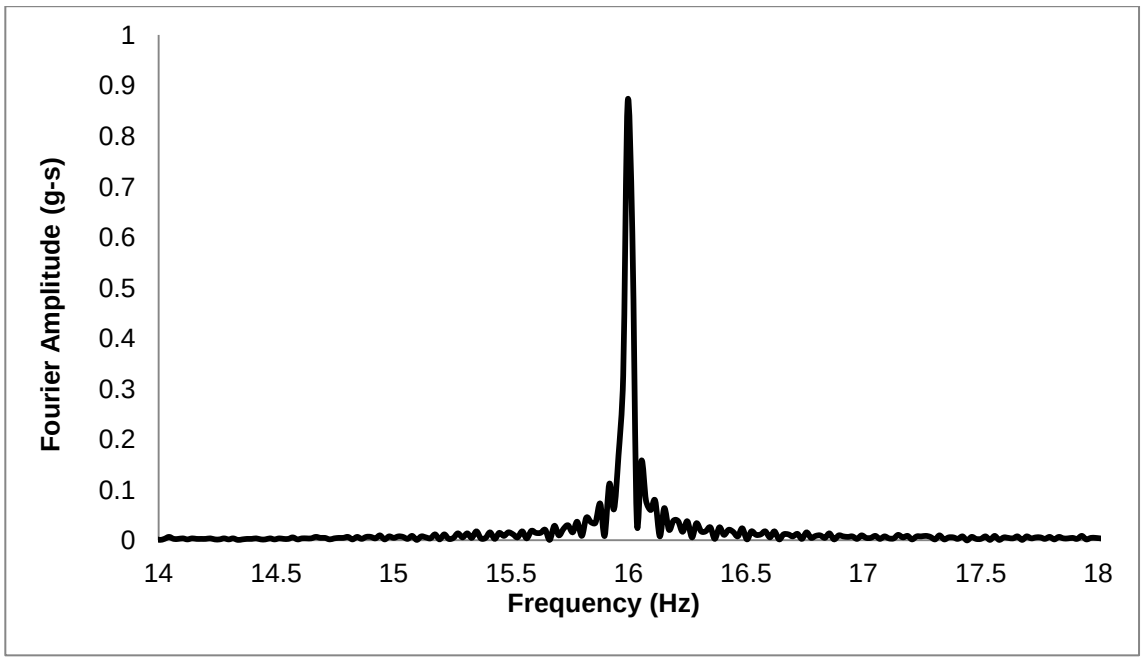

Figure 4-3: Fourier spectrum of the input motion used in the shaking table test

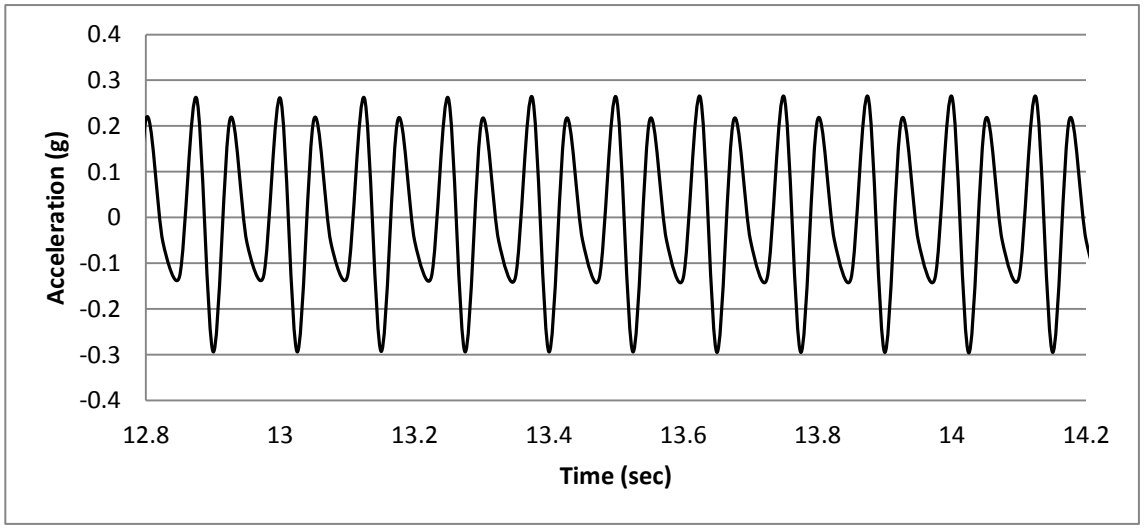

Figure 4-4: Pile cap acceleration response

4.3 The numerical model

4.3.1 Problem dimensions

Figure 4-5 shows the piles, the geogrid connectivity and pile cap dimensions. The model pile cap was fabricated from aluminum block with dimensions 200mmx200mm x6mm, representing a prototype concrete pile cap of dimensions 4.00x4.00x0.7m. The model piles were fabricated of four acrylic tubes 600 mm long and 20 mm in diameter, representing steel piles 12 m long and 380 mm in diameter. These piles were rigidly connected to a pile cap. Four plastic rings were fabricated and installed to connect the microgrid mesh to the piles. The microgrid mesh was extended and affixed to the rings using four steel bolts. Rings were fixed in their vertical position using a plastic bolt. The microgrid mesh had a stiffness of 110 kN/m at 2% strain, representing a prototype geosynthetic material (e.g. polymer strips) with stiffness of 44,000 kN/m.

Figure 4-6 shows the 3D finite element model of the geosynthetic pile foundation composite system. This model simulated the dimensions of the real soil column, geogrid, pile and cap dimensions of the shaking table test setup. The soil column consisted of a soft glyben layer sandwiched between an aggregate layer from top and a bedding sand layer. The geogrid mesh was introduced within the aggregate layer at a depth of 3.5 times the pile diameter (i.e. 66 mm).

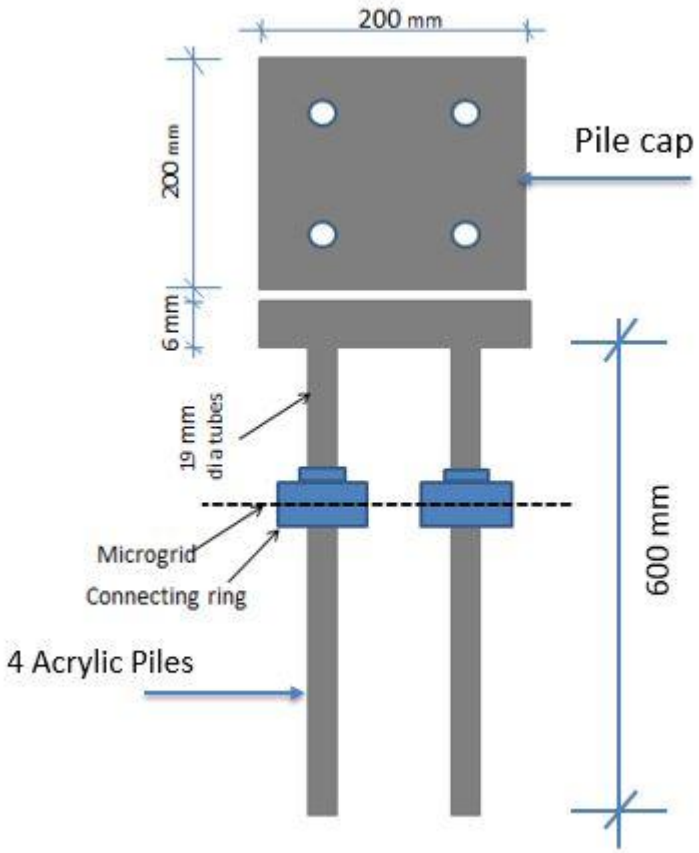

Figure 4-5 : Model pile foundation and microgrid connectivity

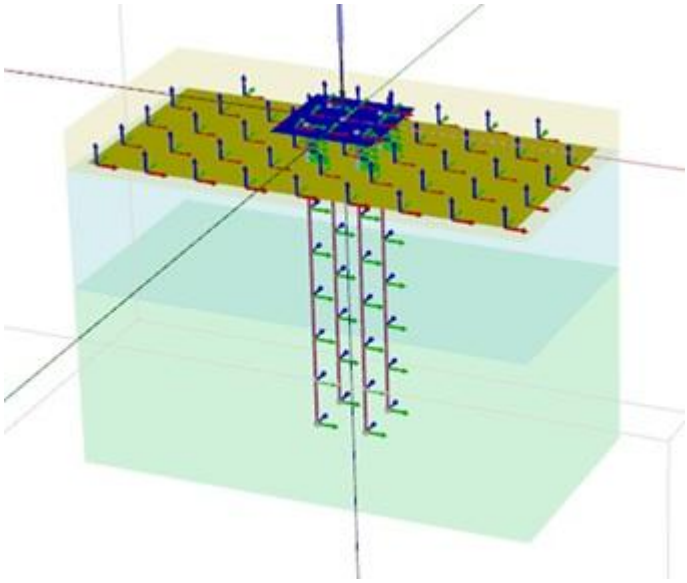

Figure 4-6: 3D FE model of geosynthetic reinforced pile-cap system

4.3.2 Interface conditions

During the shaking table test, it was noticed that relative movement of the pile cap with respect to the top aggregate layer had occurred. This behaviour was modeled using interface elements at the bottom of the pile cap with reduced pile cap-soil interface strength that was assumed to be 1 % of the soil strength. In contrast, the interlock behaviour, which is expected to occur at the geogrid-aggregate interface was modeled with nodal deformation compatibility which constrains the relative translation between the geogrid mesh and the surrounding soil (Brinkgreve et. al, 2012). To facilitate these two modeling procedures, the aggregate layer was split into two layers 3 cm and 5 cm in which the reduced interface strength was allocated to the top layer and the rigid interface layer was assumed at the bottom.

4.3.3 Material models and parameters:

The following section presents the description of the material models used in the dynamic numerical analysis and the methodology followed to obtain the engineering parameters that were used in these models.

4.3.3.1 Linear elastic soil model and parameters

The stress strain behavior of the bottom sand layer was simulated as a liner elastic soil model to reduce the computational effort and time. This is justified since non-linearity was not expected to occur in this layer due to its relatively high strength and stiffness, and the relatively low shaking excitation amplitude applied and the associated small strain amplitude experienced. Figure 4.7 provides the stress-strain hysteretic loop calculated at a soil element within the sand layer indicating a maximum strain of 0.006% ($6x10^{-5}$), which is considered to be small strain and the soil stiffness can be represented by the low strain shear modulus (i.e. maximum shear modulus, G_{max}). The angle of internal friction and shear modulus parameters of the sand layer was obtained via laboratory direct shear tests. The sand (and aggregate) shear modulus were evaluated using the equation proposed by Seed and Idriss (1970), i.e.:

$$G_0 = 1000\ K_{2max}\ (\sigma'_m)^{0.5} \qquad [1]$$

where:

G_0 is the maximum (low strain) shear modulus in (psf)

K_{2max} is the shear modulus number for the soil = 50 for loose sand and 75 for dense sand

σ'_m is the mean effective confining stress of the soil in psf

The shear wave velocity can then be calculated as,

$$V_s = \sqrt{\frac{G_o}{\rho}} \qquad [2]$$

Table 4-1: Model granular Soil parameters

Parameter	Sand
Unit weight, (kN/m^3)	17.35
Relative density Dr (%)	80
Vsm (m/s)	50
ϕ_{peak}	40
G_{max} (kPa)	4427
Poisson's ratio (ν)	0.3
Damping ratio %	2

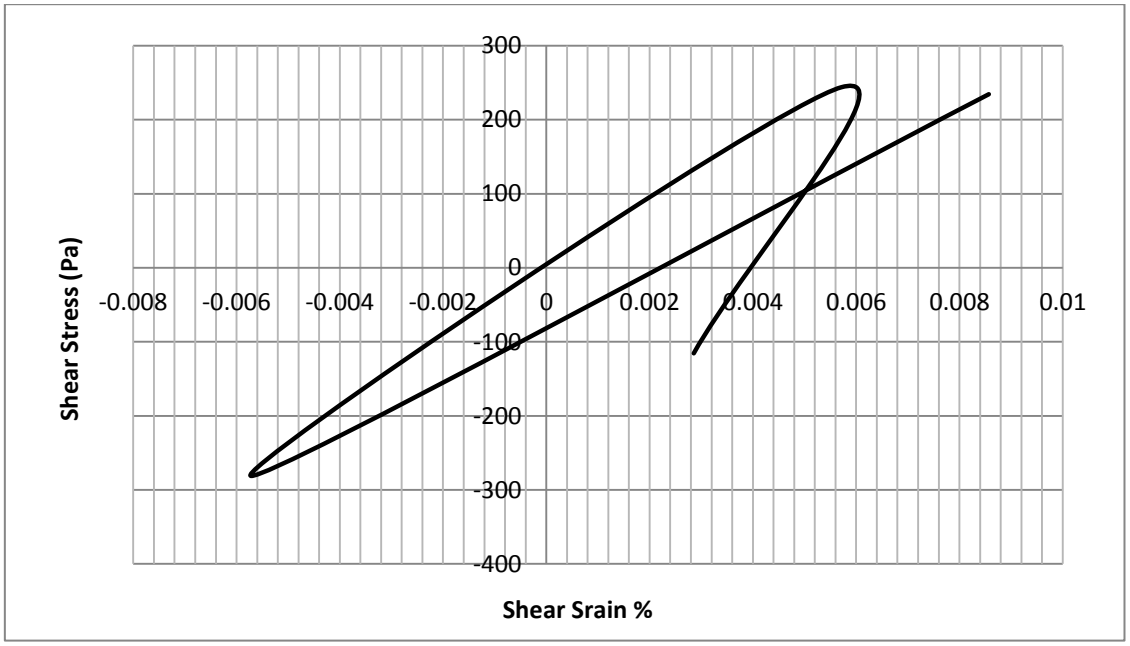

Figure 4-7: Typical sand shear stress-strain loop (calculated from the shaking table tests).

4.3.3.2 Nonlinear soil model and parameters

In contrast to the sand layer, it was expected that the aggregate and glyben layers would undergo nonlinear stress-strain behavior due to the significant amplification of the input motion and the relatively lower strength and stiffness of the two layers due to reduced overburden pressure. Figures 4.8 and 4.9 provide the stress-strain hysteretic loops calculated at soil elements within the aggregate and glyben layers, respectively, indicating maximum strains of 0.05% ($5x10^{-4}$) and 0.025% ($2.5x10^{-4}$), which are considered to be relatively high strain and the soil stiffness should be represented by shear modulus corresponding to the strain level. Therefore, the nonlinear stress-strain behaviors of the aggregate and glyben layers were modeled using the Plaxis built-in Hardening Soil (HS) model with small strain stiffness (HSSMALL model).

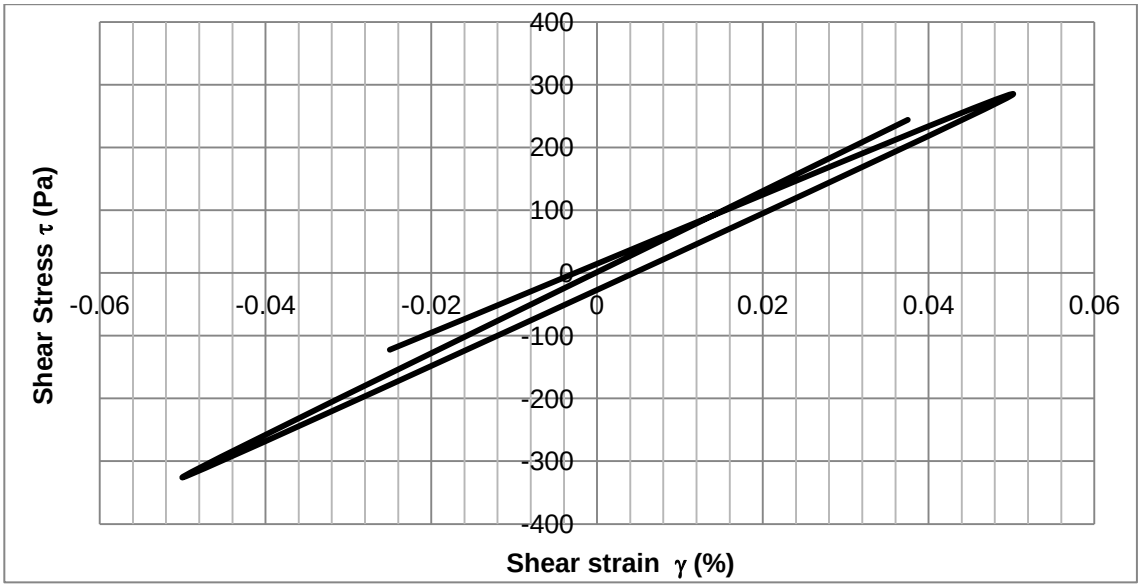

Figure 4-8: Typical aggregate shear stress-strain loop (calculated from the shaking table tests).

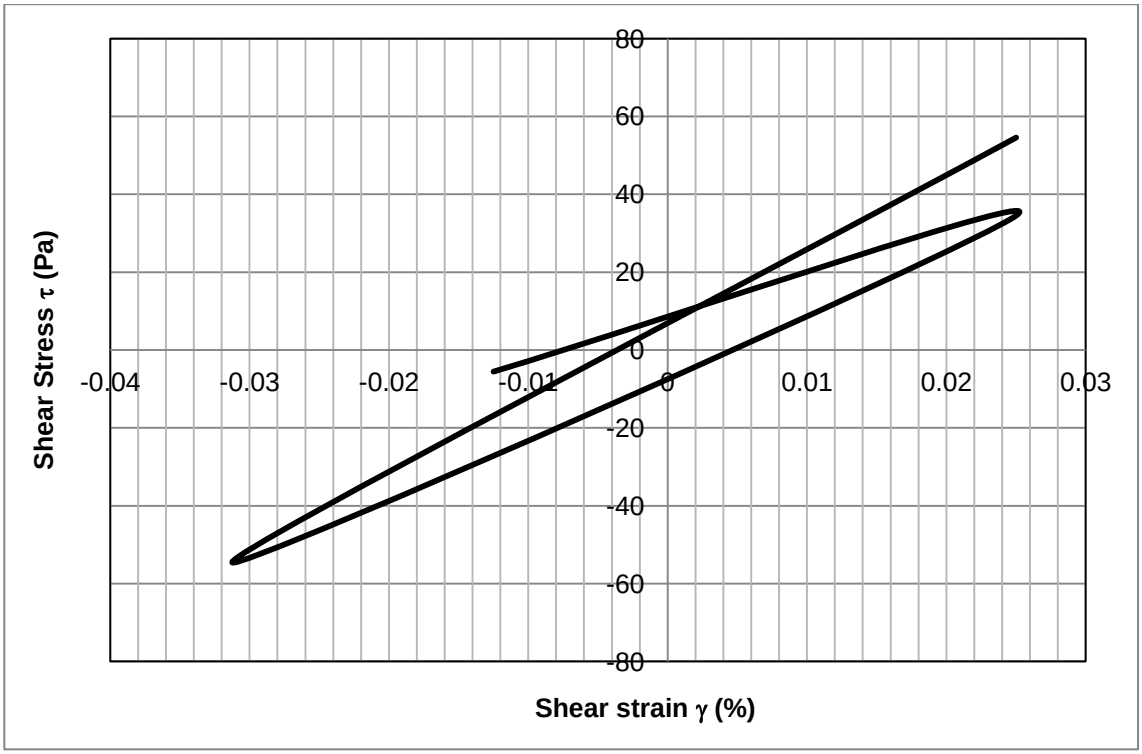

Figure 4-9: Glyben shear stress-strain loop (calculated from the the shaking table tests).

The Plaxis (HSSMALL) model accounts for the stiffness degradation for different types of soils when subjected to primary deviatoric loading (Brinkgreve et al., 2012). Simultaneous irreversible plastic strains develop in soils during deviatoric loading causing the yield surface to change in size. In contrast to the elastic perfectly-plastic soil models, the yield surface of the HS model expands due to plastic straining and varies in the principle stress space. Also, the HS model captures the variation of the plastic axial strain with the deviatoric stress by using the theory of plasticity rather than the theory of elasticity and introducing a yield cap. The granular soil dilatancy is also considered in the HS model. The model is characterized by stress dependent stiffness according to power law, i.e., the unloading-reloading Young's modulus is given by:

$$E_{ur}^{ref} = E_{ur} / \left(\frac{c\cos\varphi - \sigma_3' \sin\varphi}{c\cos\varphi + P^{ref} \sin\varphi} \right)^m \quad [3]$$

where, E_{ur}^{ref} is the reference soil elastic modulus , and the cohesion (c), angle of internal friction (ϕ) are the soil effective strength parameters; P^{ref} is the reference confining stress taken at 100 kPa; σ_3': is the confining stress calculated at the mid depth of the clay layer; and m is an exponent taken as 1 for soft clay.

The plastic straining due to primary deviatoric loading is represented by the reference secant stiffness in standard drained triaxial test, E_{50}^{ref}, and the plastic straining due to primary compression is represented by the reference tangent stiffness for primary odometer loading, E_{eod}^{ref}. E_{50}^{ref} can be estimated as a fraction of the soil elastic modulus, E_{ur}^{ref} using the relation:

$$E_{50}^{ref} = E_{ur}^{ref}/3 \qquad [4]$$

while, E_{oed}^{ref} is estimated as a fraction of E_{50}^{ref}, i.e.:

$$E_{oed}^{ref} = E_{50}^{ref}/1.25 \qquad [5]$$

The elastic unloading / reloading is described by the reference soil elastic modulus E_{ur}^{ref}, and Poisson's ratio (ν_{ur}). Finally, the shear strength is evaluated according to the Mohr-Coulomb failure criterion in terms of the strength parameters cohesion (c), angle of internal friction (ϕ) and dilatancy angle (ψ).

The basic equation of the HS model is the hyperbolic relation between the vertical strain, ε_1, and the deviatoric stress, q, in primary triaxail loading is formulated as:

$$-\varepsilon_1 = \frac{1}{E_i}\frac{q}{1-q/q_a} \quad \text{for} \quad q < qf \qquad [6]$$

The hyperbolic relation can be visualized in figure 4-10 as follows:

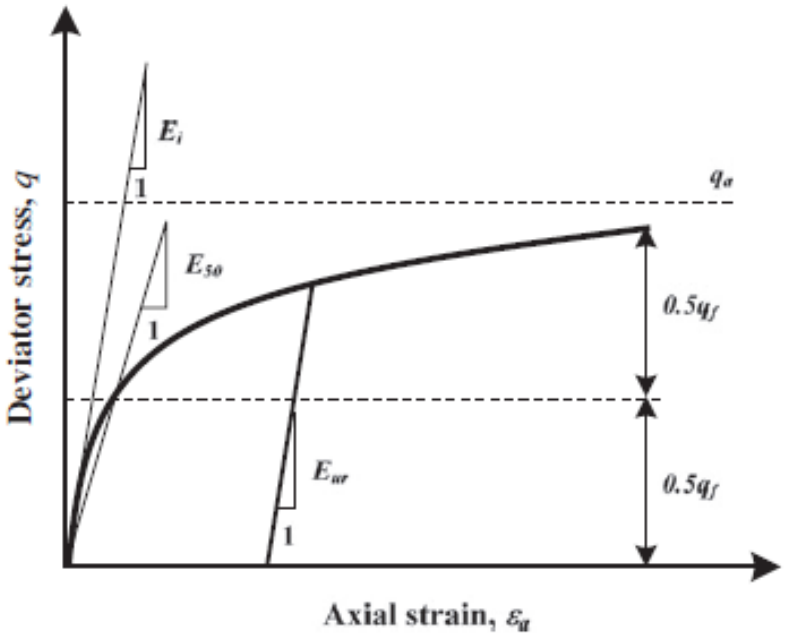

Figure 4-10 : Hyperbolic stress-strain relationship in primary loading for a slandered drained triaxial test (Schanz et al., 1999)

Where

E_i: is initial stiffness

$$Ei = \frac{2E_{50}}{2-R_f} \qquad [7]$$

q: is the current shear stress

q_a: is the asymptotic value of the shear stress

q_f: is the ultimate diviatoric stress , where:

$$q_f = (c \cot \varphi - \sigma_3') \frac{2 \sin \varphi}{1-\sin \varphi} \qquad [8]$$

$R_f = q_f / q_a$

In the cyclic loading applications, the HS model is limited to the assumption that soil undergoes elastic loading and reloading behavior with no hysteretic damping. Some of the limitations of the HS model in dynamic applications can be resolved by using the HS-Small Strain (HSSMALL) model. The HSSMALL model accounts for soil stiffness at

small strain and non-linear degradation at large strain levels (Brinkgreve et al., 2012). The HSSMALL model uses the Hardin and Drenvich (1972) hyperbolic law to relate the shear modulus at large strains to small-strain properties. The Hardin and Drenvich (1972) hyperbolic law is formulated as:

$$\frac{G_s}{G_0} = \frac{1}{1+\left|\frac{\gamma}{\gamma_r}\right|} \quad [9]$$

where the threshold strain γ_r is given by:

$$\gamma_r = \frac{\tau_{max}}{G_0} \quad [10]$$

Hence, in order to generate stiffness modulus reduction curve that covers the range of soil stiffness from the low strain value (i.e. dynamic stiffness, G_0) to the observed hysteretic behaviour, two more parameters are required:

- The initial or very small-strain shear modulus, G_0.
- The shear strain parameter $\gamma_{0.7}$ at which the secant shear modulus is reduced to about 70% of G_0.

Evaluation of the nonlinear soil model parameters for glyben layer:

Surarak et.al (2012) carried out comprehensive triaxial and odometer testing on Bangkok soft clay to determine its Hardening Soil model parameters E_{oed}^{ref}, E_{50}^{ref}, and E_{ur}^{ref}.The obtained parameters were used to calibrate a Plaxis triaxial test model. The research revealed that the experimental stress strain curves were comparable with the Plaxis curves. Therefore, the HS model parameters of the soft Bangkok clay were adopted in this numerical calibration with undrained (B) analysis (Brinkgreve et al, 2012). Glyben undrained shear strength value was obtained from the average measured undrained shear strength c_u.

The shear modulus at a given shear strain level is obtained using Equation [9] and the shear strain parameter $\gamma_{0.7}$ was estimated from the shear modulus degradation curve of modified glyben at $G/G_{max} = 70\ \%$,as shown in Figure 4-11 (Turan et al., 2009b).

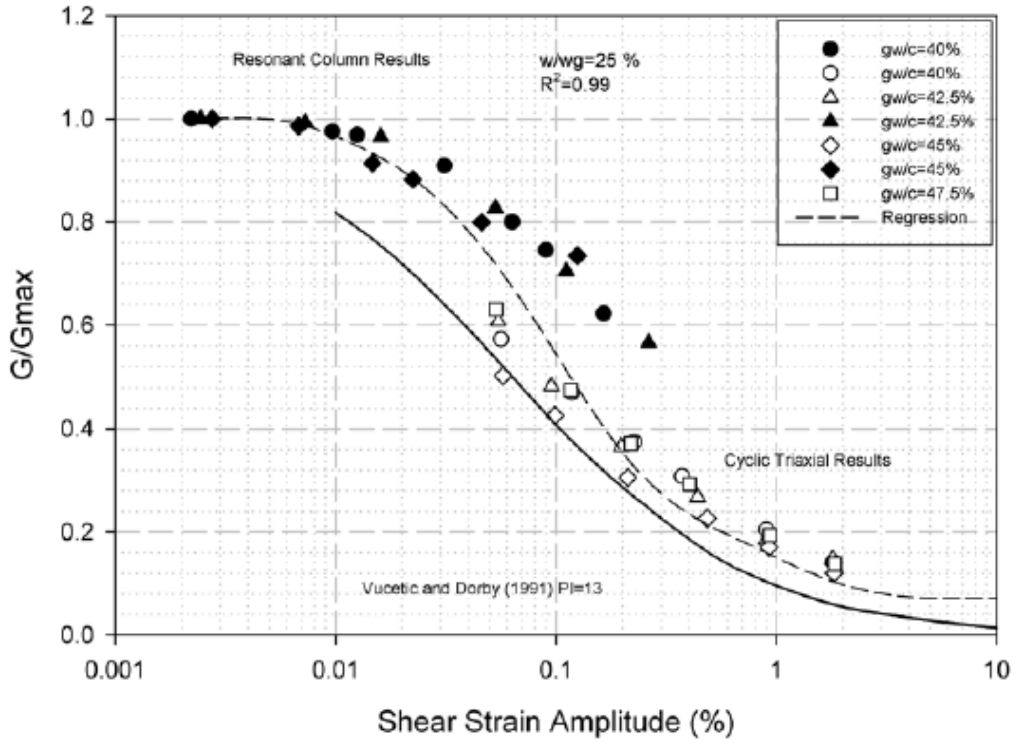

Figure 4-11: Stiffness degradation for modified glyben (Turan et al., 2009a)

Evaluation of the nonlinear soil model parameters for aggregate layer:

In this research the HS small strain model parameters for the aggregate layer were calculated as follows. Instead of running traxial tests, the low strain shear modulus, G_0, was calculated using Equation [1]. In order to reflect the difference in overburden pressure, the aggregate layer was subdivided into two sub-layers: top layer (above geogrid); and bottom layer (below geogrid). HSSMALL stiffness parameters were estimated based on the static shear modulus G_{static} . The G_{static} was estimated as 10% of G_o and the soil elastic modulus E_{ur} is calculated as $2G_{static}(1+\nu)$. Knowing E_{ur} and estimating the confining stress σ_3 from:

$$\sigma_3 = K_o \sigma_v \qquad [11]$$

Where

$K_o = 1\text{-}\sin\varphi$ [12]

$\sigma_v = \gamma_{soil}\, h$ [13]

The reference unloading reloading Young's modulus E_{ur}^{ref} was calculated using Equation [3]. The angle of friction of aggregate was measured as 50º (Appendix A). Then, E_{50}^{ref} and E_{oed}^{ref} were calculated from Equations [4] and [5] respectively. G_0^{ref} was estimated from the following equation:

$$G_0^{ref} = G_0 / \left(\frac{c\cos\varphi - \sigma_3' \sin\varphi}{c\cos\varphi + P^{ref}\sin\varphi}\right)^m \quad [14]$$

The shear modulus at any strain level is obtained from Equation [9].The shear strain parameter $\gamma_{0.7}$ was estimated from the shear modulus degradation curve of aggregate at $G/G_{max} = 70$ % ,as shown in Figure 4-12 (Rollins et al., 1998). Table 4.2 summarizes the clay and aggregate HSSMALL model parameters,

Table 4-2: The model HSSMALL clay and aggregate parameters:

Parameter	Symbol	Top Aggregate	Bottom Aggregate	Glyben
Soil unit weight (kN/m^3)	γ	16	16	13.8
Secant stiffness in standard drained triaxial test (kN/m^2)	E_{50}^{ref}	2783	4680	800

Tangent stiffness for primary oedometer loading (kN/m^2)	E_{oed}^{ref}	2227	3750	850
Unloading/reloading stiffness (kN/m^2)	E_{ur}^{ref}	8350	14.4X10^3	8000
Power for stress-level dependency of stiffness	M	1	1	1
Cohesion	c'_{ref}	1	1	1
Friction angle	φ	50	50	NA
Dilatancy angle	Ψ	20	20	NA
Undrained Shear Strength	c_u	NA	NA	15
Reference shear modulus at small strains (kN/m^2)	G_0^{ref}	36.3 X 10^3	61.1X10^3	377X10^3
Threshold strain, $\gamma_{0.7}$		0. 007	0.007	0.06
Poisson's ratio	v'_{ur}	0.2	0.2	0.2

4.3.3.3 Soil damping

The damping ratio of soils is an important parameter in numerical modelling of the dynamic behaviour of soil-supported structures (Ju and Ni, 2007). The damping ratios of the aggregate, glyben and sand layers were calculated from the stress strain loops obtained from the acceleration data collected during the shaking table tests. Figures 4-7 to 4-9 show typical shear stress-strain hysteretic loops of the sand, aggregate and glyben layers, respectively. The damping ratio was simulated in the numerical model via the two Rayleigh damping coefficients α_R and β_R (Ju and Ni, 2007). These coefficients were used to determine the damping matrix C, which is formulated as a function of the mass and stiffness matrices as follows:

$$C = \alpha_R M + \beta_R K \quad [15]$$

Rayleigh damping coefficients α_R and β_R were determined from the damping ratio and two different circular natural frequencies (ω_1 and ω_2) through the relationship :

$$\alpha_R = 2\,\omega_1\omega_2\,(D_1\,\omega_2 - D_2\,\omega_2) / (\omega_2^2 - \omega_1^2) \quad [16a]$$

$$\beta_R = 2\,(D_2\,\omega_2 - D_1\,\omega_2) / [\pi(\omega_2^2 - \omega_1^2)] \quad [16b]$$

4.3.4 The numerical model elements and mesh configuration

The soil was modeled using 10 node tetrahedral elements. The piles were modeled as three node beam column elements using the built-in embedded piles elements. The pile cap was modeled using plate elements. The Interface elements were introduced at the bottom of the pile cap in order to simulate the separation that was noticed during the shaking tests. The interface elements were modeled as 6 nodes triangular elements that allow separation and relative deformation between the cap and soil as the deformation exceeds the stiffness of the interface layer.

In the calibration phase, the numerical model simulated the configuration, dimensions and boundary conditions of the physical model test setup. The vertical boundaries of the model were surrounded with prescribed displacement surfaces that allow free translation in the 1-D horizontal X and Z directions while restraining the translation at the transverse Y direction. This scheme simulates the free horizontal translation of the lamina section during 1-D shaking. At the bottom of the model, a prescribed surface was attached through which a harmonic base excitation signal of 16 Hz and 0.06g amplitude was introduced.

4.3.5 The numerical calculation process

The dynamic calculation process was divided into four main stages, namely: the initial condition stage (to evaluate initial geostatic stresses); the construction of the geogrid-pile-cap system stage; and the forced vibration analysis stage. In the fourth stage, the

geogrid mesh was deactivated in order to simulate the case where the geogrid mesh was removed from the model pile cap system.

Before starting the initial phase, all structural elements were deactivated and the soil body was activated. Once the initial stage was executed, the stresses in the soil body were calculated using the K_0 procedure and vertical stresses in equilibrium with the soil self-weight were created. Hence, an initial stress field was generated within the finite element mesh. Then, in the construction phase the soil, geogrid and structural elements were activated together and an elastic-plastic deformation analysis was executed (Brinkgreve et. al, 2012).

In the dynamic response analysis stage, the basic dynamic equation is solved using the Newmark implicit time integration scheme (Rao , 2005):

$$[M]\frac{d^2\vec{X}}{dt^2} + [C]\frac{d\vec{X}}{dt} + K\vec{X} = \overrightarrow{F}\left(\overrightarrow{X}, t\right), \quad t > 0 \qquad [17a]$$

$$\vec{X} = \overrightarrow{X_0} \; and \; \frac{d\vec{X}}{dt} = \overrightarrow{Y_0} \qquad t = 0 \qquad [17b]$$

Where M, C, K and F denote the known n x n mass, damping, stiffness and force matrices, respectively. The Newmark method solves the above equation by using a step-by-step procedure in which $\vec{X}(t)$ is obtained at discrete time intervals Δt apart (Rao, 2005).

4.4 Free Field Ground Response Analysis Using Deep Soil

The free field ground response analysis was carried out using the software DeepSoil (Hashash. et al., 2002). A harmonic signal having the scaled frequency of the Upland earthquake with amplitude of 0.06g was used as the input motion for the three layer soil column in a Deep soil model. The equivalent linear analysis method was carried out to calculate the soil column response. The stiffness degradation and damping curves of the surface aggregate layer under light confinement stress was obtained from the curves developed by Rollins et al. (1998) (Figure 4-12 and 4-13). The stiffness degradation and

damping curves of glyben were obtained from Turan et al. (2009b). The Seed and Idress (1975) stiffness degradation and damping curves of sand (built-in within DeepSoil) was employed for the base sand layer. Figure 4-14 compares the acceleration response calculated by DeepSoil and the acceleration measured by accelerometer AC-7 that was placed at the surface of the gravel layer in the shake table test. The input motion used was a harmonic signal of 16 Hz and 0.06 g amplitude. Figure 4-14 shows a close agreement between the measured and calculated responses.

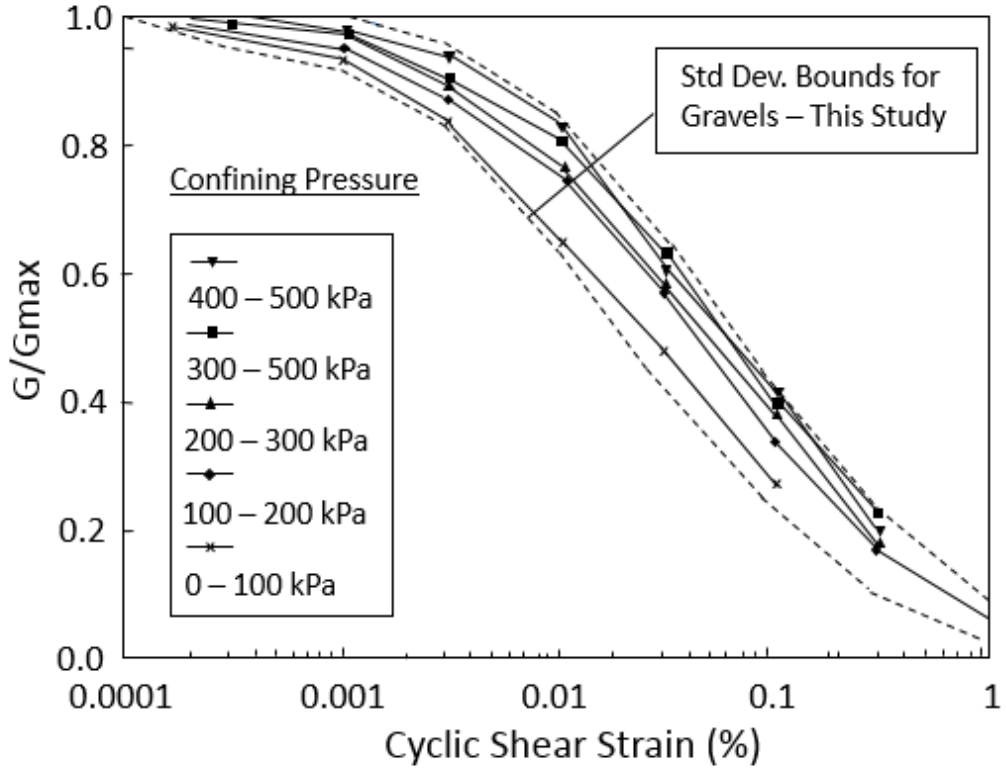

Figure 4-12 : Mean curves defining G/G_{max} versus γ relationships for gravelly soils at various confining pressures along with standard deviation boundaries for reduced data set (Rollins et al. ,1998).

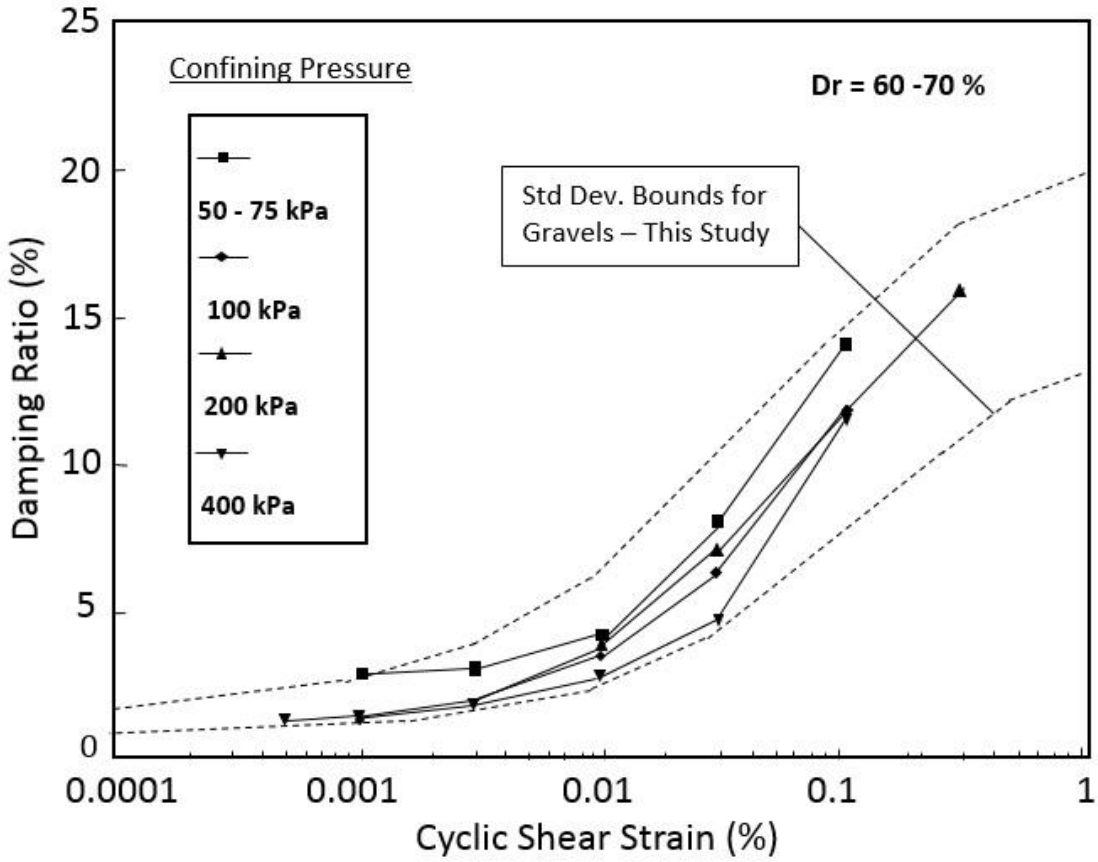

Figure 4-13 : Mean Curves Defining D versus γ relationships for gravelly soils at various confining pressures along with standard deviation boundaries for entire data set (Rollins et al. ,1998).

The input parameters used to generate the soil column response are summarized in Table 4-3. The average soil column natural frequency was calculated as 16 Hz which matches a scaled natural frequency of 3.5 Hz.

Table 4-3: DeepSoil input parameters; model soil column.

Layer #	Layer Name	Model Thickness (cm)	Prototype Thickness (cm)	Unit Weight (kN/m^3)	Model Shear Wave Velocity (V_{sm}) (m/s)
1	Aggregate	8	160	16	15
2	Glyben	23	460	14	40
3	Sand	36	720	18	50

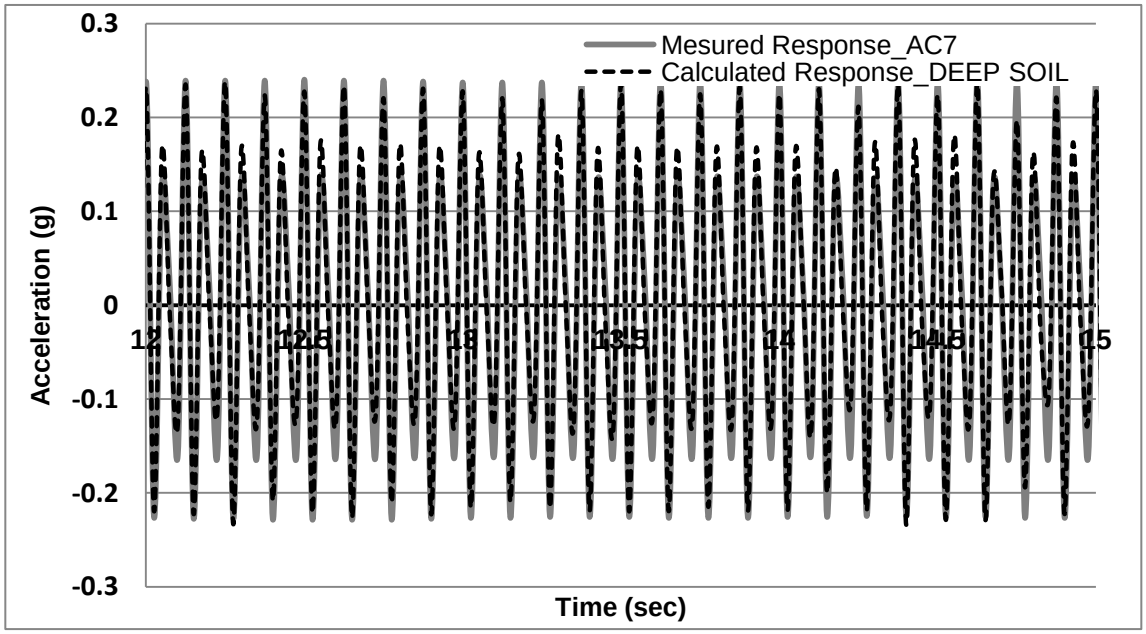

Figure 4-14: Measured vs. calculated acceleration using DeepSoil.

4.5 Numerical Model Calibration Results

The same harmonic input signal was used to calibrate the Plaxis model with geogrid being embedded within the top aggregate layer. Figure 4-15 compares the measured results for the pile cap horizontal acceleration time history and the numerical model predictions. Figure 4-15 shows excellent agreement between the measured and calculated responses.

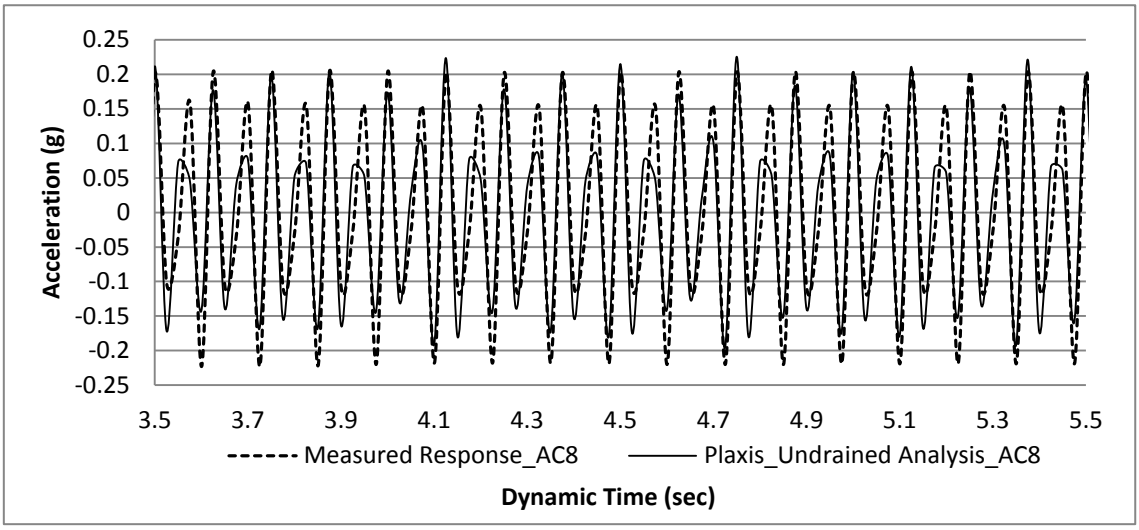

Figure 4-15: Calculated vs. measured responses of pile cap reinforced with geogrid

4.6 Dynamic Model and Its Verification

This section describes a prototype scale model developed to study the dynamic behavior of the geogrid-soil-pile foundation system. It also includes a parametric study carried out to investigate the influence of geogrid stiffness depth and length on the kinematic pile soil interaction. The prototype scale model was subjected to a lateral harmonic shaking signal applied at the base of the supporting soil. The results obtained from the parametric study were discussed in order to explore the beneficial effects of the geogrid reinforcement in reducing the acceleration of the pile foundation system.

4.6.1 Soil Model

The soil model extends 100 meters from the foundation center in the direction of dynamic shaking and 25 meters from the foundation system in the transverse direction (see Figure 4-16). The model boundaries in the perpendicular direction were set as viscous boundaries to absorb the shaking energy while the boundaries parallel to the shaking direction were set as free boundaries. The soil finite element volume was constructed out of 4 m tetrahedron elements with 10 nodes per element and 3 translational degrees of freedom per node.

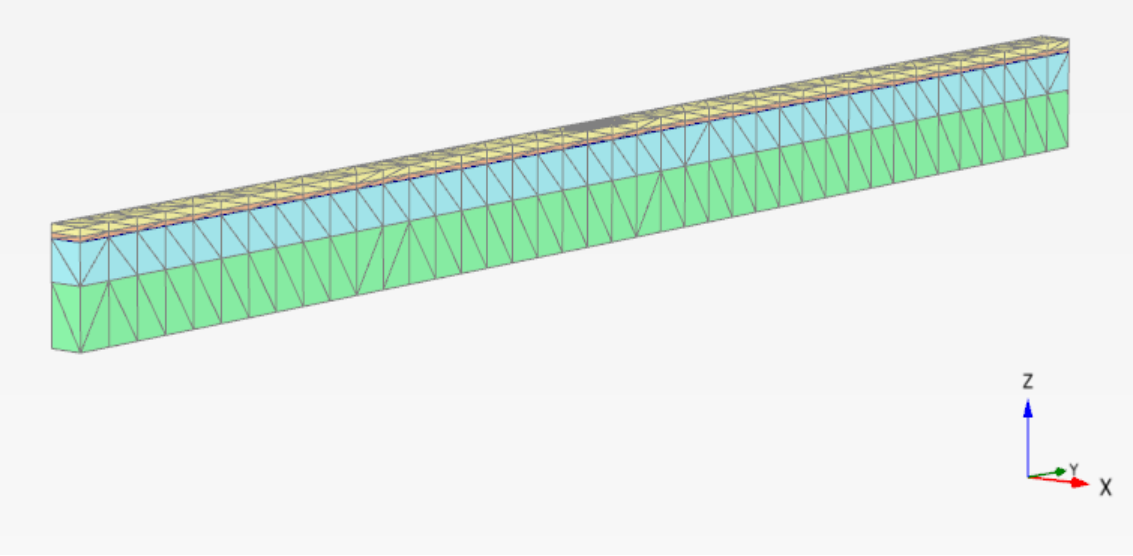

Figure 4-16 : Soil model general view

As shown in Figure 4-17, the model soil profile is subdivided into three main layers: a surface granular layer (aggregate); a soft clay layer; and a granular layer. The depth of the three layers is equivalent to their scaled model depth on a geometric scale of 20. The granular layers were assumed to follow a drained behavior while the soft clay layer was assumed to follow the Undrained (A) behavior due to the nature of quick loading associated with the shaking signal (Brinkgreve et. al, 2012). The stress-strain behavior of the three layers was modeled using the HSSMALL model. The G_0 values of the soil layers were calculated from Equation 4.2 after assuming practical Vs values so that the

fundamental frequency of the prototype soil column was set at 3.7 Hz. The method of calculating the HSSMALL parameters is similar to that used for the model granular layer; as explained in section 4.3.3.2. Table 4-4 shows the Vs values and HSSMALL parameters associated with each soil layer.

(a)

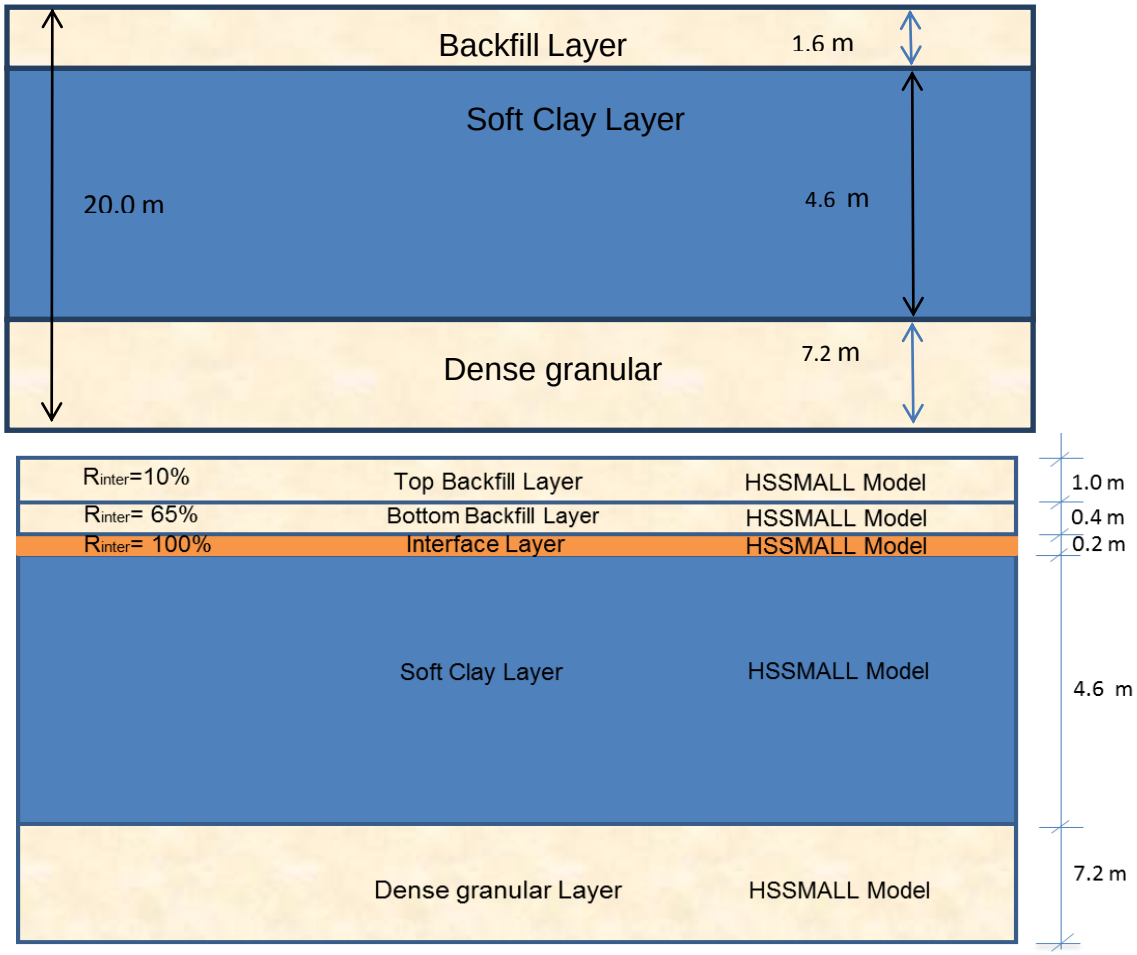

(b)

Figure 4-17 : a) Soil column stratigraphy without geogrid, b) Soil column stratigraphy after adding geogrid

Table 4-4: The HSSMAL prototype parameters of each soil layer

Parameter	Symbol	Top Backfill layer	Interface Layer	Soft clay layer	Dense Granular layer
Soil unit weight (kN/m^3)	γ	20	20	17	20
Shear wave velocity (m/s)	Vs	220	300	170	220
Secant stiffness in standard drained triaxial test (kN/m^2)	E_{50}^{ref}	31.6 X 10^3	58.8X 10^3	4.91 X 10^3	31.6 X 10^3
Tangent stiffness for primary oedometer loading (kN/m^2)	E_{oed}^{ref}	25.3 X 10^3	47.0 X 10^3	3.93 X 10^3	25.3 X 10^3
Unloading/reloading stiffness (kN/m^2)	E_{ur}^{ref}	94.8 X 10^3	176.0X 10^3	14.7 X 10^3	94.8 X 10^3
Power for stress-level dependency of stiffness	m	1	1	1	1
Cohesion	c'_{ref}	5	5	5	NA
Friction angle	φ	40	40	25	40
Reference shear modulus at small strains (kN/m^2)	G_0^{ref}	98.8 X 10^3	184.0 X10^3	50.1X10^3	98.8X10^3

Poisson's ratio	v'_{ur}	0.2	0.2	0.2	0.2

4.6.2 Piles-cap-geogrid-foundation model

Taking advantage of symmetry, the foundation model involved two steel piles 12 m long, 0.5 m in diameter with 6 mm wall thickness. The piles were spaced at 2.5 m and supported a reinforced concrete cap, with dimensions 2 m X 4 m x 0.4 m depth (see Figure 4-18). A geogrid mesh was embedded within the surface granular layer at a depth of 1.6 m (as shown in Figure 4-17).

The linear elastic stress-strain model was used to simulate the behavior of the piles and pile cap. The surfaces of the piles and the pile cap were modeled using 6 nodes triangular shell elements with 6 degrees of freedom per node, three translational and three rotational. The geogrid mesh was represented by 6-nodes triangular elements with 3 translational degrees of freedom per node. The geogrid elements were set to carry tension loads with axial stiffness of 500 kN/m and no bending stiffness. The goegrid elements were connected to the pile shell elements and the soil tetrahedron elements and share the translational degrees of freedom at the connecting nodes. In the parametric study, the geogrid mesh stiffness was increased up to 44,000 kN/m to study the influence of higher stiffness polymer strips.

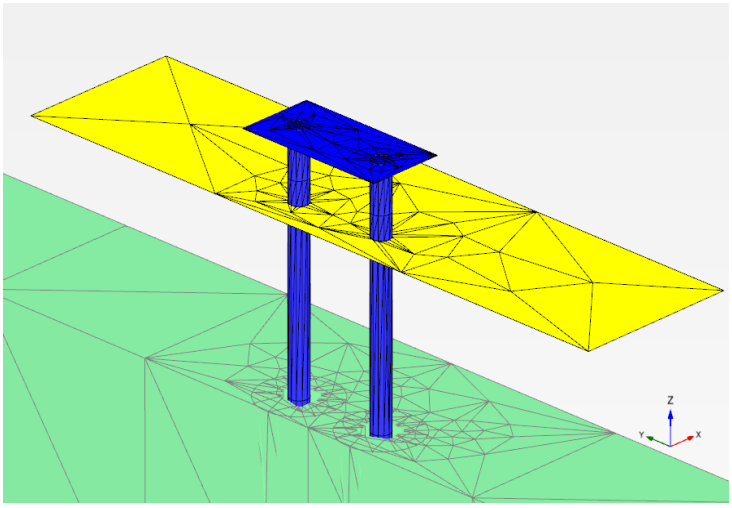

Figure 4-18: Pile-Cap–geogrid finite element mesh.

4.6.3 Interface model

Soil-pile interface nonlinearity is a major source of pile foundation stiffness degradation. Due to cyclic loading, gapping and slippage occur at the pile-soil interface and cause interface nonlinearity. El Nagger and Novak (1995) accounted for interface slippage using rigid sliders connecting both piles and soil nodes. The pile and soil nodes were allowed to move relative to each other when the shear force in the slider exceeded the maximum shear force. Wu and Finn (1996) accounted for gapping by not allowing any tension to occur between the pile and soil. This was achieved by keeping the normal stresses at the pile soil-interface smaller than the assigned tensile strength. El Naggar and Bentley (2000) modeled the pile-soil interface using non-tension springs connecting both soil and piles elements. In the case of clays, gapping is allowed when these springs is disconnected under tension loading. In the case of sand, the interface springs do not allow gapping and sand follows the pile on the tension side with zero soil stiffness. Maheshwari et al. (2003) considered separation between piles and soils using no tension elements.

Similarly, for earth retaining structure, the mechanism in which shear forces are transferred between geogrid and soil is of major importance and influences the overall seismic wall behavior. Several researchers (e.g. Ling et al., 2004; Burke and Ling, 2004; Cai and Bathrust, 1995; Helwany et al., 2001; and Ling, 2009) modeled soil-geogrid interface elements as thin layer elements, thin shell membrane elements or slip elements The slip elements are assumed to follow the Mohr-Coulomb criterion in which slip occurs when the shear stress reaches the yield shear strength at the interface The interface slip is initiated when the applied stress exceeds the yield strength and the shear stiffness reduced with a fraction (α).

In this study, the pile-soil and geogrid-soil interfaces were modeled as surfaces with frictional slip elements having their strength equivalent to a percentage of the adjacent soil shear strength, denoted as $R_{interface}$. The interface elements were 6 nodes triangular

elements connecting both sides of pile shell and geogrid elements to the soil tetrahedron elements. These interface surfaces allow relative movement between piles, geogrid and soil elements (Brinkgreve et al., 2012).

At the surface backfill layer, the Pile-Soil $R_{interface}$ strength is assumed to be 10 % of the adjacent soil strength up to a depth of 1 m to account for the slippage associated with the dynamic loading. At the geogrid mesh level, the geogrid-soil interface strength was assumed equivalent to the strength of the adjacent granular soil. In order to simulate the real strengthening effect of the geogrid interlocking forces, the shear strength of the soil adjacent to the geogrid mesh was assigned a value higher than that of the top granular backfill. The soil strength of at the interface was assigned a shear stiffness value equivalent to 35 % higher than that of the backfill soil.

This stiffness increase was established from matching the results of the experimental static pull test of the case where geogrid was embedded in deep backfill with the results of the numerical model of the deep backfill with an interface layer with thickness equal to approximately 2 times the average particle size of the aggregates (i.e. 2 x 5 mm) x 20 (scale factor). To achieve the best match between the measured and calculated pile cap responses, the shear modulus of the interface layer was increased by 35 % of the backfill shear modulus in order to account for the positive effects of interlocking. Figure 4-18 compares the measured lateral displacements of the pile cap with those calculated from 2 numerical models, one considering the microgrid only and one considering the geogrid and an interface layer with shear modulus increased by 35%. As can be noted from Figure 4-19, there is good agreement between the calculated response considering the interface layer and the measured response. This agreement demonstrated the ability of the numerical model to reproduce the observed behavior of the geosynthetics-reinforced pile foundation system. This approach was considered in the rest of the numerical models in the rest of this chapter as it allowed the size of elements within the interface layer to be smaller to accommodate the large nonlinearity in this region, without increasing the number of elements of the entire model significantly.

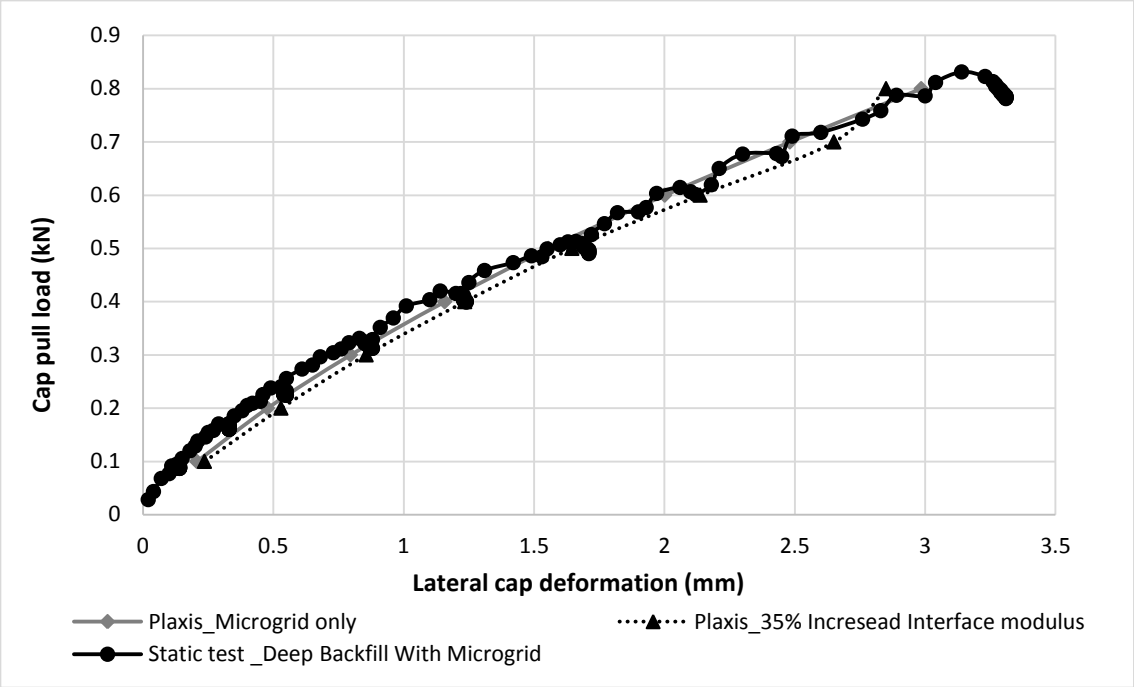

Figure 4-19: Pile cap translation, Static pull test vs. 35% improved interface modulus

4.6.4 Ground response analysis

Free field ground response analyses of the prototype soil model were carried out using the 3D finite element model developed herein and the ground response analysis software DeepSoil. A harmonic signal with frequency = 3.6 Hz and an amplitude = 0.1g was used as the input motion for both models. The equivalent linear analysis method was used in the DeepSoil analysis. The stiffness degradation and damping curves of the surface aggregate layer under light confinement stress was obtained from the curves developed by Rollins et al. (1998). The stiffness degradation and damping curves of the clay were obtained from Vucetic, and Dobry (1991), while the Seed and Idriss (1975) stiffness degradation and damping curves of sand were employed for the base sand layer. Figure 4-19 shows the acceleration responses obtained from the DeepSoil and the 3D finite element models at the surface of the backfill layer. Figure 4-20 shows that there is

excellent agreement between the two responses. This excellent agreement demonstrated the ability of the numerical model to simulate the dynamic behavior of the layered soil profile. The input parameters used to generate the soil column response are summarized in Table 4-5. The average soil column natural frequency was calculated as 3.7 Hz which approximately corresponds to the scaled natural frequency of the model soil column as explained in section 4.4.

Table 4-5: DeepSoil input parameters; prototype soil column.

Layer #	Layer name	Thickness (cm)	Unit Weight (kN/m^3)	Shear Wave Velocity (V_{sp}) (m/s)
1	Aggregate	1.6	20	220
2	Glyben	4.6	17	170
3	Sand	7.2	20	220

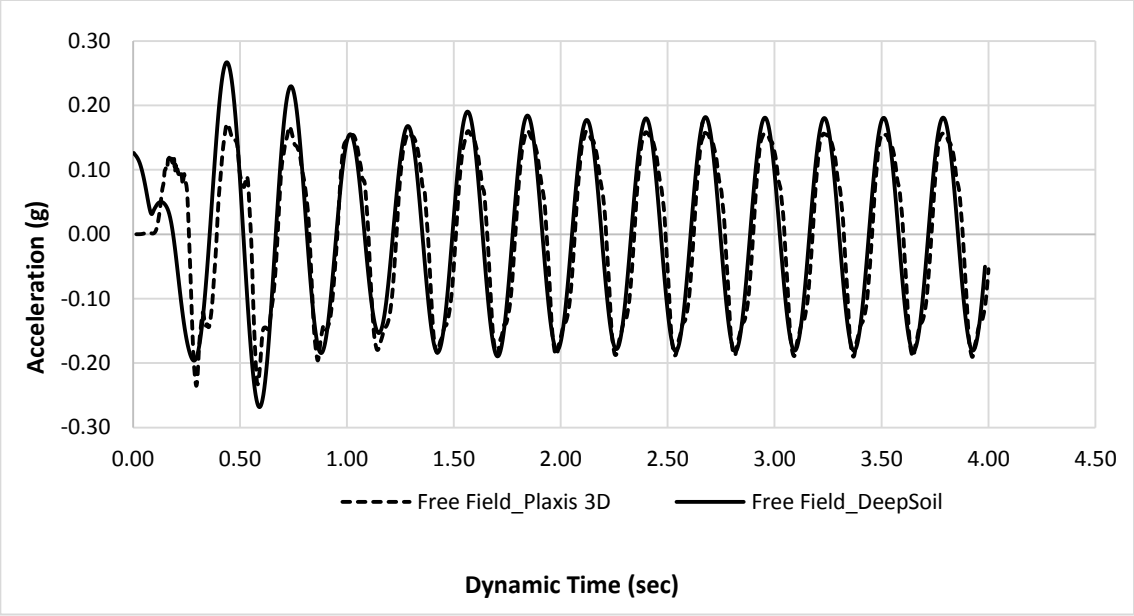

Figure 4-20: Ground response analysis, 3D finite element model vs. DeepSoil.

4.7 Parametric Study Considering Dynamic Analysis

A parametric study was conducted using the verified numerical model to evaluate the influence of different parameters on the performance of geosynthetics-reinforced Pile foundation system. Table 4.6 summarizes the cases considered.

Table 4-6: Summary of numerical model verification analyses

Numerical Case No.	Test case description	Base Excitation Amplitude	Base Excitation Frequency
1	Harmonic excitation, 2.0 m backfill with and without geogrid	0.1 g	3Hz
2	Harmonic excitation, 2.0 m backfill with and without geogrid	0.2g	3Hz
3	Harmonic excitation, 2.0 m backfill with and without geogrid	0.3g	3Hz
4	Harmonic excitation, 2.0 m backfill with and without geogrid	0.2g	2Hz
5	Harmonic excitation, 2.0 m backfill with and without geogrid	0.2g	5Hz
6	Harmonic excitation, 6.0 m backfill with and without geogrid	0.2g	3Hz
7	Harmonic excitation, 1.6 m backfill with polymer strips	0.2g	3Hz

4.7.1 Effect of geogrid reinforcement on response to shaking with varying intensity

This section investigates the effectiveness of geosynthetics reinforcement for pile foundations subjected to input motion with different amplitude. The base motion amplitude was increased from 0.1 to 0.3 g, while the excitation frequency was kept constant at 3Hz.

Figure 4-21 shows the response calculated at the pile cap due to the applied harmonic excitation for the cases of 2 m backfill with and without geogrid. The input motion was set at amplitude = 0.1 g. Figure 4-21 shows that the addition of the geogrid has reduced the acceleration amplitude by an average of 20% when the response reached a steady state, which indicates beneficial effect in reducing acceleration, as well as lateral response of the pile foundation.

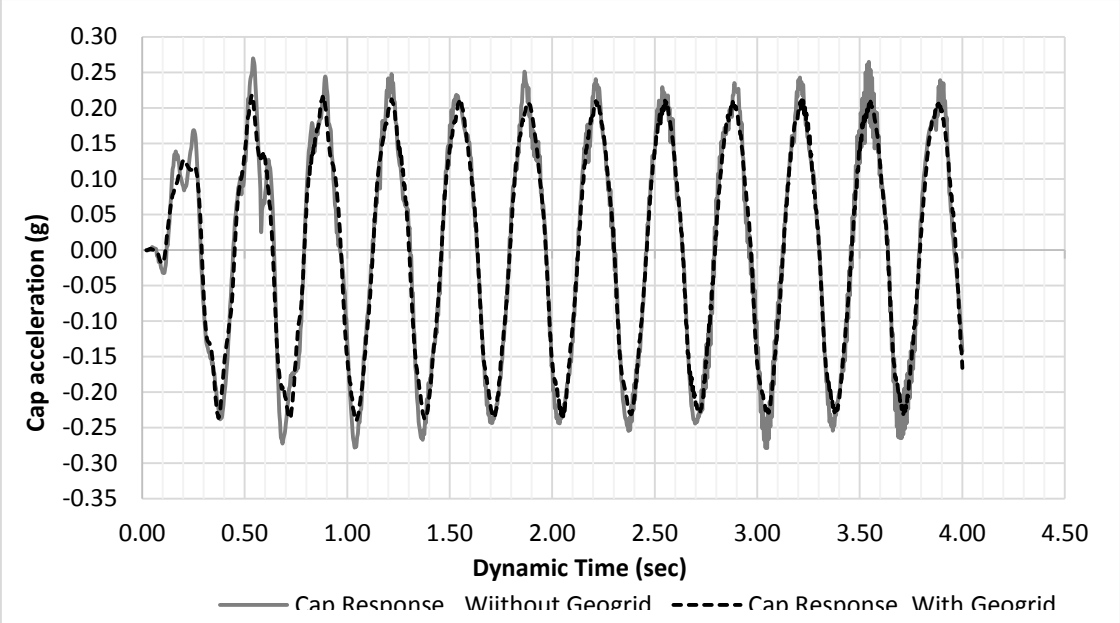

Figure 4-21: Cap motion comparison, Cases of 2 m backfill with and without geogrid (0.1 g, 3 Hz).

Figure 4-22 shows the response of the pile cap with and without the geogrid reinforcement subjected to input motion with amplitude = 0.2g. It can be noted from Figure 4-22 that the geogrid reinforcement reduced the cap acceleration by almost 50 %. This indicates increased effectiveness for stronger ground input motion. This can be attributed to the stiffening effect of the geogrid-soil interlock which enhanced the lateral resistance of the pile cap.

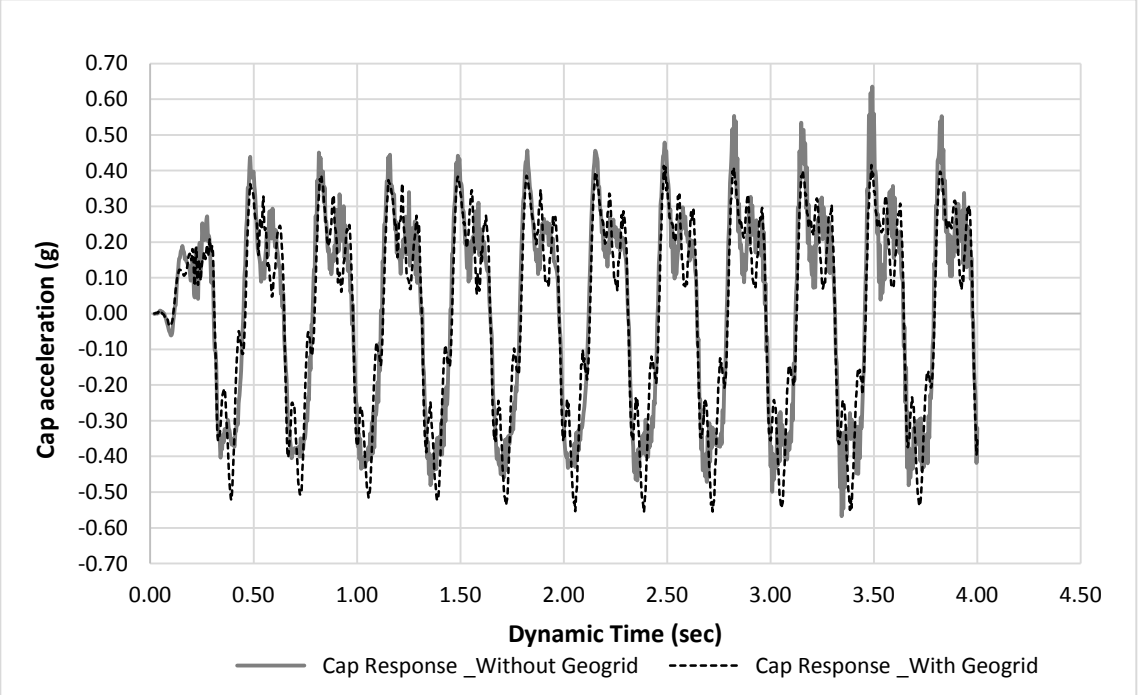

Figure 4-22: Cap motion comparison, Cases of 2 m backfill with and without geogrid (0.2 g, 3 Hz).

Figure 4-23 shows the cap response to an excitation with amplitude = 0.3g. Similar to the previous case, the geogrid reinforcement resulted in reduced cap acceleration by almost 30 %. It appears that for much increased input motion, the shear stresses at the geogrid-soil interface exceeded its maximum shear resistance, hence limiting the favorable effect of the geogrid to an average of 30 %.

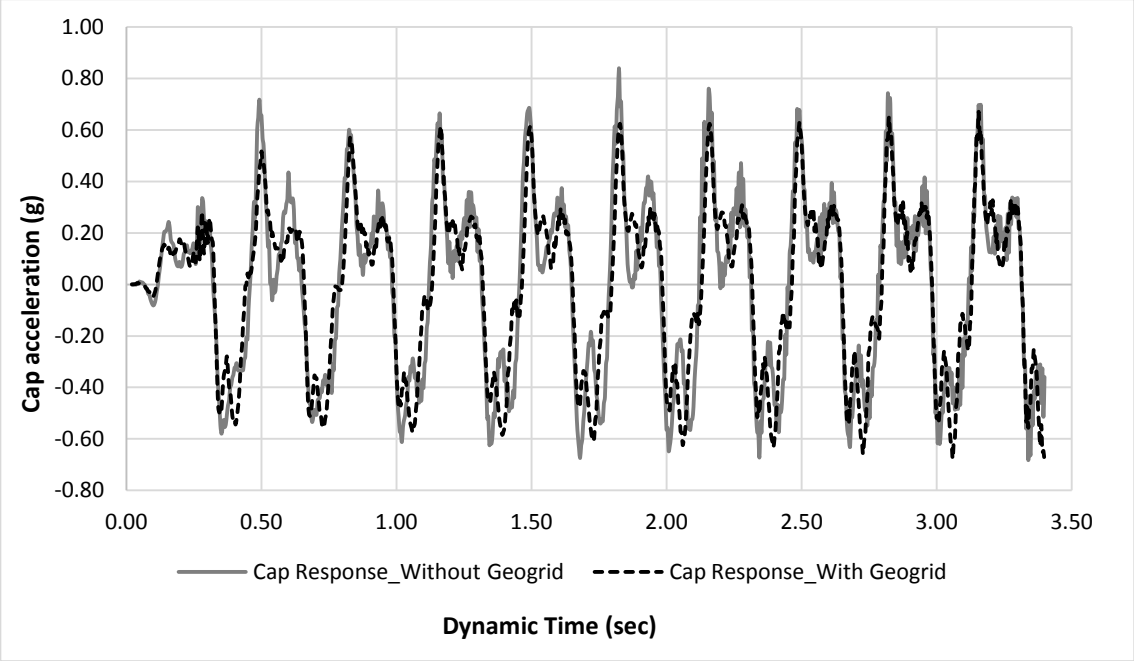

Figure 4-23: Cap motion comparison, Cases of 2 m backfill with and without geogrid (0.3 g, 3 Hz).

4.7.2 Effect of geogrid reinforcement on response of foundation subjected to shaking with different frequency

The effect of the input motion frequency on the behavior of the pile-cap-geogrid system was investigated by subjecting the pile foundation system to base motion with two different frequencies, 2 Hz and 5 Hz g, while keeping its amplitude constant at 0.2 g. This frequency range represents the typical predominant frequencies of medium to high frequency earthquakes in North America.

Figures 4-24 and 4-25 show the cap response with and without the geogrid reinforcement for excitation frequencies 2 Hz and 5 Hz, respectively. Figures 4-24 and 4-25, along with Figure 4-22 reveal that the geogrid advantageous effect was sustained over the studied range of frequencies. This confirms the effectiveness of the geosynthetics-strengthened pile foundation system in a wide range of seismic activities.

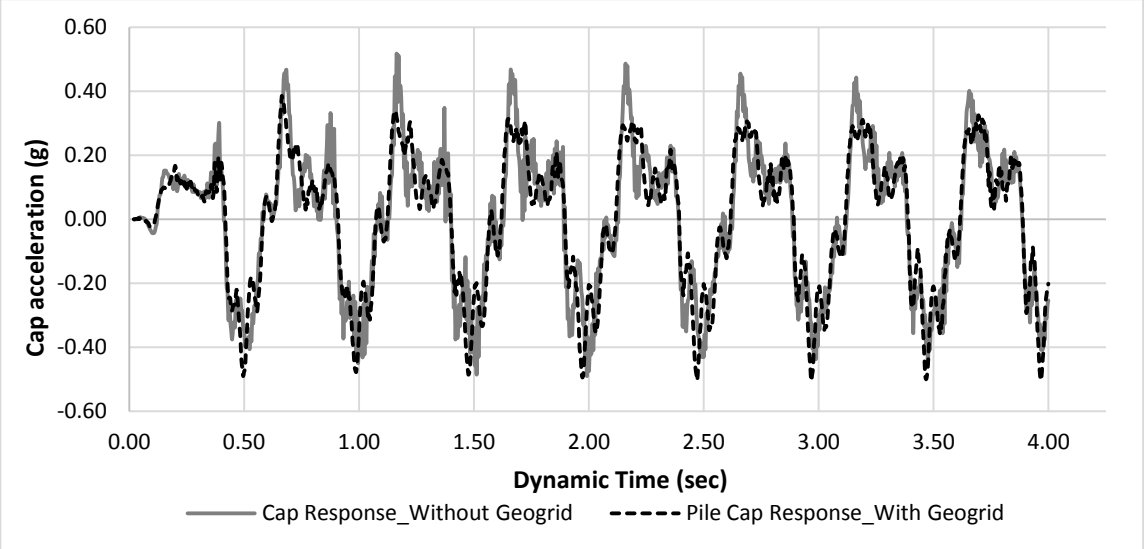

Figure 4-24: Cap motion comparison, Cases of 2 m backfill with and without geogrid (0.2 g, 2 Hz).

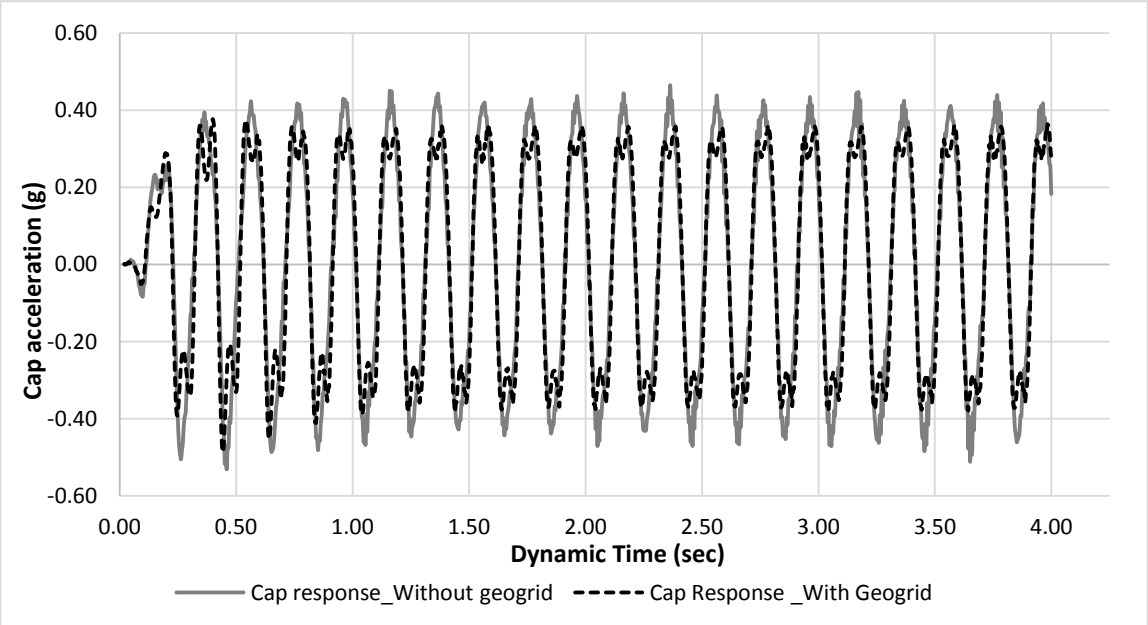

Figure 4-25: Cap motion comparison, Cases of 2 m backfill with and without geogrid (0.2 g, 5 Hz).

4.7.3 Effect of engineered backfill thickness

Figure 4-26 shows the acceleration time history of the pile cap response for the cases of 6 m backfill without geogrid, 1.6 m backfill with geogrid and 1.6 m backfill without backfill. It can be noted from Figure 4-26 that both cases of 1.6 m backfill with geogrid and 6 m backfill without geogrid produced similar acceleration time histories. This demonstrates that the geogrid-reinforcement can reduce the requirements for ground improvement significantly, while maintaining the same acceptable performance. This can represent significant savings in cost and construction time. In contrast, the acceleration time history of the pile cap for the case of 1.6 backfill without geogrid is almost 40 % higher than the other two cases. These results confirm the effectiveness of the geosynthetics reinforcement to improve the seismic performance of pile foundations.

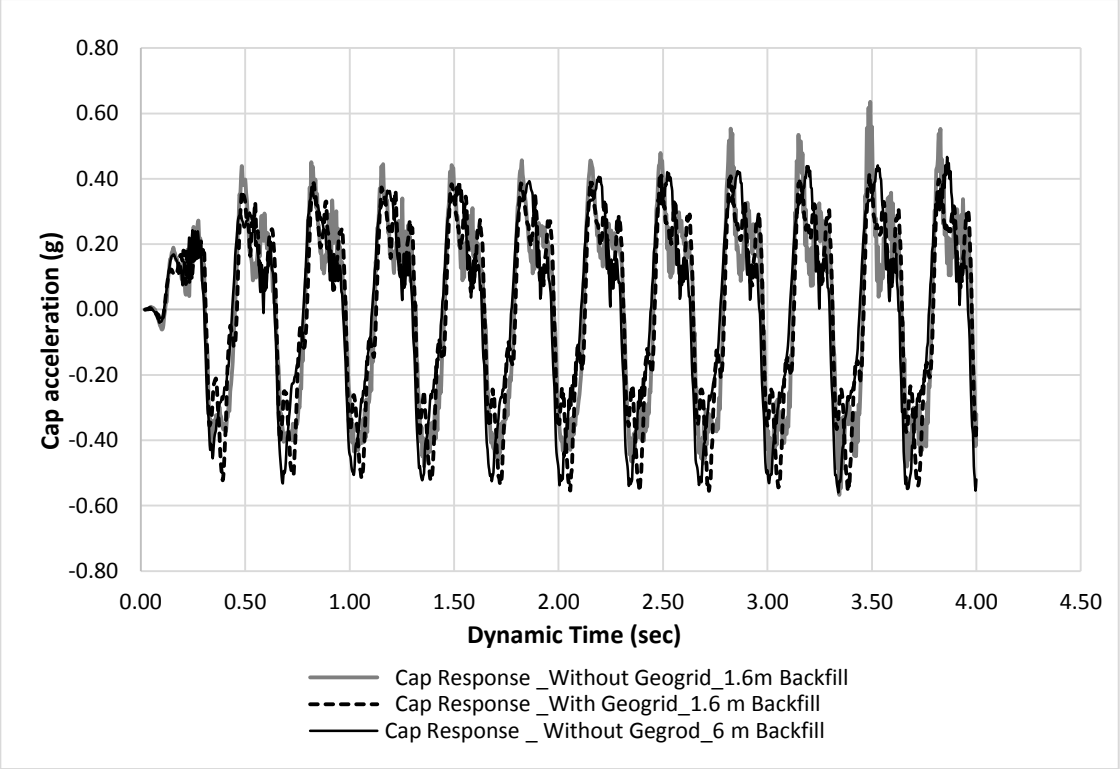

Figure 4-26: Pile cap acceleration time history comparison , (cases of 1.6 m with geogrid, 1.6m without geogrid and 6 m backfill without geogrid).

4.7.4 Effect of stiffness of geosynthetics reinforcement on the system performance

The stiffness of the geosynthetic reinforcement used in the aforementioned sections (500 KN/m) represented the stiffness of typical geogrids. However, polymer strips can have a stiffness of as much as 44000 kN/m. Additional dynamic analyses were carried out to investigate the beneficial effect of using polymer strips instead of geogrids as reinforcing element.

Figure 4-27 compares the responses of a pile cap reinforced with polymer strips and geogrids when subjected to base excitation with amplitude = 0.2g and frequency = 3Hz. Figure 4-26 shows that the polymer strips resulted in further reduction of the pile cap response compared to the conventional geogrid. This additional improvement, however, should be weighed against the extra cost of using the polymer strips. The final design should be optimized considering the level of seismic intensity and the specified performance criterion for the pile foundation.

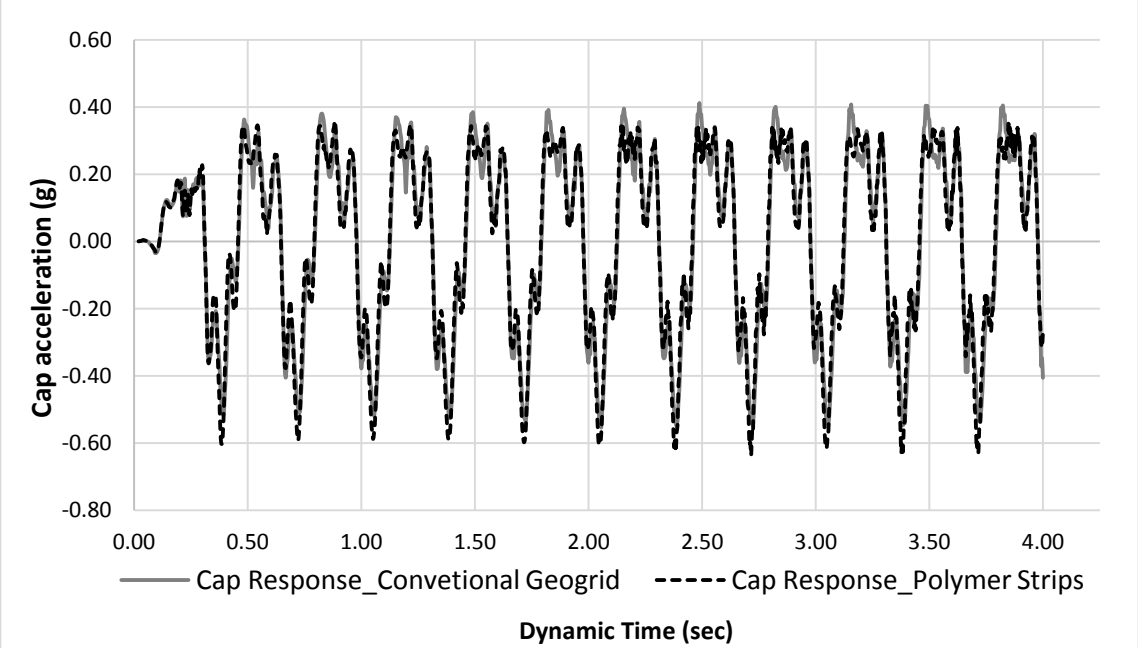

Figure 4-27: Effectiveness of conventional geogrid vs. polymer strips in reducing pile cap response

4.8 Parametric Study Considering Pseudo-Static Analysis

This section presents the results of a parametric study carried out to evaluate the performance of the proposed geogrid-strengthened piled foundation system considering the typical seismic design loads stipulated by the National Building Code of Canada (NBCC, 2010). The objective of the design exercise is to optimize the ground replacement effort (i.e. thickness of engineered backfill).

The seismic loading is given by the pseudo-static inertial force generated for 20 m high (6 stories) reinforced concrete building. The parametric study investigates the effects of geogrid depth and stiffness on the lateral pile deflection. The soil profile considered in this study was modified to reflect a practical case of an engineered backfill and a week native soil layer.

4.8.1 Building, pile cap model and geogrid

The example building was assumed to be located in Vancouver, BC. The total building height is 20.0 m covering an area of 22.5 m X 22.5 m. The building is supported on a raft 0.5 m thick and supported by 100 steel piles spaced at 2.5 m centre-to-centre. The piles were 12 m long, 0.5 m in diameter and had 9.5 mm wall thickness. The pile raft was supported on the soil surface over an interface mesh which allows maximum free translation in the direction of loading. For the purpose of reducing the analysis time, only an area of 4 m X 4 m within the core of the building was modeled. The core of the building was assumed to support part of the lateral seismic load through two shear walls in the direction of the seismic loading. Therefore, only one pile group (2X2) was considered in the analysis.

The soil model boundary and geogrid width were extended 4.5 and 4.25 meters in the lateral direction beyond the line of symmetry , as previously shown in figure 4-17 and 4-18 .The piles, pile cap, and soil finite element mesh characteristics were all similar to the ones modeled in the previous prototype dynamic study. Figures 4-28 and 4-29 show the vertical shear walls, pile cap and geogrid layout plus the soil profile in 2D and 3D views.

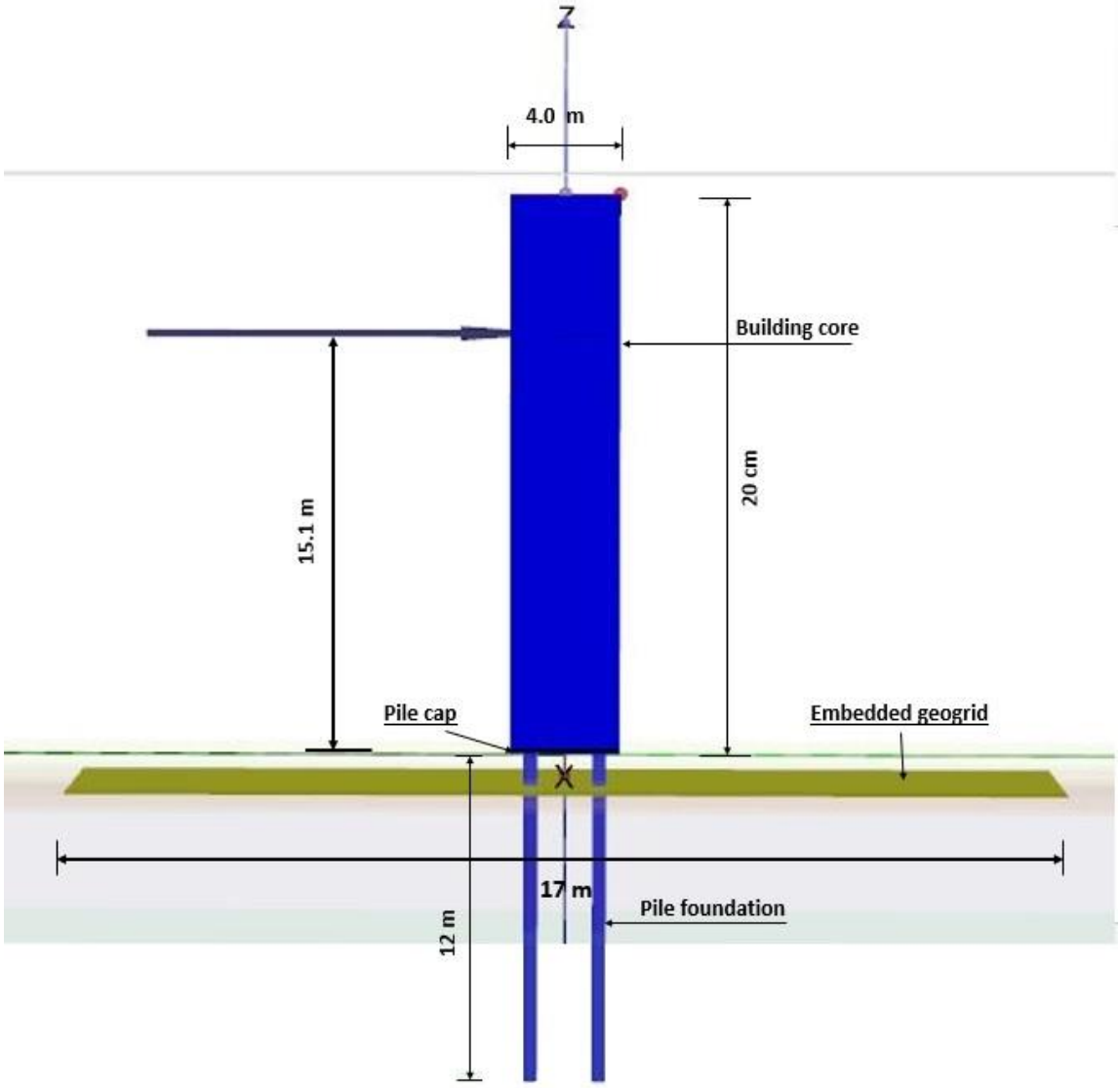

Figure 4-28 : Pile, cap, geogrid and superstructure model

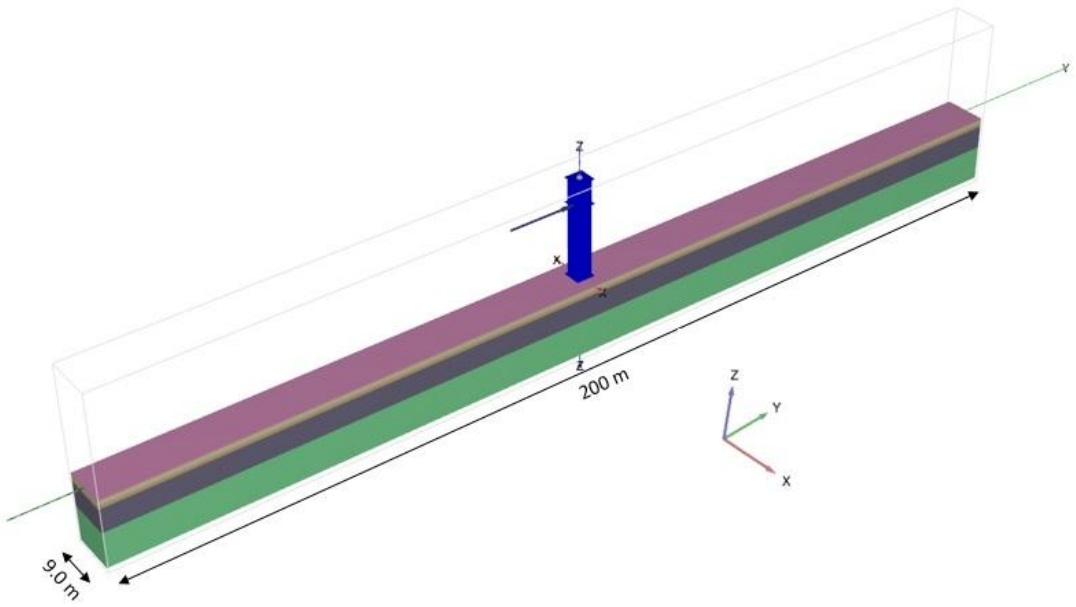

Figure 4-29 : Plaxis model 3D view

The method of analysis for the nonlinear soil model was similar to that adopted in the dynamic prototype study. However, for practical consideration, the shear wave velocity V_s of the backfill used in this study was increased to 300 m/s and a softer clay layer with V_s equals 113 m/s was used to simulate a weaker native soil. Table 4-7 summarizes the HSSMALL model parameters used in this investigation. The soil layers depths were modified so that the total depth of native clay layer is 6 m and the depth of the bedding layer is 13 m. The backfill layer replaced the native clay layer in three stages: 2, 4 and 6 m.

Table 4-7: HSSMALL Soil parameters of each soil layer adopted for the equivalent static study

Parameter	Symbol	Top Backfill layer	Interface Layer	Soft clay layer	Dense Granular layer
Soil unit weight (kN/m^3)	γ	20	20	17	20
Shear wave velocity (m/s)	V_s	300	405	113	220
Secant stiffness in standard drained triaxial test (kN/m^2)	E_{50}^{ref}	58.8 X 10^3	107 X 10^3	2.17 X 10^3	31.6 X 10^3
Tangent stiffness for primary oedometer loading (kN/m^2)	E_{oed}^{ref}	47.0 X 10^3	85.7 X 10^3	1.74 X 10^3	25.3 X 10^3
Unloading/reloading stiffness (kN/m^2)	E_{ur}^{ref}	176.0X 10^3	321.0 X 10^3	6.51 X 10^3	94.8 X 10^3
Power for stress-level	m	1	1	1	1
Cohesion	c'_{ref}	5	5	5	NA
Friction angle	φ	40	40	25	40
Reference shear modulus at small strains (kN/m^2)	G_0^{ref}	184.0 X10^3	335.0 X10^3	22.1X10^3	98.8X10^3
Poisson's ratio	v'_{ur}	0.2	0.2	0.2	0.2

There were two types of geosyenthetics considered in the pseudo-static analysis. The first is the polymer strips with stiffness of 44,000 kN/m. The second is a conventional geogrid

with a stiffness of 2900 kN/m at 2% strain. The conventional geogrid stiffness was taken from the technical data sheet of TMP Geosyenthetics – Uniaxial Geogrid GG200PE. Table 4-8 shows the specification of the conventional geogrid.

Table 4-8 : Uniaxial Geogrid GG200PE specifications

Index Properties	Test Method	Units	MD Value
Polymer	-	-	HDPE
Minimum Carbon Black	ASTM D 4218	%	2
Tensile Strength @ 2% Strain	ASTM D 6637	kN/m (lb/ft)	58 (3.970)
Tensile Strength @ 5% Strain	ASTM D 6637	kN/m (lb/ft)	116 (7,950)
Ultimate Tensile Strength	ASTM D 6637	kN/m (lb/ft)	200(13,700)
Strain @ Ultimate Strength	ASTM D 6637	kN/m (lb/ft)	11.5
Junction Efficiency	GRO GG2-87	kN/m (lb/ft)	90

4.8.2 Pseudo-static seismic lateral loading calculation

The equivalent seismic base shear has been calculated as per the NBCC (2010) provisions. The site was assumed to be located in Vancouver area with soft soil and site Class E classification (NBCC 2010, Table 4.1.8.4.A). The strength level design base shear is given by:

$$V = \frac{S(T_a)\, M_v\, I_E}{R_d R_0}\, W \qquad \text{(NBCC 4.1.8.11)} \qquad [18]$$

Where

- The Fundamental period of the structure in seconds $T_a = 0.05\ (h_n)^{3/4} = 0.5$ sec (CI.4.1.8.11.3(c)).

- For Vancouver , the 5% damped spectral response acceleration ratios, Sa(T), are provided in Table-C2 of NBCC2010 as :

Sa(0.2)	Sa(0.5)	Sa(1.0)	Sa(2.0)	PGA
0.95	0.65	0.34	0.17	0.47

- The design spectral acceleration value S(T):

  From Table 4.1.8.4.b, the value of acceleration-based site coefficient, $F_a = 0.9$.

  From Table 4.1.8.4.c, the value of velocity-based site coefficient, $F_v = 1.8$.

  For T=0.5 sec, $S(T) = F_v \cdot Sa(0.5)$ or $S(T) = F_a \cdot Sa(0.2)$, Smallest S(T) = 0.855.

  Therefore, for T=0.5 sec, S(T) = 0.855

- From Table 4.1.8.11, $Sa(0.2)/Sa(2.0) = 0.95/0.17 = 5.6 < 8.0$, Therefore higher mode factor $M_v = 1.0$.

- The seismic importance factor was set at 1.5.

- From Table 4.1.8.9, and considering the building has limited ductility shear walls, $R_d = 1.5$, $R_o = 1.5$.

- Seismic dead load W = 15220 kN.

- Total lateral seismic force is obtained from Eq. [18].

  V= 8726.13 kN

The calculated base shear force was applied at the vertical centroid of the distributed lateral floor forces. The vertical centroid was calculated from the division of the total seismic overturning moment by the total base shear. Table 4.9 shows the distribution of the lateral earthquake forces Fi and determines the total overturning moment and the vertical centroid.

Table 4-9: Equivalent static forces and overturning moment calculation

Floor height	W(kN)	wiXhi	LTFi*(kN)	LFi**(kN)	OM***(KN.m)
20	3961.25	79225.00	3546.41	141.85	0
15	3961.25	59418.75	2659.80	106.39	709.28
10	3961.25	39612.50	1773.20	70.92	1950.52
5	3336.25	16681.25	746.72	29.87	3546.40
Total	15220.00	194937.50	8726.13	349.05	5291.63

* Total lateral force over 100 piles
**Lateral force over 4 piles
***Overturning moment over 4 piles

The vertical centroid = 5291.63/349 = 15.16 m

4.8.3 Summary of numerical pseudo-static analyses

This section describes the cases investigated in this parametric study. The equivalent static load was applied to the model geogrid-strengthened foundation system considering various soil profiles and different configurations for the geosyenthetics reinforcement including: embedment depth and stiffness. Table 4.10 summarizes the different cases analyzed.

Table 4-10: Equivalent static analysis cases

Case No.	case description
1	Native soil, no backfill without geosynthetic reinforcement
2	2 m backfill without geosynthetic reinforcement
3	4.0 m backfill without geosynthetic reinforcement
4	6.0 m backfill without geosynthetic reinforcement
5	2.0 m backfill with one high tensile geogrid mesh placed at 1.0 m depth
6	2.0 m backfill with one high tensile geogrid mesh placed at 1.25 m depth
7	2.0 m backfill with two high tensile geogrid mesh placed at 1.0 and 1.5 m
8	2.0 m backfill with one polymer strips placed at 1.25 m depth

4.9 Results and Discussion

The results of the parametric study are presented and discussed in this section. The results are discussed with respect to the effect of geosynthetic material stiffness, depth and length on: the building maximum lateral displacement, pile head maximum deflection, pile maximum bending moment and pile maximum shear. Figure 4-30 depicts the deformed shape of the building, pile cap and piles as a result of the equivalent seismic loading.

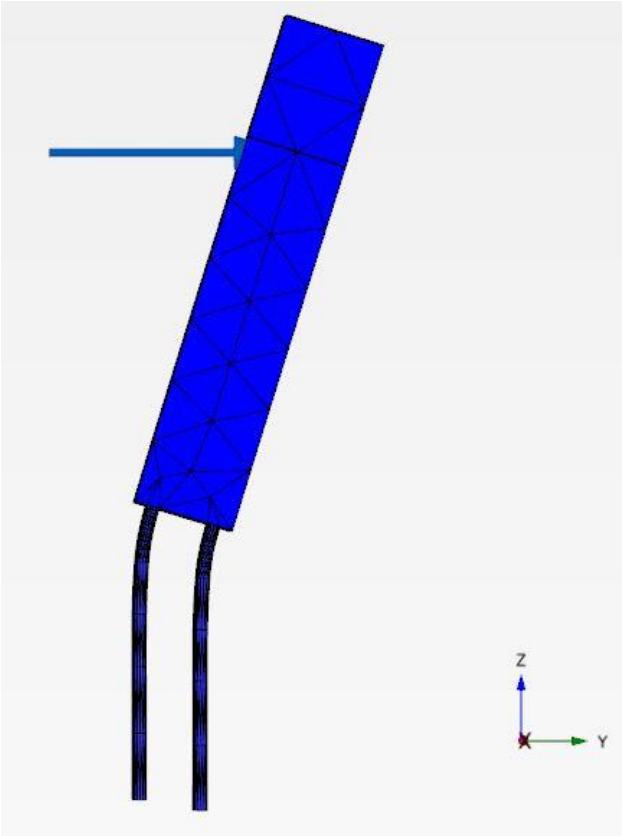

Figure 4-30: Deformed model shape

4.9.1 Effect of geosynthetic material stiffness and depth

Table 4-11 provides the results of cases 1-8 with respect to building maximum lateral drift, pile head maximum deflection, pile maximum bending moment and pile maximum shear.

Table 4-11: Cases 1-8 results comparison.

Case No.	Max pile cap vertical deflection (mm)	Max pile cap lateral deflection (mm)	Max pile bending moment (Nm/m)	Max pile shear (kN/m)
1	19.4	19.6	209	208.0
2	17.4	14.3	215.7	268.3
3	16.1	12.2	265.7	279.2
4	15	11.3	259.4	272.6
5	16	11	146	285
6	16.2	12	135	260
7	15.7	10.4	150.4	272.3
8	16.3	9.4	133.1	291

It can be noticed from the results of cases 1-3 that the pile cap lateral deflection decreases as the conventional backfill depth increases. Also, the results show that increasing the backfill induced higher bending moment and shear force in the piles.

Cases 4 and 5 compare the 6 m plain backfill results to the results of the 2 m backfill with high tensile geogrid embedded at 1.0 m depth. It can be noticed that embedding the high tensile geogrid at 1.0 depth within 2m of backfill resulted in the same performance as the case of 6m backfill, while reducing the bending moment of the piles by 44%. However, the shear force increased by 5 %. This comparison indicates that by using the geogrid, the backfill depth can be reduced by 67% while achieving the same reduction in the lateral displacement (i.e. 44 % reduction in lateral displacement).

Comparing the results of Cases 5 and 6 demonstrates the effect of the geogrid layers depth on the performance of geosynthetics-reinforced pile foundation system. It can be noticed that embedding the geogrid mesh at depth of 1.25 m has reduced the bending moment and shear forces while improving the serviceability of the foundation system. Case 6 demonstrates that by using the geogrid reinforcement, the backfill depth can be reduced by 67% (compared to Case 3) while achieving 39 % improvement in lateral pile foundation performance relative to the native soil case.

In addition, the comparison of Cases 6 and 7 indicates that the lateral performance of the foundation can be improved further by increasing the number of geogrid layers. Also, the comparison of Cases 1, 4 and 7 indicates that through using 2 layers of geogrid, the backfill depth can be reduced by 67% while achieving 47 % improvement in the lateral pile foundation performance and reducing the bending moment and shear forces in the piles.

Moreover, comparing Cases 4, 6 and 8 indicates that the lateral performance of the pile foundation with polymer strips embedded in 2 m backfill was better than that of the pile foundation system with 6.0 m backfill and the 2 m backfill enhanced with one geogrid layer. Using the polymer strips, the backfill depth can be reduced by 67 % while achieving 52 % improvement in the lateral pile foundation performance. In addition, using the polymer strips as reinforcement induced the least bending moment, but polymer strips induced bigger shear force in the piles. This behavior can be attributed to the large stiffness of the polymer strips resulting in high lateral force at the pile shell nodes.

4.10 Summary and Conclusions

This chapter presents the finite-element (FE) model for simulating the dynamic performance of geogrid-reinforced pile foundation system. A numerical dynamic model of geogrid-reinforced pile foundation system was calibrated using the results of the experimental dynamic model. A parametric study was carried out to study the effect of the base motion amplitude and frequency on the dynamic behavior of the geogrid piled foundation system. The parametric study also evaluated the efficiency of pile foundation-

geogrid against the performance of a conventional pile foundation with ground replacement (i.e. deep engineered backfill). The following conclusions may be drawn from the results:

- The numerical results compared well with the experimental results demonstrating that the HSSMALL model was able to simulate the nonlinear stress-strain behavior of the experimental soil bed.

- The numerical results revealed that embedding the geogrid mesh has enhanced the lateral performance of the pile foundation system and reduced its acceleration response.

- The geogrid reinforcement favorable effect was observed for a range of base shaking frequencies and amplitudes.

- Increasing the geogrid stiffness further enhanced the lateral performance of the pile foundation. However, the results indicated that conventional geogrid could replace high stiffness geosynthetic grids as the performance using both materials was comparable.

- The dynamic numerical parametric study suggested that it is possible to reduce the depth of granular backfill by using geogrid while achieving improved lateral performance of the pile foundation system.

- The pseudo-static analysis showed that, as expected, the lateral performance of the pile foundation was improved as the thickness of the conventional backfill increased. However, increasing the backfill thickness induced higher bending moment and shear force in the piles.

- The pseudo-static analysis indicated that embedding the high tensile geogrid in 2m thick engineered backfill at 1.0 m depth reduced resulted in almost the same performance of the pile foundation with 6 m backfill. This means using the

googrid reinforcement can reduce the backfill by 67% while achieving the same improved performance (i.e. 44% reduction in lateral displacement and pile bending moment). However, the shear force increases by 5 %.

- Embedding the geogrid mesh at a depth of 1.25 m, within 2m backfill, have reduced the bending moment and shear forces of the piles while improving the performance of the foundation system (39 % reduction in lateral pile foundation displacement).

- The lateral performance of the pile foundation can be improved further by adding another geogrid layer. It was found that using 2 layers of geogrid, the backfill thickness can be reduced by 67% while achieving 47 % reduction in lateral displacement of the pile foundation, and reduced bending moment and shear force in the piles.

- The lateral performance of the pile foundation reinforced with polymer strips embedded in 2 m thick backfill was better than the performance of the pile foundation with 6m thick backfill and that with the 2 m backfill strengthened with one and two geogrid layers.

References:

[1] Angelides, D. C., and Roesset, J. M. 1980. Nonlinear dynamic stiffness of piles. Department of Civil Engineering, Massachusetts Institute of Technology, Cambridge, Maass. Research Report R80-13

[2] Bathurst RJ, Alfaro MC. Review of seismic design, analysis and performance of geosynthetic rein- forced walls, slopes and embankments. International Symposium on Earth Reinforcement, keynote lecture, Kyushu, 1996. p. 23-52.

[3] Bentley , K.J., and El Naggar, M.H. 2000, Numerical analysis of kinematic response of single piles, Canadian Geotechnical Journal, **37**:1368-1382.

[4] Brinkgreve, R., Egin, E. and Swolfs, W. User's Manual for Plaxis 3D 2012 , Delf University of Technology & PLAXIS bv, The Netherlands.

[5] Cai, Z., and Bathurst, R.J. 1995. Seismic response analysis of geosynthetic reinforced soil segmental retaining walls by finite element method. Computers and Geotechnics, **17** (4), 523-546.

[6] Christopher Burke C, Hoe I. Ling and Huabei Liu, 17th ASCE Eng Mech Conf, June 13-16, Univ of Delaware, Newark, DE, 2004 SEISMIC RESPONSE ANALYSIS OF A FULL-SCALE REINFORCED SOIL RETAINING WALL.

[7] El-Emam, M.M., and Bathurst, R.J. 2007. Influence of reinforcement parameters on the seismic response of reduced-scale reinforced soil retaining walls. Geotextiles and Geomembranes, **25** (1), 33-49.

[8] Fakharian, K., and Attar, I.H. 2007. Static and seismic numerical modeling of geosynthetic-reinforced soil segmental bridge abutments. Geosynthetics International, **14** (4), 228-243.

[9] Faruque, M. O., and Desai, C.S. 1983. 3-D material and geometric nonlinear analysis of piles. In Proceedings of the 2nd International Conference on Numerical

Methods in Offshore Piling, The Univesity of Texas at Austin, Austin, Tex. pp. 553-575.

[10] Hardin, B.O., and Drnevich, V.P. (1972). Shear modulus and damping in soils: Design equations and curves. Proceedings. ASCE: Journal of Soil Mechanics and Foundations Division, 98(SM7), 667-692.

[11] Hashash, Y., Park, D.,Tsai, C., and Groholski, D. 1-D Wave Analysis Program for Geotechnical Site Response Analysis of Deep Soil Deposits. 2002.V5.0. University of Illinois at Urbana-Champaign.

[12] Helwany, S.M.B., Budhu, M., and McCallen, D. 2001. Seismic analysis of segmental retaining walls. I: Model verification. Journal of Geotechnical and Geoenvironmental Engineering, **127** (9), 741-749.

[13] Ju, S. H., and Ni, S. H. 2007. Determining Rayleigh damping parameters of Soils for finite element analysis. International journal of numerical and analytical methods in geomechanics, **31**, 1239-1255.

[14] Ling, H.I., Liu, H., Kaliakin, V.N., and Leschchinsky, D. 2004 .Analyzing dynamic behavior of geosynthetic-reinforced soil retaining walls. Journal of Engineering Mechanics, **130** (8), 911-920.

[15] Liu, H. 2009. Analyzing the reinforcement loads of geosynthetic-reinforced soil walls subject to seismic loading during the service life. Journal of Performance of Constructed Facilities, **23** (5), 292-302.

[16] Michalowski R L. 1998. Soil reinforcement for seismic design of geotechnical structures. Computers and Geotechnics, **23** (1-2), 1-17.

[17] Randolph, M. F. 1981, Response of flexible piles to lateral loading. Geotechnique, **31**(2), 247-259.

[18] Rao, S. S., 2005, The finite element method in engineering, Elsevier Butterworth Heinemann, Amsterdam.

[19] Rollins, K. M., Evans, M. D., Diehl, N. B., and Daily, W. D. 1998. Shear Modulus and Damping Relations for Gravels. Journal of Geotechnical and Geoenvironmental Engineering, **124** (5), 396–405.

[20] Seed, H. B. and Idriss, I. M. Soil moduli and damping factors for dynamic response analysis, report EERC 70-10, Earthquake Research Center, University of California, Berkeley; 1969.

[21] Surarak, C., Likitlersuang S., Wanatowski D., Balasubramaniam A., Oh E., and Guan H. 2012. Stiffness and strength parameters for hardening soil model of soft and stiff Bangkok clays. Soils and Foundations, 52 (4), 682-697.

[22] Trochanis, A., Bielk, J., and Christiano, P. 1988. A three dimensional nonlinear study of piles leading to the development of a simplified model. Department of Civil Engineering, Carnegie Institute of Technology. Report R-88-176.

[23] Trochanis, A.M., Bielak, J., and Christiano, P, 1991, Simplified model for analysis of one or two piles. Journal of Geotechnical Engineering, ASCE, **117**(3),448-466.

[24] Turan, A., Hinchberger, S.D., and El Naggar, M.H. 2009. Design and commissioning of a laminar soil container for use on small shaking tables. Soil Dynamics and Earthquake Engineering, **29** (2), 404-414.

[25] Turan, A., Hinchberger, S.D., and El Naggar, M.H. 2009. Mechanical characterization of an artificial clay. Journal of Geotechnical and Geoenvironmental Engineering, **135** (2), 280-290.

[26] Vucetic, M., and Dobry, R. 1991. Effect of soil plasticity on cyclic response. Journal of Geotechnical Engineering, ASCE, **117**(1),89-107.

[27] Wu, G., and Finn, W, 1997. Dynamic nonlinear analysis of pile foundations using finite element method in the time domain, Canadian Geotechnical Journal, **34**(1), 44-52.

[28] Yegian, M., and Wright, S. 1973. Lateral soil resistance displacement relationships for pile foundations in soft clays. In Proceedings of the 5th Offshore Technology Conference, Houston. Tex, Vol.2, pp. 663-676. OTC Paper 1893.

Chapter 5

5. Summary and Recommendations for Further Research

This thesis investigated the effect of geogrid reinforcement on the lateral response of pile foundations. The investigation was carried out on two model superstructure mounted on a model piles-cap foundation and subjected to 1-G shaking on a shaking table. The research also investigated the static lateral response of the geogrid-piled foundation composite system through subjecting the foundation cap to a static lateral pull. The results derived from the composite system are compared with the base case where the model piled foundation with ground replacement using thick engineered backfill is not reinforced with geogrid and another case where the granular backfill is reduced significantly. The thesis presents static and dynamic numerical models of the piled-geogrid reinforcement composite system that could be used for the analysis and design. The numerical models were verified against the results of the reduced scaled model tested on 1-G shaking table.

5.1 Summary of thesis findings

The following conclusions may be drawn from the thesis findings.

Considering the configuration of the foundation system investigated in this study, and based on the results of reduced scale physical pull tests and corresponding static numerical analyses:

- The lateral resistance of the foundation system was increased by 15 % due to the addition of the model microgrid mesh.
- The lateral resistance of the foundation system decreased by 20 % due to reducing the thickness of the surficial granular backfill layer.
- The numerical results show that the addition of the polymer strips would allow reducing the required soft ground replacement by 50%, while providing improved lateral performance.

- The numerical results showed that the addition of the geosynthetic reinforcement reduced the bending moment by 8% and reduced the shear force by 2%.
- The numerical results also showed that extending the geosynthetic reinforcement increased the lateral stiffness of the foundation system and reduced the lateral displacement by 12 %.
- The numerical results indicated that extending the microgrid mesh farther from the pile foundation bending decreased the bending moment by around 5%.
- The parametric study indicated that the extent of the geosynthetic reinforcement influences the level of enhancement it provides. Thus, the length of the reinforcement should be optimized for the specific case considered.
- Overall, the model scale experimental and numerical results showed that the beneficial effects of the geosynthetic reinforcement increased as the applied load increased. Thus, further improvement of the lateral performance of the geosynthetic-reinforced foundation is expected if the foundation is allowed to experience larger displacement.

The results of a series of reduced scale shaking table tests performed to study the influence of a model polymer strips, the microgrid, reinforcement on the dynamic response of a SDOF superstructures and a supporting piled foundation are summarized herein. The experimental results presented here provide physical evidence on the effectiveness of the proposed foundation concept and can be used to calibrate numerical models. Following are a summary of the conclusions from this experimental study;

- As expected, increasing the thickness of the backfill layer reduced the ground motion amplification and the maximum dynamic response of the soil column to harmonic loading. The addition of the microgrid mesh further reduced the lateral response by 23%.
- The scaled earthquake and sine sweep tests indicated that the microgrid reinforcement resulted in reducing lateral response of the pile foundation, even for the case with thicker engineered backfill. The maximum lateral response of the pile cap decreased farther for the case of the geosynthetics-reinforced backfill.

- The lateral response of the SDOF systems to the scaled earthquake and sine sweep tests decreased for the case of microgrid-reinforced backfill. The sine sweep tests results indicated that the thick backfill reduced the maximum lateral response of the low frequency SDOF structure and the microgrid reinforcement reduced it further. The effectiveness of the microgrid reinforcement in reducing the dynamic response was more pronounced at higher inertial interaction associated with the low frequency SDOF due to the larger dynamic loads associated with larger deformations in the microgrid.
- The rocking vibrations of the pile cap due to the sine sweep tests and harmonic loading were reduced due to the geosynthetics reinforcement. The sine sweep tests revealed that increasing the backfill thickness from 3 cm to 8 cm reduced the peak cap rocking motion by 15 % and the addition of microgrid reinforcement further reduced the peak rocking motion by 9 %.

Finite element analyses were carried out to simulate the dynamic performance of geogrid-reinforced pile cap system. A numerical dynamic model of geogrid-reinforced pile cap system was calibrated against the experimental dynamic model. A parametric study was carried out to study the effect of the base motion amplitudes and frequencies on the dynamic behavior of the geogrid piled foundation system. The study also included comparing the efficiency of pile cap-geogrid embedded in relatively shallow backfill against the performance of a conventional pile foundation embedded in deep backfill using pseudo-static analysis. The following points present the summary of results:

- The numerical results compared well with the experimental results demonstrating that the HSSMALL model was able to simulate the nonlinear stress-strain behavior of the experimental soil bed.

- The numerical results revealed that embedding the geogrid mesh has enhanced the lateral performance of the pile foundation system and reduced its acceleration response.

- The geogrid reinforcement favorable effect was observed for a range of base shaking frequencies and amplitudes.

- Increasing the geogrid stiffness further enhanced the lateral performance of the pile foundation. However, the results indicated that conventional geogrid could replace high stiffness geosynthetic grids as the performance using both materials was comparable.

- The dynamic numerical parametric study suggested that it is possible to reduce the depth of granular backfill by using geogrid while achieving improved lateral performance of the pile foundation system.

- The pseudo-static analysis showed that, as expected, the lateral performance of the pile foundation was improved as the thickness of the conventional backfill increased. However, increasing the backfill thickness induced higher bending moment and shear force in the piles.

- The pseudo-static analysis indicated that embedding the high tensile geogrid in 2m thick engineered backfill at 1.0 m depth reduced resulted in almost the same performance of the pile foundation with 6 m backfill. This means using the googrid reinforcement can reduce the backfill by 67% while achieving the same improved performance (i.e. 44% reduction in lateral displacement and pile bending moment). However, the shear force was increases by 5 %.

- Embedding the geogrid mesh at a depth of 1.25 m, within 2m backfill, have reduced the bending moment and shear forces of the piles while improving the performance of the foundation system (39 % reduction in lateral pile foundation displacement).

- The lateral performance of the pile foundation can be improved further by adding another geogrid layer. It was found that using 2 layers of geogrid, the backfill thickness can be reduced by 67% while achieving 47 % reduction in lateral

displacement of the pile foundation, and reduced bending moment and shear force in the piles.

- The lateral performance of the pile foundation reinforced with polymer strips embedded in 2 m thick backfill was better than the performance of the pile foundation with 6m thick backfill and that with the 2 m backfill strengthened with one and two geogrid layers.

5.2 Recommendations for Future Research

It is recommended to evaluate the performance of a full-scale geogrid-reinforced piled foundation system. A small group of piles, 2X2, can be driven in soft soil and lateral dynamic and static forces can be applied to the pile cap. The lateral displacements of the pile cap and the deformations in the piles can be recorded with sensitive accelerometers, LVDT's and strain gages. The surface clay layer can then be removed in stages and replaced with engineered backfill. The foundation can be tested for each backfill case with the same loading conditions and instruments. For each backfill case, a high tensile geogrid mesh can be embedded within the backfill layer and the testing procedure can be repeated to evaluate the effect of geogrid reinforcement. The data gathered from the field tests can be used for numerical model calibration. The calibrated model can be used to execute a parametric study that establishes a detailed design guidelines and procedure for this novel foundation system.

Appendix A

Direct shear tests results:

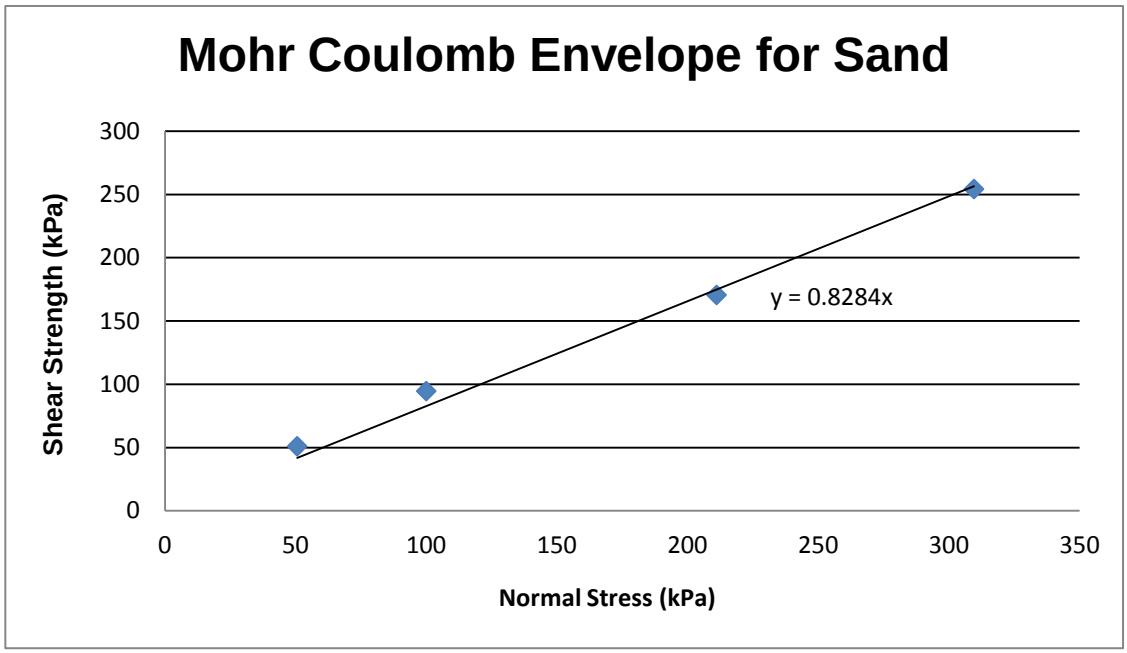

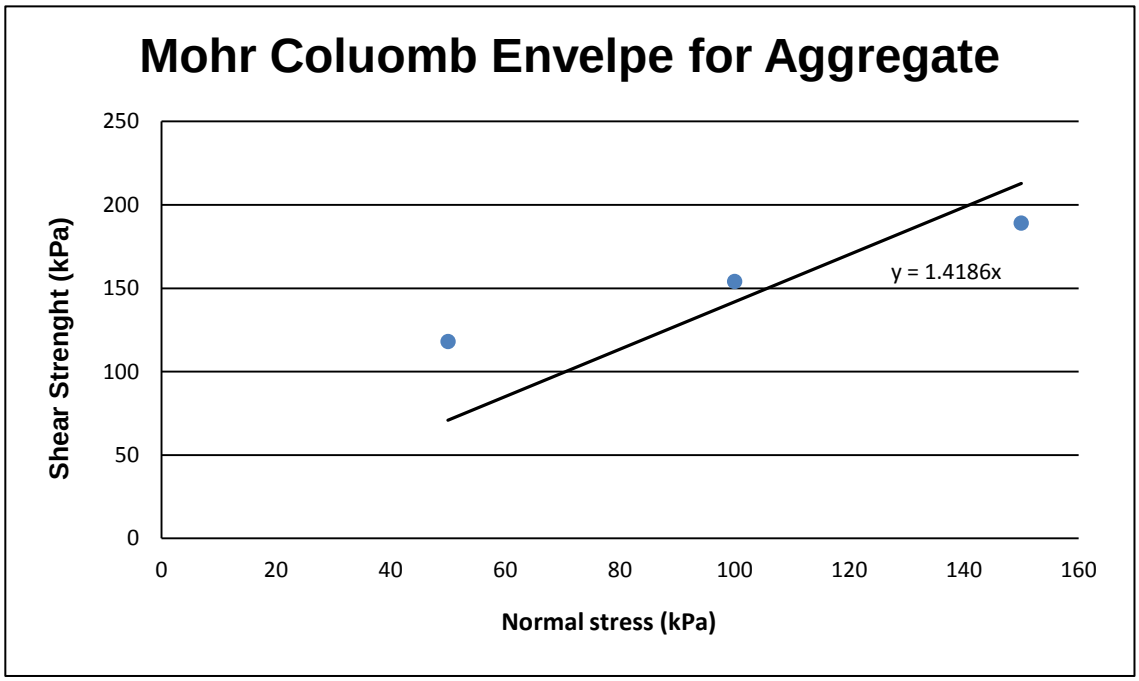

Curriculum Vitae

Name: Ahmed Mohammed A Taha

Post-secondary Education and Degrees:

King Fahd University of Petroleum and Minerals
Dhahran, Kingdom of Saudi Arabia
1992-1997 B.Sc.

The University of Ottawa
Ottawa, Ontario, Canada 2008-2010 M.Sc.

The University of Western Ontario
London, Ontario, Canada 2010-2013 Ph.D.

Related Work Experience:

The Saudi Arabian Oil Company
Project Engineer 1998-2008

Teaching Assistant
The University of Western Ontario 2012-2013

Publications:

Taha A, and Fall M, (2013) " Shear Behavior of Sensitive Marine Clay-Concrete Interfaces" *Journal of Geotechnical and Geoinvironmental Engineering*, Vol 139, No. 4, PP: 644-650.